

A Sodium Wasting Phenotype and Disrupted Collecting Duct Function in Ae1 R607H and L919X Knock-In Mice

by

Priyanka Mungara

A thesis submitted in partial fulfillment of the requirements for the degree of

Master of Science

Department of Physiology
University of Alberta

© Priyanka Mungara, 2024

ABSTRACT

The kidney collecting duct, composed of principal and intercalated cells (ICs), fine-tunes urine composition by regulating fluid, electrolyte, and acid-base homeostasis. Type A intercalated cells (A-ICs) facilitate proton secretion into the urine through an apical proton ATPase and mediate bicarbonate reabsorption into the blood via a basolateral kidney anion exchanger 1 (kAE1). Genetic mutations that impact IC function, for example mutations to *SLC4A1* (kAE1), can lead to distal renal tubular acidosis (dRTA). dRTA results in metabolic acidosis, failed urinary acidification, and an unexplained urinary sodium-wasting phenotype. *In vivo* data from transgenic mice and dRTA patients' kidney biopsies indicate that a loss of kAE1 results in a decreased abundance of ICs. This is evident in the previously published Ae1 R607H knock-in (KI) mouse model (orthologous to human AE1 R589H mutation) that recapitulates classical metabolic acidosis. Our lab obtained a second, unpublished mouse model, the Ae1 L919X KI mice (orthologous to human AE1 R901X mutation). We hypothesize that these mice, with a decreased abundance of A-ICs, are an effective model for studying the persistent urinary sodium loss. The objectives of our work were to 1) characterize the Ae1 L919X KI mice, 2) determine whether the two mouse models accurately reflect the urinary ion loss seen in dRTA patients, and 3) begin investigating the mechanisms causing the urinary sodium loss in these mice. To test our hypothesis, wildtype and dRTA mutant mice were fed a salt-depleted diet, an acid diet, or a salt-depleted acid diet. Following these dietary challenges, analysis of plasma and urine ion concentrations and pH, and qRT-PCR and immunoblots on whole kidney tissues was completed. At baseline, similar to homozygous R607H KI mice, the homozygous L919X KI mice exhibit typical dRTA features including alkaline urine and a reduced number of A-ICs. The salt-depletion and acid challenge alone revealed preliminary evidence of disrupted collecting duct function in the

mutant animals compared to WT. Following the salt-depleted acid diet, both dRTA mutant mice exhibited a urinary sodium loss. Additionally, both homozygous mutant mice showed evidence of upregulated gene and protein expression of tight junction proteins claudin-4 and claudin-10b, suggesting an involvement of the paracellular pathway to compensate for the failing transcellular pathways within the collecting duct. Overall, our findings reveal that both mutant mice appropriately model dRTA pathophysiology, including the urinary sodium wasting phenotype seen in human patients, and suggest a compensatory upregulation of the paracellular transport pathway. As kidney disease is a prominent health concern in Canada, this project contributes to the growing body of knowledge on how various nephron segments communicate with each other to regulate ion homeostasis in our body. Our understanding of the relationship between acid-base balance and sodium reabsorption, can not only provide improved treatment options for dRTA patients, but also to those living with other electrolyte imbalance disorders.

PREFACE

Chapter 1

Parts of Chapter 1 of this thesis have been expanded from a published review article **Mungara, P., Waiss, M., Hartwig, S., Burger, D. & Cordat, E.** Unraveling the Molecular Landscape of kAE1: A Narrative Review. *Canadian Journal of Physiology and Pharmacology* (2024) doi:10.1139/cjpp-2023-0482

Chapter 2

All research in this thesis was approved by the University of Alberta Research Ethics board. Animal protocols were approved by the University of Alberta's Animal Care and Use Committee (AUP #1277) and were in accordance with the national and institutional animal care guidelines.

Chapter 3

Information on L919X KI mice generation was provided from the lab of Dr. Christian A. Hübner (Institute of Human Genetics, Jena University Hospital, Friedrich Schiller University, Jena, Germany). Preliminary characterization found in Appendix A was performed in Dr. Dominique Eladari's laboratory (Université de Picardie Jules Verne, France).

Data from initial experiments of the "salt-depleted acid diet" (Chapter 3) was provided by laboratory technician Kristina MacNaughton prior to the commencement of my master's degree. Subsequently, I assumed responsibility for the investigation and continued its progression.

Saron Gebremariam, an undergraduate student in the PHYSL 461 course, completed RNA isolation and all qRT-PCR of baseline markers (Chapter 3: Figures 3.31, Figure 3.32). This work was done under the supervision of Priyanka Mungara and Dr. Emmanuelle Cordat.

Unless stated otherwise above, all work in this thesis is the work of Priyanka Mungara.

ACKNOWLEDGEMENT

I would like to express my gratitude to my supervisor, Dr. Emmanuelle Cordat. Thank you for welcoming me into your lab and providing me with so many opportunities for growth and success. Your mentorship and support will accompany me for the rest of my career. Thank you for fostering a safe environment for my learning.

I would like to thank our lab technician, Kristina MacNaughton. Your guidance has been vital to my project and my growth as a scientist and person. To my fellow graduate students, Forough Chelangarimiyandoab and Grace Essuman, and all my other colleagues, thank you for supporting me, teaching me, and for your friendship. Thank you also to lab technician Wanling Pan for her guidance and teachings.

My supervisory committee members Dr. Todd Alexander and Dr. Shereen Hamza, I thank you for your helpful recommendations and for sharing your immense knowledge. It has helped me at every stage of my project and challenged me to think about my work in different ways.

Thank you to the Canadian Institutes of Health Research (CIHR) and the Faculty of Graduate and Postdoctoral Studies providing me with scholarships during my master's degree which allowed me to focus on my studies properly.

Thank you to those outside the lab, like my family and friends, for supporting me as well.

TABLE OF CONTENTS

ABSTRACT	ii
PREFACE	iv
ACKNOWLEDGEMENT	v
TABLE OF CONTENTS	vi
LIST OF TABLES.....	viii
LIST OF FIGURES	ix
LIST OF ABBREVIATIONS	xii
Chapter 1: Introduction.....	1
THE NEPHRON.....	2
THE COLLECTING DUCT.....	4
THE THICK ASCENDING LIMB	8
SODIUM TRANSPORT THROUGH THE NEPHRON.....	11
<i>Transporters in the Tubules</i>	<i>11</i>
<i>Hormonal Regulation.....</i>	<i>13</i>
DISTAL RENAL TUBULAR ACIDOSIS	16
<i>The Sodium Wasting Phenotype Persistent Despite Correction of Acidosis</i>	<i>16</i>
(KIDNEY) ANION EXCHANGER 1 PROTEIN.....	17
<i>Protein Structure and Function</i>	<i>17</i>
<i>Post-Translation Modifications and Protein Interactions</i>	<i>18</i>
<i>kAE1 Mutations That Cause Distal Renal Tubular Acidosis</i>	<i>22</i>
HYPOTHESIS AND RATIONALE.....	25
Chapter 2: Materials and Methods.....	26
ANIMALS AND ETHICS APPROVAL	27
METABOLIC CAGE STUDIES WITH SPECIALIZED DIETS.....	28
URINE AND SERUM ANALYSIS.....	30
RNA ISOLATION AND REVERSE TRANSCRIPTASE QUANTITATIVE POLYMERASE CHAIN REACTION.....	30
PROTEIN EXTRACTION AND IMMUNOBLOTTING.....	35
COOMASSIE BLUE STAINING FOR RELATIVE QUANTIFICATION OF URINE ALBUMIN.....	35
TAIL-CUFF BLOOD PRESSURE MEASUREMENTS.....	38
STATISTICAL ANALYSIS.....	38
Chapter 3: Results.....	39
CHARACTERIZATION OF dRTA MUTANT MICE AT STEADY STATE.....	40
DIETARY CHALLENGE 1: 24 HOURS OF SALT-DEPLETED DIET.....	50

DIETARY CHALLENGE 2: 6 DAYS OF ACID LOAD.....	61
DIETARY CHALLENGE 3: SALT-DEPLETED ACID LOAD.....	74
<i>Chapter 4: Discussion</i>	<i>102</i>
SUMMARY OF FINDINGS	103
THE TWO MOUSE MODELS HAVE INCOMPLETE dRTA.....	104
THE NEPHRON'S RESPONSE TO THE DIETARY CHALLENGES.....	104
<i>Urinary Ion Imbalances</i>	<i>104</i>
<i>Urine Acidification</i>	<i>107</i>
<i>Paracellular Ion Transport</i>	<i>108</i>
<i>Hormonal/Systemic Influence</i>	<i>109</i>
STUDY LIMITATIONS AND FUTURE DIRECTIONS.....	110
BIBLIOGRAPHY.....	115
APPENDIX A	127

LIST OF TABLES

Table 2.1	Primers and Probes Used for qRT-PCR on Mouse Genes	32
Table 2.2	Primary Antibodies Used on Mouse Kidney Tissues	37
Table 3.1	Metabolic Cage Parameters of R607H KI/KI and L919X KI/KI Mice at Steady State	43
Table 3.2	Steady State Plasma Characterization of WT and R607H AE1 KI/KI Mice	46
Table 3.3	Steady State Plasma Characterization of WT and L919X AE1 KI/KI Mice	47
Table 3.4	Plasma Characterization of WT and R607H AE1 KI/KI Mice Following 24 hours of Salt-Restriction	54
Table 3.5	Plasma Characterization of WT and L919X AE1 KI/KI Mice Following 24 hours of Salt-Restriction	55
Table 3.6	Plasma Characterization of WT and R607H AE1 KI/KI Mice Following 6 Days Acid Challenge	65
Table 3.7	Plasma Characterization of WT and L919X AE1 KI/KI Mice Following 6 Days Acid Challenge	66
Table 3.8	Summary of the Major Findings Presented in this Thesis	101

LIST OF FIGURES

- Figure 1.1** A schematic highlighting the vascular and tubular components of the nephron. 3
- Figure 1.2** Illustration of the cellular composition and transporters in the kidney collecting duct. 7
- Figure 1.3** Cartoon diagram of the thick ascending limb major apical and basolateral transporters. 10
- Figure 1.4** A visual guide on transporters and influences of sodium transport along the nephron. 15
- Figure 1.5** AlphaFold structure of band 3/kidney anion exchanger 1 transport protein (kAE1). 20
- Figure 1.6** A simplified graphic illustrating the diverse protein interactions of kAE1 with key partners. 21
- Figure 1.7** Visual summary of findings on the Ae1 R607H Knock-In dRTA mutant mouse model at baseline and following acid challenge. 24
- Figure 2.1** Metabolic cage experiment protocol with specialized diets. 29
- Figure 3.1** mRNA levels of Ae1 are lower in dRTA mutant mice compared to WT mice at baseline. 41
- Figure 3.2** Urinary pH is higher while urine ammonium excretion is lower in dRTA mutant mice than WT counterparts at baseline. 42
- Figure 3.3** Comparison of urinary sodium, potassium, and chloride excretion between dRTA mutant mice and WT counterparts. 45
- Figure 3.4** Preliminary examination of NBCn1 protein abundance suggests a trend for higher NBCn1 protein abundance in dRTA mutant mice compared to WT mice. 49
- Figure 3.5** Both L919X KI/KI mice and WT mice reduce their chow and water consumption, and fecal mass after 24 hours of salt-restriction. 51
- Figure 3.6** Both R607H KI/KI mice and WT mice reduce their chow and water consumption, and fecal mass after 18 hours of salt-restriction. 52
- Figure 3.7** Urinary pH is alkaline before and after a 24-hour salt-restriction diet in dRTA mutant mice compared to WT mice. 57

- Figure 3.8** There is no significant difference in urinary sodium, potassium, and chloride excretion in R607H KI/KI mice compared to WT mice. 58
- Figure 3.9** L919X KI/KI mice excrete less urinary potassium than WT mice without differences in sodium and chloride excretion. 59
- Figure 3.10** Urine osmolality in the R607H KI/KI and L919X KI/KI mice is not significantly different compared to WT, following the 24-hour salt-restriction diet. 60
- Figure 3.11** R607H KI/KI mice reduce their urine output and trend for reduced fecal mass compared to WT mice on a 6-day acid challenge. 62
- Figure 3.12** L919X KI/KI mice reduce their urine output compared to WT mice and their fecal mass compared to baseline on a 6- day acid challenge. 63
- Figure 3.13** Urinary pH remains alkaline in dRTA mutant mice compared to WT before and after a 6-day acid challenge. 68
- Figure 3.14** L919X KI/KI mice significantly increase urinary sodium excretion on acid diet. 69
- Figure 3.15** R607H KI/KI have concentrated urine than WT littermates on the acid diet. 70
- Figure 3.16** Gene expression of IC marker *Ae1* is decreased in L919X KI/KI mice compared to WT mice. 72
- Figure 3.17** Gene expression of tight junction protein *claudin-10b* is higher in L919X KI/KI mice compared to WT mice. 73
- Figure 3.18** Both L919X KI/KI mice and WT mice drink less, produce less urine and feces over a 14-day salt-depleted acid load. 75
- Figure 3.19** R607H KI/KI mice produce less urine than WT mice after a 14-day salt-depleted acid load, although both genotypes reduce their water consumed and fecal mass produced. 76
- Figure 3.20** After the salt-depleted acid load, R607H KI/KI mice are acidotic, hypernatremic, hyperchloremic, and their kidneys have elevated renin gene expression compared to WT mice. 78
- Figure 3.21** L919X KI/KI mice are hypernatremic, hyperchloremia, have elevated BUN, reduced TCO₂ and trend for higher renal renin mRNA abundance compared to WT mice. 79
- Figure 3.22** R607H KI/KI have a higher systolic blood pressure at Day 14 compared to WT mice at Day 8. 80

- Figure 3.23** There is no significant difference in urine osmolality between the R607H KI/KI 81
or L919X KI/KI mice and WT littermates following the salt-depleted acid load.
- Figure 3.24** The dRTA mutant mice have alkaline urine and R607H KI/KI mice secrete less 83
urinary ammonium than WT littermates at Day 14 of the salt-depleted acid
challenge.
- Figure 3.25** R607H KI/KI mice excrete more urinary sodium but less urinary potassium and 84
chloride than WT mice on Day 14 of a salt-restricted acid load.
- Figure 3.26** L919X KI/KI mice excrete more urinary sodium and chloride than WT mice on 85
Day 14 of a salt-restricted acid load.
- Figure 3.27** Gene expression and protein abundance of markers of the IC, TAL, and distal 88
convoluted tubule are decreased, while ENaC (PC marker) is significantly
increased in R607H KI/KI mice versus WT littermates.
- Figure 3.28** Although gene expression and protein abundance of markers of the IC are 90
decreased, PC and TAL markers do not vary significantly in L919X KI/KI mice
versus WT littermates.
- Figure 3.29** Claudin-4 and claudin-10b are upregulated in both L919X and R607H KI/KI 93
mice after a salt-depleted acid diet.
- Figure 3.30** Paracellular markers claudin-3 and -7 expressed in the distal nephron are up- 95
regulated in L919X KI/KI mice but not in R607H KI/KI after a salt-depleted
acid diet.
- Figure 3.31** kAe1 gene expression of IC and is down regulated in R607H KI/KI mice 97
compared to WT mice at baseline.
- Figure 3.32** kAe1 gene expression is downregulated and claudin 4 is up-regulated in L919X 98
KI/KI mice compared to WT mice at baseline.
- Figure 3.33** Urine albumin abundance is higher in the R607H and L919X KI/KI mice after 100
the salt-depleted acid challenge compared to WT littermates.
- Figure 3.34** The generation and preliminary characterization of the L919X KI mice. 127
- Figure 3.35** Further preliminary characterization of the L919X KI mice via Von Kossa and 129
Masson Trichome Staining.
- Figure 3.36** R607H KI/KI and L919X KI/KI mice following the salt-depleted acid load show 131
changes in urinary creatinine excretion

LIST OF ABBREVIATIONS

A-IC	Type A intercalated cell
ADH	Antidiuretic hormone
AE4 (Ae4)	Anion exchanger 4
AnGAP	Anion gap
ANP	Atrial natriuretic peptide
AQP	Aquaporin
B-IC	Type B intercalated cell
BE _{ecf}	Base excess in the extracellular fluid
BUN	Blood urea nitrogen
BW	Body weight
CAII	Carbonic anhydrase
CaSR	Calcium sensing receptor
CD	Collecting duct
dRTA	Distal renal tubular acidosis
ENaC	Epithelial sodium channel
FOXI1	Forkhead box protein I1
GFR	Glomerular filtration rate
H ⁺ -ATPase	Vacuolar-type proton ATPase
Hb	Hemoglobin
HCT	Hematocrit
HEK	Human embryonic kidney 293 cells
IC	Intercalated cell

kAE1 (kAe1)	Kidney anion exchanger 1
KI	Knock in
MDCK	Madin-Darby canine kidney cells
MR	Mineralocorticoid receptor
NBCn1	Sodium/bicarbonate cotransporter
NCC	Sodium chloride cotransporter
NDCBE	Sodium-dependent chloride/bicarbonate exchanger
NHE	Sodium/proton exchanger
NKCC2	Sodium, potassium, chloride co-transporter
PC	Principal cell
RAAS	Renin angiotensin aldosterone system
ROMK	Inward rectifier potassium channel 1
qRT-PCR	Quantitative reverse transcription polymerase chain reaction
SDS-PAGE	Sodium dodecyl sulfate polyacrylamide gel electrophoresis
SEM	Standard error of mean
SGLT	Sodium glucose cotransporters
TAL	Thick ascending limb
TM	Transmembrane domain
WT	Wildtype

Chapter 1: Introduction

THE NEPHRON

The kidneys are bean-shaped organs located on the posterior side of the abdomen on either side of the spine ²⁵. This organ system plays a pivotal role in electrolyte regulation, acid-base balance, innate immunity ¹³, hormonal secretion, detoxification, and blood volume/pressure control ²⁵. The nephron is the functional unit of the kidney, with over one million nephrons present per kidney of a healthy adult (**Figure 1.1**). The nephron consists of a vascular and tubular component ²⁵. The vascular component contains the renal vasculature and the glomerulus. The glomerulus, housed in the Bowman's capsule, is a sophisticated blood filtration system which allows the passage of small solutes and water, but prevents passage of large protein molecules and red blood cells ²⁵. The resulting filtrate, resembling plasma but devoid of macromolecules, accumulates in the Bowman's capsule before entering the nephron's tubular component ²⁵. The tubular component executes two primary functions: reabsorption and secretion and is divided into four principal segments ²⁵. First is the proximal tubule, which initiates the reabsorption of the majority of the filtered ions, glucose, vitamins, amino acids, and water. Subsequently, the filtrate progresses to the next segment, the Loop of Henle. The descending limb of this segment reabsorbs water only while the ascending limb is a watertight epithelium, which facilitates reabsorption of various ions and salt, diluting the filtrate. Exiting the loop, the now dilute filtrate moves to the distal convoluted tubule where further secretion and reabsorption processes occur ²⁵. The final nephron segment, and the focus of this thesis project, is the collecting duct (**Figure 1.1**).

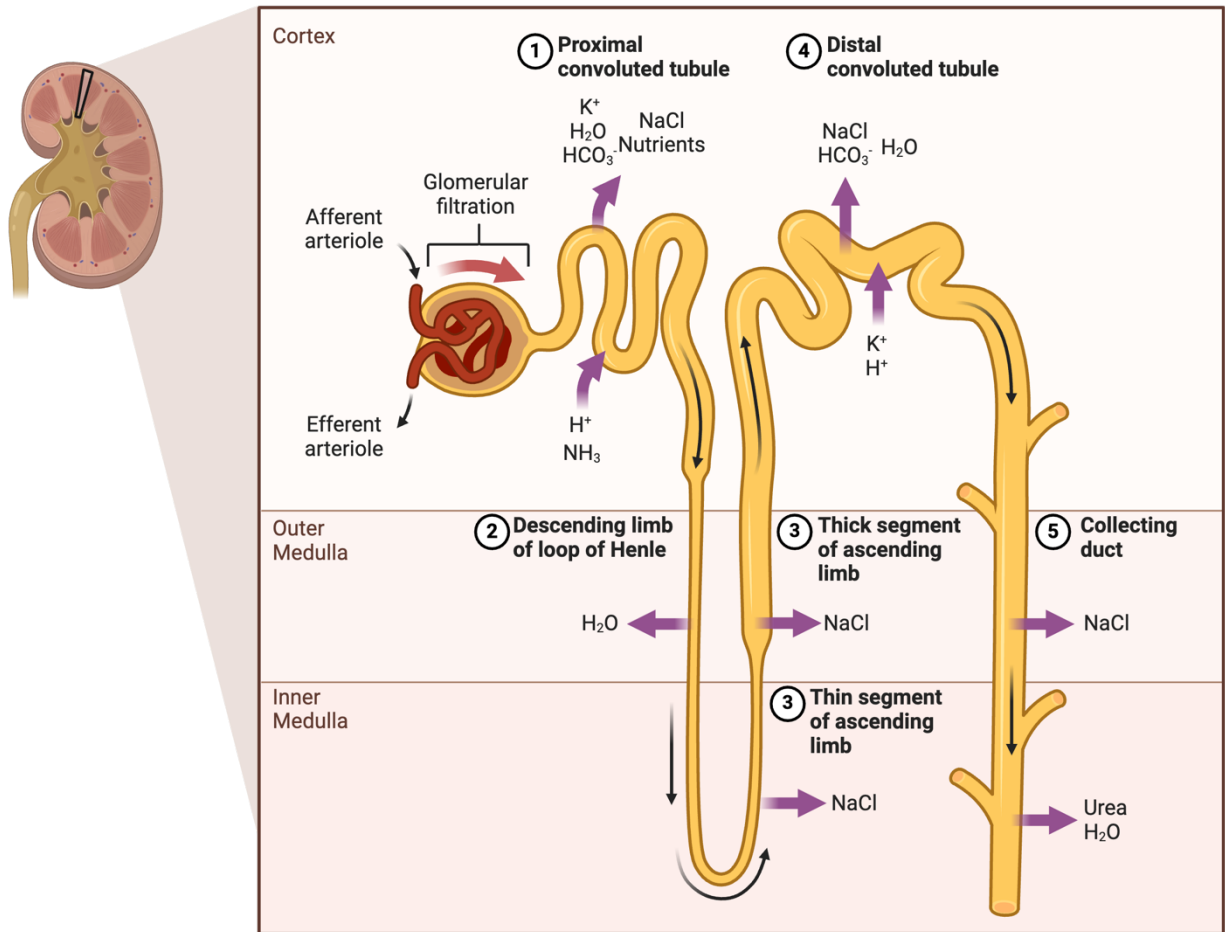


Figure 1.1 A schematic highlighting the vascular and tubular components of the nephron.

This image shows the anatomy of a nephron. It highlights the vascular components with the arterioles and the glomerulus. It also highlights the tubular component, including the proximal tubule, Loop of Henle, distal convoluted tubule, and collecting duct. The specific ions reabsorbed or secreted in each segment are also shown. *This image was obtained from and altered in BioRender.com.*

THE COLLECTING DUCT

The collecting system of the nephron consists of the late distal convoluted tubule, the connecting tubule, and the cortical and medullary (inner and outer) collecting duct (CD) ^{63,94}. Specifically, the CD is the final nephron segment, crucial for finetuning urine composition and mediating acid-base homeostasis and electrolyte and fluid status (**Figure 1.2**) ^{63,99}. This regulation involves control over the transcellular and paracellular transport of water, sodium, chloride, potassium, bicarbonate, and protons ⁸³. The CD epithelium comprises two major cell populations: principal cells (PCs) and intercalated cells (ICs), with a ratio of 2:1 in the outer medullary CD and 3:1 in the cortical CD, respectively ⁹⁴ (**Figure 1.2**). Despite the structural and functional differences between PCs and ICs, both cells differentiate from aquaporin 2 (AQP2) expressing precursor cells ^{34,94,123}.

Principal Cells

PCs are majorly involved in sodium and water reabsorption and potassium excretion to and from primary urine ^{14,42,83}. A move towards PC lineage occurs when NOTCH1/2 ligand JAG1, activates NOTCH1/2 via a mechanism involving proteases such as ADAM10 and γ -secretase, which ultimately activates transcription factors leading to the expression of PC genes and suppression of transcription factors involved in IC lineage ¹²³. PCs are characterized by expression of the apical epithelial sodium channel (ENaC), apical inward rectifier potassium channel 1 (ROMK) and AQP2 and AQP3 water channels ⁸² (**Figure 1.2**). The function of these epithelial cells is tightly regulated by aldosterone and arginine vasopressin (**Figure 1.2**), which modulate ENaC, ROMK, and AQP2 in their sodium, potassium, and water transport (described further in later section) ^{63, 83}.

Intercalated Cells

ICs are mitochondria-rich epithelial cells with basolateral membrane infoldings and cytoplasmic vesicles⁹⁴. ICs perform acid-base homeostasis, salt transport, and even innate immune roles in the distal segments of the kidney^{13,63,83}. Cell differentiation towards IC lineage occurs from forkhead box protein I1 (FOXI1) transcription factor and NOTCH signalling¹²³. The major subcategories of ICs include type A (A-ICs), type B (B-ICs), and non-A, non-B ICs⁹⁶ (**Figure 1.2**). A-ICs are acid-secreting cells, identified by an apical vacuolar proton ATPase (H⁺-ATPase) and H⁺/potassium-ATPase, and a basolateral chloride/bicarbonate exchanger called kidney anion exchanger 1 (kAE1)⁹⁶. In the kidney, acid-base balance occurs through the reabsorption and *de novo* synthesis of bicarbonate, coupled with proton secretion⁴³. Hence in the CD, carbon dioxide diffuses into the cells and is hydrated to form H₂CO₃, catalyzed by carbonic anhydrase II (CAII). From there, the dissociated bicarbonate ion is reclaimed through the basolateral membrane, via kAE1, while the protons are secreted into the urine through the H⁺-ATPase⁴³. A-ICs also contain Rhesus glycoproteins, recently recognized as ammonia transporters in the distal nephron^{20,94}. B-ICs mirror the polarity and function of A-ICs and are responsible for facilitating bicarbonate ion secretion. They are identified via an apical chloride/bicarbonate exchanger called pendrin, a basolateral H⁺-ATPase, and sodium and chloride/bicarbonate exchanger, AE4^{42,94,122,123} (**Figure 1.2**). In addition to bicarbonate secretion, B-ICs contribute to electroneutral salt reabsorption through the coupled activity of pendrin and the apical sodium-dependent chloride/bicarbonate exchanger (NDCBE)⁴². Little is known about the function of non-A, non-B ICs. They express an apical H⁺-ATPase and pendrin and therefore may play a role in electrolyte homeostasis⁹⁴.

To carry out the paracellular transport, the CD (and other nephron segments) rely on tight junctions⁴⁸, which connect the epithelium of this segment. Within the tight junctions specifically,

claudin proteins mediate ion movement and form a protective barrier ¹¹⁸. Claudins have four transmembrane domains, with one short intracellular loop and two large extracellular loops. The first extracellular loop confers ion selectivity while the second extracellular loop mediates interactions with claudins in adjacent cells ¹¹⁸. Claudin-4 is prominently expressed in the CD ⁶² (**Figure 1.2**). Claudin-4 exhibits specificity towards anions, functioning as a selective pore for chloride while blocking the permeability to sodium ^{39,62}.

The CD system has a high degree of plasticity. It can adapt to changes in systemic electrolyte and acid–base status ⁸. For example, chronic alkalosis increases B-ICs. Opposingly, chronic acidosis increases the relative number of A-ICs, possibly at the expense of B-ICs ⁷², decreasing pendrin and AE4 expression or plasma membrane abundance in these cells ^{35,122}. Recent studies have also found evidence of crosstalk between PCs and ICs. For example, knock out of the B1 subunit of the H⁺-ATPase (present on ICs), resulted in impaired sodium and chloride conservation through altered ENaC activity and reduced levels of pendrin ⁴². In this same model, prostaglandin E2 and ATP released from B-IC cells exerted altering paracrine effects on PCs ⁴². Therefore, the CD system is marked by responsiveness to the dynamic tubular environment.

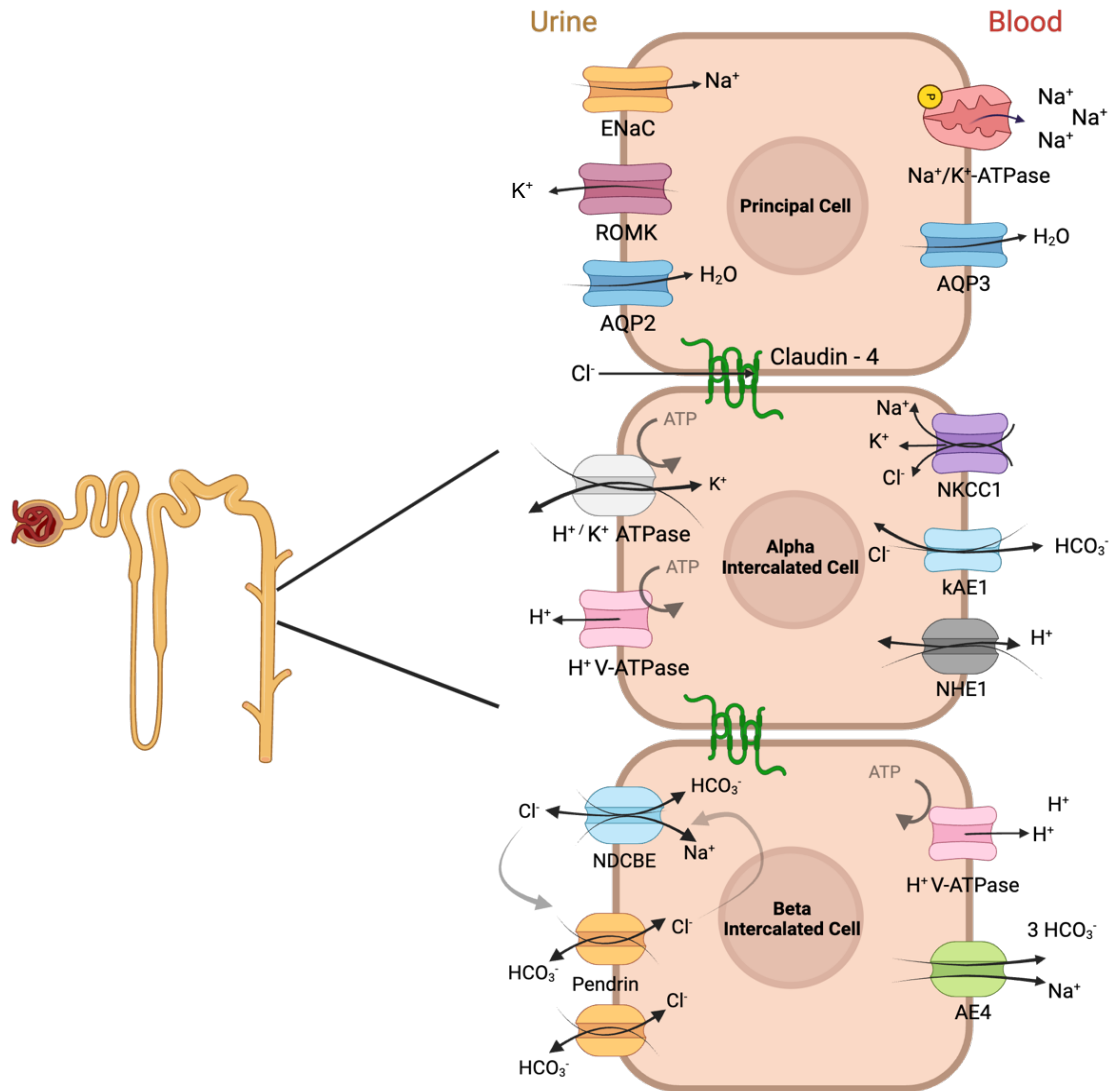


Figure 1.2 Illustration of the cellular composition and transporters in the kidney collecting duct. The collecting duct in the final nephron segment. Principal and intercalated cells (Type A, Type B, and Non-A Non-B which are not illustrated here) comprise this segment. Principal cells express ENaC, ROMK, and AQP proteins. Alpha-intercalated cells (A-ICs) feature H⁺-ATPase and kAE1, while beta-intercalated (B-ICs) cells express pendrin, NDCBE, and AE4. Tight junction proteins connect collecting duct cells, with claudin-4, a chloride pore, being a major component of the tight junction. *This figure was created in Biorender.com.*

THE THICK ASCENDING LIMB

Another nephron segment relevant to this research project is the Loop of Henle. Preceding the CD system, it consists of a thin descending limb, thin ascending limb, and a thick ascending limb (TAL). The TAL is another crucial site of electrolyte, fluid, and acid-base balance where it actively reabsorbs salt to dilute the luminal fluid and drive the countercurrent multiplication ¹³² (**Figure 1.3**). The TAL apical membrane contains three major proteins: the sodium, potassium, chloride co-transporter (NKCC2), ROMK, and sodium/proton exchanger 3 (NHE3) ⁴⁰. Ammonium can also be transported by NKCC2 as it has the same ionic radius as potassium, and this capacity increases during acidosis ⁷⁹. ROMK channels facilitate potassium recycling into the lumen, which aids salt transportation via NKCC2 and creates a net positive luminal voltage (5 - 10 mV) to promote paracellular cation transport ⁴⁰. NHE3 reabsorbs sodium in exchange for protons, contributing to the medullary interstitial gradient. It is especially responsible for sustained urine acidification during administration of furosemide (NKCC2 inhibitor) ^{23,129}. Here, the increased driving force of sodium reabsorption by NHE3 subsequently increases tubular fluid acidification ¹²⁹. The basolateral membrane of the TAL features invaginations nearly reaching the lumen membrane, amplifying its surface area ⁸⁹. Notably, the basolateral membrane contains the sodium/potassium ATPase, NHE1 ⁶⁰, NHE4 ⁷², calcium-sensing receptor, CaSR ³³, and the chloride channel *Ka/b* ⁹⁰. The apical extrusion of protons via NHE3 coincides with the basolateral efflux of bicarbonate via another basolateral protein called the sodium/bicarbonate cotransporter (NBCn1) ^{40,59,79}. NBCn1 is responsible for buffering plasma pH and facilitating ammonium excretion by the CD ⁷⁹ (**Figure 1.3**).

Like the CD, the cells of the TAL are also connected by tight junctions that express major claudin species including claudin-3, 10b, -14, -16, and -19 ⁷⁸. The TAL is a major site of

paracellular sodium, magnesium, and calcium transport through these claudins ⁷⁸. Claudin-10b is a protein of interest in this thesis. It is enriched in the inner stripe of the outer medulla and the TAL, so consequently, this region exhibits a higher permeability to sodium (PNa^+) to PCl^- ratio ^{40, 89}. It is expressed in the tight junctions and the basolateral infoldings of the cortical TAL, shown to stabilize the membrane and contribute to high flux salt reabsorption ⁸⁹ (**Figure 1.3**).

The TAL's activity, akin to the CD, is regulated by local milieu and hormones ^{72,76,132}, for example vasopressin ^{37,72} and uromodulin ⁷⁶, which increase TAL salt transport activity or prostaglandin E2 ^{114,76}, which has an inhibitory influence on ion movement in the TAL.

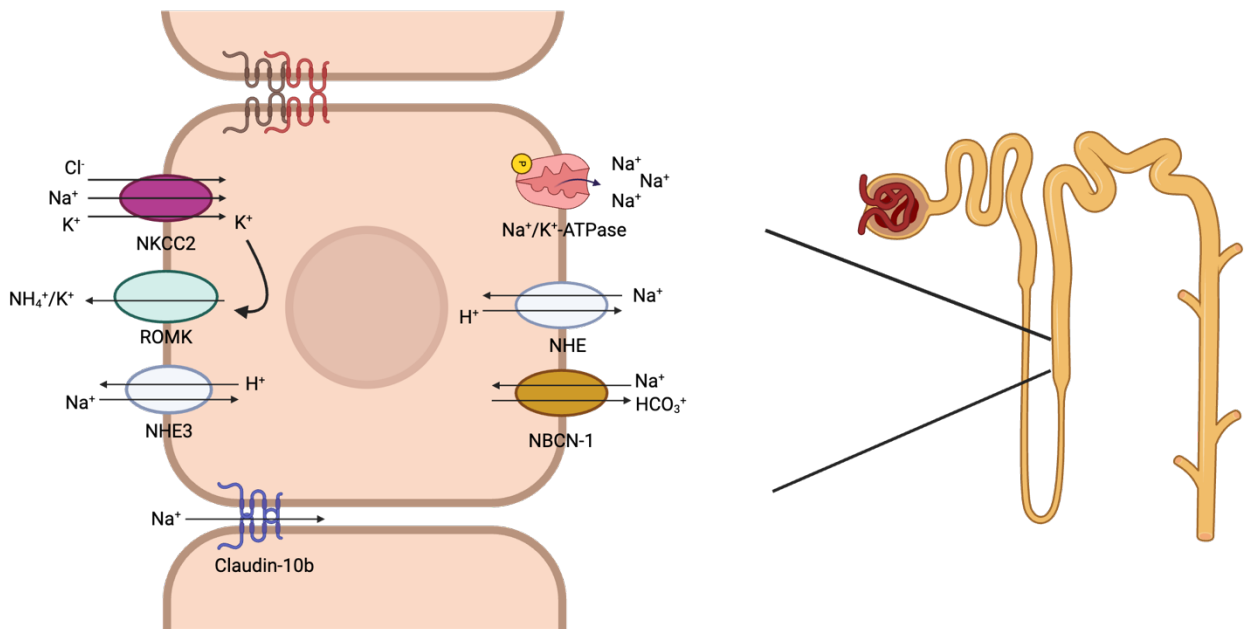


Figure 1.3 Cartoon diagram of the thick ascending limb major apical and basolateral transporters. NKCC2, ROMK, and NHE3 on the apical membrane facilitate salt reabsorption and acid secretion. Sodium will exit the basolateral membrane primarily through the sodium/potassium ATPase and NHE proteins. Bicarbonate and proton movement occurs through NBCN1 and NHE transporters also present on the basolateral side. The thick ascending limb cells are also connected by tight junction proteins, including claudins. Claudin-10b, a sodium pore, is in the tight function but also potentially TAL basolateral membrane. *This figure was created in Biorender.com.*

SODIUM TRANSPORT THROUGH THE NEPHRON

As the primary extracellular cation, sodium homeostasis is essential for survival. The kidney plays a central role in achieving a balance between dietary intake and excretion of sodium and water, as seen through the functions of the TAL and CD. This ensures that the extracellular fluid volume and cardiovascular homeostasis are maintained at appropriate levels¹²⁰. Control of sodium transport along the nephron is accomplished by feedback mechanisms^{25,80}, a unique set of sodium transport mechanisms on each segment, and through hormonal regulation (**Figure 1.4**)

Transporters in the Tubules

- Proximal Tubule

The proximal tubule reabsorbs approximately 60 - 70 % of filtered sodium, predominantly (~ 90 %) through the transcellular pathway¹⁸. Active transport, electrodiffusion, and solvent drag each contributes to total sodium reabsorption here³⁰. Sodium transport is mainly facilitated by the apical sodium-hydrogen exchanger (NHE3). It also involves the coupling of sodium with bicarbonate or neutral organic solutes such as glucose or amino acids via co-transporters^{120,130}, so proteins such as sodium-glucose transport proteins (SGLT1/2) also facilitate sodium movement¹²⁰. In the late proximal tubule, a lumen-positive voltage is present, resulting in a driving force suitable for paracellular sodium movement through claudin-2^{4,130}. The actions in this segment are driven by the electrochemical potential generated by the basolateral sodium/potassium ATPase¹⁸ and the electrogenic sodium-bicarbonate cotransporter (NBCe1-A). (**Figure 1.4**).

- Thick Ascending Limb and Macula Densa Cells

The TAL is responsible for 25 - 30 % of total sodium reabsorption; 50 - 70 % of this being transcellular and 30 - 50 % being paracellular^{40, 72, 80}. NHE3 and NKCC2 are the predominant

mechanisms of sodium transport here ¹⁰⁴, again facilitated by the electrochemical potential generated by the basolateral sodium/potassium ATPase. Like the proximal tubule, lumen positive transepithelial voltage promotes paracellular sodium movement ⁵⁰. This voltage is generated through paracellular calcium and magnesium reabsorption via claudin-16 and claudin-19 ^{130, 131}, and the recycling of potassium back to the lumen via ROMK ¹²⁰. Net chloride absorption from the lumen coupled to depolarization of basolateral membrane from chloride efflux also creates a positive voltage which drives sodium movement ⁴⁷. This paracellular movement occurs through claudin-10b, enriched in the inner stripe of the outer kidney medulla of the TAL ⁸⁹ (**Figure 1.4**). The macula densa consists of specialized cells located in the transition between the TAL and the distal convoluted tubule, near the afferent and efferent arterioles. They can detect tubular lumen salt concentration and accordingly regulate vascular tone ¹³⁰. Microelectrode and patch clamp experiments revealed that macula densa cells possess NKCC2, NHE2, and a sodium/potassium ATPase protein, and therefore share sodium transport properties with the TAL ^{61, 80}.

- Distal Nephron

The distal convoluted tubule accounts for the remaining 7 - 10 % of sodium reabsorption through the activity of the apical sodium chloride cotransporter (NCC) and basolateral NHE2 protein ¹²⁰. The later portions of the distal convoluted tubule contain an apical ENaC, which can mediate electrogenic sodium reabsorption as well ⁶⁸. Finally, the CD fine-tunes the urine concentration and therefore is responsible for reclaiming the last 2 - 5 % of sodium within the filtrate ^{26,120}. This action occurs primarily through electrogenic sodium reabsorption via ENaC located on PCs. B-ICs also contribute to salt homeostasis, through the coupled action of pendrin and NDCBE. Here, apical chloride efflux through pendrin is linked to the sodium influx via NDCBE in a fashion that is ENaC-independent and electroneutral ⁶⁵. These processes, especially

ENaC activity, are possible through the sodium/potassium ATPase generated gradients ²⁶ (**Figure 1.4**).

Hormonal Regulation

Varying body sodium content is often sensed by hormonal effector systems. One such axis is the renin-angiotensin-aldosterone system (RAAS), activated during decreased extracellular fluid volume or sodium delivery to the distal tubules ²⁹. Renin, secreted by the juxtaglomerular cells, converts angiotensinogen to angiotensin I, which is then converted into angiotensin II by the angiotensin-converting enzyme ^{25,29}. Angiotensin II is a potent vasoconstrictor and can have independent effects on sodium and water homeostasis. For example, angiotensin II augments sodium/proton exchange in the proximal tubule through increasing NHE3 insertion to the apical membrane ²⁴. It can also stimulate increased ENaC activity in the late distal convoluted tubule ¹²⁷ and chloride channel activity in ICs ⁵⁴. Indirectly, angiotensin II stimulates antidiuretic hormone (ADH/vasopressin) release from the pituitary gland. This hormone regulates water reabsorption and urine osmolality but can also enhance sodium reabsorption in the TAL by increasing NKCC2 abundance and phosphorylation ³⁷. ADH directly increases ENaC activity and insertion at the membrane as well ¹⁰⁸. Importantly, angiotensin II stimulates aldosterone secretion from the adrenal glands ^{25,29}. Aldosterone can increase NCC apical abundance and activity via phosphorylation ^{93, 112}. Aldosterone mainly acts on CD cells to increase ENaC and the sodium/potassium ATPase expression and activity ⁹⁵. Clearly, hormones play a pivotal role in regulating transport through the tubules to maintain sodium and water balance within the body (**Figure 1.4**).

Notably, sodium reabsorption is not only driven by the electrochemical gradients or concentrations in the filtrate, but is also influenced by the tubular glomerular feedback and the sympathetic nervous system ¹²⁰. Interestingly rodent studies reveal that dietary sodium changes predominantly impact distal nephron sodium reabsorption, while the proportion of sodium reabsorption in the proximal tubule remains stable ²⁷. But disturbances to proper sodium reabsorption and excretion, or an imbalance of other electrolytes like potassium or calcium, can lead to significant pathology and disease. One such pathology is renal tubular acidosis. This is a group of disorders in which dysregulation of acid-base and electrolyte homeostasis occurs due to improper bicarbonate reabsorption or non-volatile acid excretion by the nephron ³. Of interest to this thesis project is an affliction to the distal nephron, causing a disease called distal renal tubular acidosis.

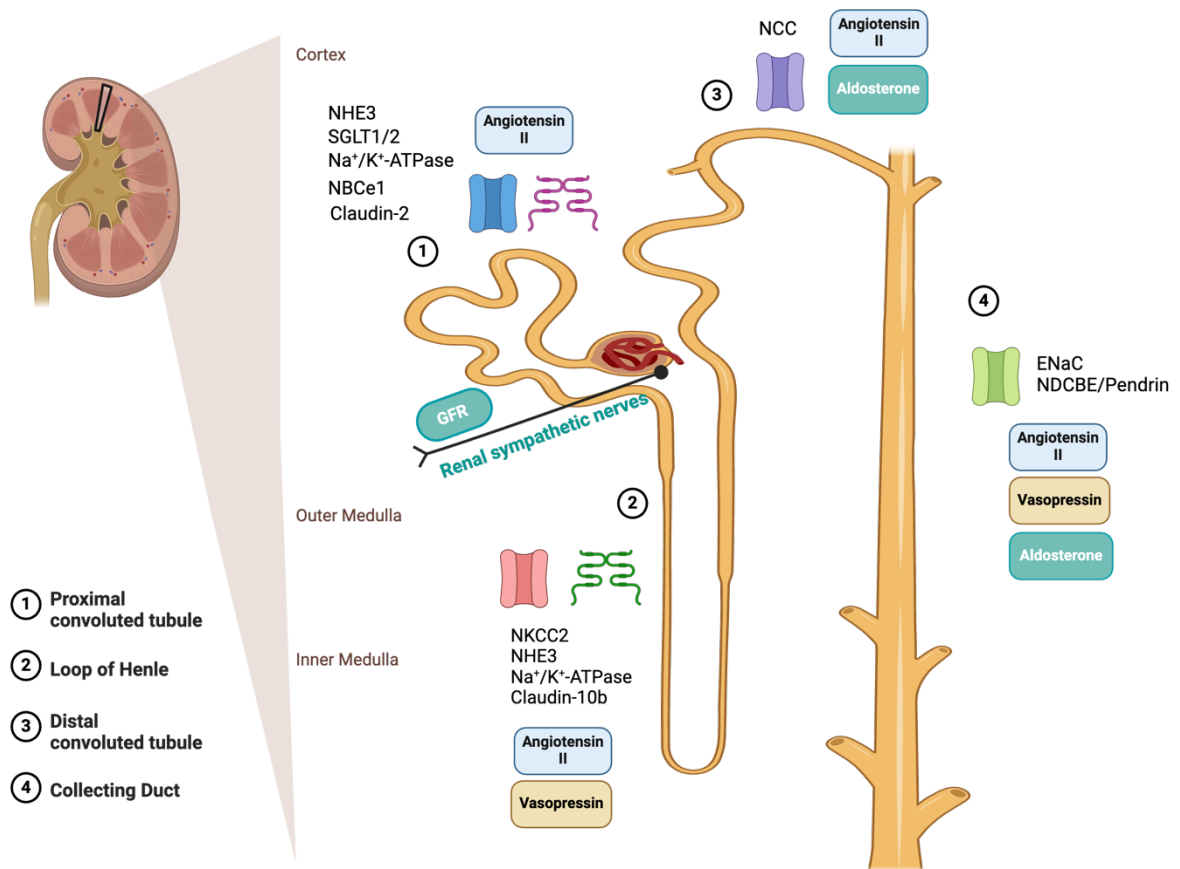


Figure 1.4 A visual guide on transporters and influences of sodium transport along the nephron. In the proximal tubule, sodium is transported through NHE3, sodium/glucose cotransporter SGLT1/2, claudin-2, driven by electrochemical gradients established by the basolateral sodium/potassium ATPase and NBCe1. In the thick ascending limb, driven by similar electrochemical gradients, transport is facilitated through NKCC2, NHE3 and claudin-10b. In the distal nephron, NCC, ENaC and the NDCBE/pendrin pair reabsorb the remaining sodium, finetuning urine composition. Hormones including angiotensin II, ADH, and aldosterone also impact sodium transport by acting on the various nephron segments (and systemically as well).

This figure was created in Biorender.com.

DISTAL RENAL TUBULAR ACIDOSIS

A dysfunction in A-ICs can lead to a rare disease called distal renal tubular acidosis (dRTA). dRTA, also referred to as Type 1 renal tubular acidosis, is characterized by improper urine acidification and metabolic acidosis ³⁶. This malfunction may be caused by inherited mutations that impact A-IC function, for example mutations to *SLC4A1* (kAE1), *ATP6V1B1*, *ATP6V0A4*, *ATP6V1C2* (H⁺-ATPase), *FOXI1* (Forkhead Box I1), and *WDR72* (a vesicle trafficking protein) ¹²³. dRTA may also be acquired consequent to tubular injury or obstruction, or secondary to other pathological conditions like autoimmune diseases or exposure to nephrotoxic medications or certain antibiotics ^{1,11,75,123}. Clinically, dRTA is delineated by metabolic acidosis, hypokalemia, hyperchloremia, nephrocalcinosis, impaired urine acidification (urine pH exceeding 5.3), and in some instances, glomerular dysfunction ¹¹. Depending on the specific mutation, extrarenal manifestations may encompass sensorineural hearing loss or deafness, hematological anomalies, male infertility due to epididymal impairment, diminished olfactory function, and compromised bone density and trabecular volume ¹²³. Management of inherited dRTA primarily involves administration of alkali salts containing bicarbonate or citrate. Additionally, interventions such as dietary modifications to reduce sodium intake and acid-releasing animal proteins can be beneficial ³⁶. While classical dRTA is diagnosed by conventional criteria, autosomal dominant dRTA mutations (in *SLC4A1*) can cause incomplete dRTA. In incomplete dRTA, acid-base imbalance is not observed at physiological state, although these patients often have kidney stone disease ^{31,36}. Only an ammonium chloride challenge or a furosemide test can uncover improper urine acidification challenges ^{1,31,123}.

The Sodium Wasting Phenotype Persistent Despite Correction of Acidosis

In 1976, a study reported for the first time a urinary salt-wasting phenotype in human dRTA patients, specifically abnormal renal sodium, and potassium handling ¹⁰⁰. In this study, some patients with classic RTA had impaired renal conservation of sodium when dietary intake of sodium was restricted during sustained acidosis correction. A few patients studied were excreting urinary sodium to levels that exceeded dietary intake by about 5 -27 mEq / day throughout at 8 – 10-day sodium restriction, while some patients showed clear chloride conservation impairment as well ¹⁰⁰. This clinical observation was the first to provide direct evidence of a tubular defect resulting in sodium wasting, independent from acid/base balance ¹⁰⁰. When this phenotype was studied using a B1 subunit of H⁺-ATPase (B1-H⁺-ATPase) knock-out mouse model, it was revealed that these mice displayed reduced pendrin expression and activity, which caused renal sodium loss. This disruption, also reduced ENaC function on PCs, further exacerbating sodium loss ⁴², providing one mechanism to explain this phenotype. However, there has been no clear evidence or mechanism defined in dRTA mutations on the *SLC4A1* gene encoding kAE1 protein.

(KIDNEY) ANION EXCHANGER 1 PROTEIN

Protein Structure and Function

Anion exchanger AE1, also known as Band 3, contains 911 amino acids arranged in 14 large transmembrane (TM) domains, a long cytoplasmic N-terminal domain, and a short cytoplasmic C-terminal domain ⁷⁴. The kidney isoform (kAE1) is truncated by amino acids 1-65 ⁸¹. This loss of residues impacts N-terminal binding to various proteins, for example ankyrins, and creates a loss of the central beta strands, helping to stabilize and open the kAE1 isoform more compared to the erythrocyte isoform ⁸¹. The TMD of AE1 performs the exchange of chloride and bicarbonate ions across the cell membrane and plays a crucial role in maintaining the structural integrity of the protein ⁶. It is divided into a core domain (TM 1-4, 8-11) and a gate domain (TM

5-7 and 12-14) (**Figure 1.5**). kAE1 protein functions as a dimer, and the two gate domains form the dimerization binding region. The TMD of each dimer is composed of 14 TM segments with a 7+7 inverted repeat fold ^{6, 133}. AE1 switches conformation during transport, alternating between an inward-facing (IF) and outward-facing conformation (OF), in an elevator like transport mechanism. TM 11 plays a major role in the switching mechanism. In the IF state, TM 11 is elongated and incorporates residues from the intracellular loop 5 (IL5), featuring a partially unfolded TM10. IL5 forms an antiparallel β -hairpin conformation in the OF state. An elevator-like transport mechanism uses the vertical movement of TM 10 and 11 to change the IL5 into a α -helix conformation and incorporate it into TM11. This movement combined with the β -hairpin-to- α -helix transition of IL5 creates a cavity in the intracellular side that exposes residues that are part of the binding pocket of AE1 ¹³³. Although the transporter is mainly in the OF state in crystals, binding of the substrate to the coordination sites causes the reorganization of the TM10-IL5-TM11 complex, leading to the exchanger to change into the IF state. This motion allows the vertical motion of the ions across the cell wall ¹³³. Specifically, TM 3 and 10 create a positive helix dipole at the N-terminal strand, creating an anion-binding site ¹³³.

Post-Translation Modifications and Protein Interactions

The post-translational modifications of kAE1 include phosphorylation, glycosylation, and ubiquitination ⁷⁴. Phosphorylation of the N-terminal Y359 and C-terminal Y904 affect kAE1 trafficking, with Y359 specifically being critical for basolateral targeting (**Figure 1.5**). Various cellular conditions such as high bicarbonate levels, hypertonicity, and hyperosmolarity regulate phosphorylation responses, in line with eAE1 phosphorylation patterns *in vitro* ^{45, 70, 71}. Both kAE1 and eAE1 feature a single glycosylation acceptor site at Asn-642 (N642) in the fourth extracellular loop ⁹¹ (**Figure 1.5**). Glycosylation at N642 influences chaperone interactions and trafficking;

mutants with altered glycosylation patterns exhibit ER retention. During kAE1 biosynthesis, the core oligosaccharide is transferred to N642 in the ER lumen and is further modified to a complex oligosaccharide as kAE1 traffics through the Golgi. The ratio of core/complex glycosylation can provide hints about trafficking defects. Elevated high mannose oligosaccharides and prevalent ER retention indicate mutant kAE1^{56,87,88}. Finally, ubiquitination targets kAE1, WT and mutants, for degradation⁸² (**Figure 1.5**). An Ae1 R607H knock-in (KI) mouse model revealed an accumulation of ubiquitin-positive structures in A-ICs which suggests a defect in the degradative pathway and/or in autophagy in these mice⁷³ (mouse model detailed further down). Therefore, there is a critical role of ubiquitination in marking kAE1 for proteasomal degradation.

kAE1 had various protein-protein interactions (**Figure 1.6**). These proteins include nephrin, found in glomerular podocytes, which binds to kAE1 impacting glomerular structural integrity¹²⁶. Integrin-linked kinase, which enhances kAE1 transport activity and stability⁵³. PDZ and LIM Domain Protein 5, which aids in kAE1 membrane targeting¹¹⁰. Glyceraldehyde-3-Phosphate Dehydrogenase, which aids in kAE1 stabilization at the basolateral membrane²⁸. Claudin-4, which interacts with kAE1 to influence epithelial permeability⁶². Peroxiredoxin 6, which protects kAE1 during metabolic acidification²⁸. The sodium/potassium ATPase, which helps to maintain kAE1 residency at the plasma membrane and impacts sodium and potassium balance¹¹¹. TMEM 139, a potential chaperone for kAE1, is involved in its transport⁷⁷. Adaptor protein, which potentially helps with kAE1 trafficking to the plasma membrane. And finally, CAII, which forms a bicarbonate transport metabolon. This specific interaction although not studied in kidney cells, likely interacts with kAE1 like in erythrocyte AE1¹⁰⁷. Brought together, the various and complex interactions of kAE1 highlight the intricate mechanisms governing its function and localization in kidney cells. These interactions are summarised in **Figure 1.6**.

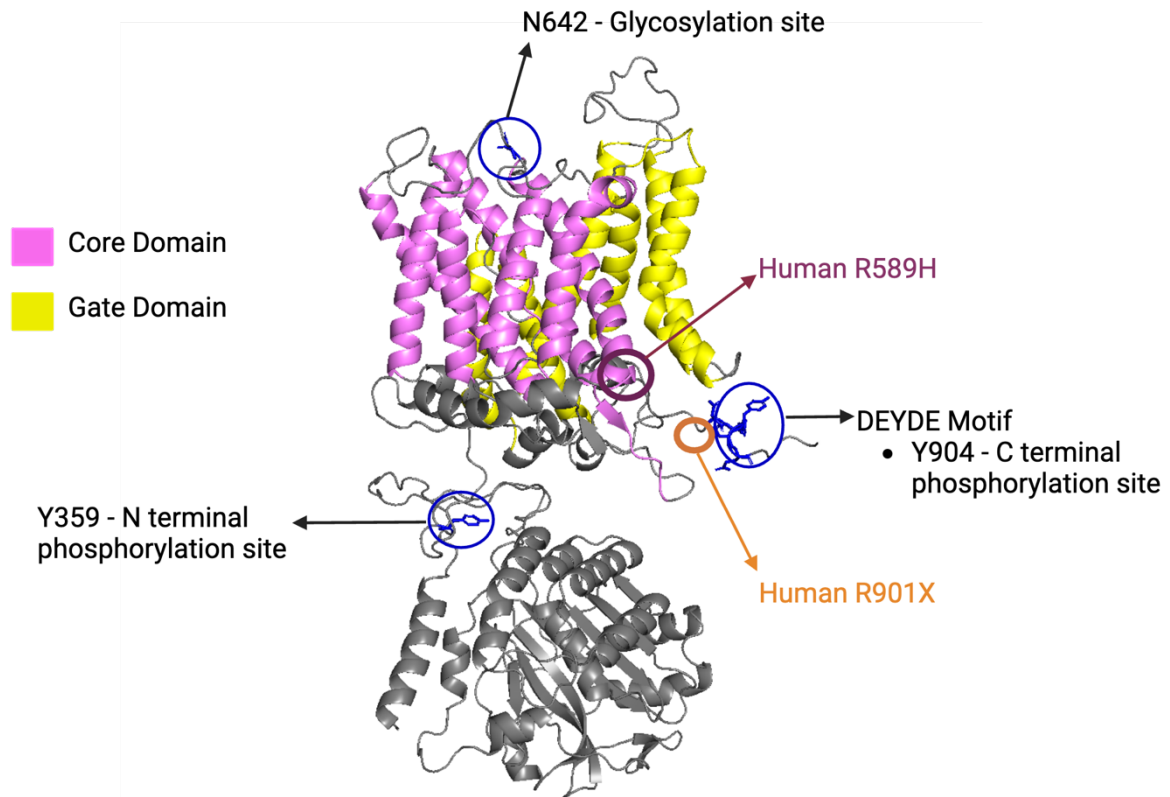


Figure 1.5 AlphaFold structure of band 3/kidney anion exchanger 1 transport protein (**kAE1**). The core (TM 1-4, 8-11) and gate (TM 5-7, 12-14) domains of the transmembrane segments are highlighted. Three key residue sites are emphasized, the N-terminal phosphorylation site Y395, the C-terminal DEYDE motif that contains the Y904 phosphorylation site, and the N642 glycosylation site. Location of the R589H and R901X human AE1 mutations are also located. *The protein structure was downloaded from AlphaFold, and it was coloured using PyMOL. This figure (with labels) was created with BioRender.com. A version of this figure is published the review article: <http://dx.doi.org/10.1139/cjpp-2023-0482>. It has been altered from what is published.*

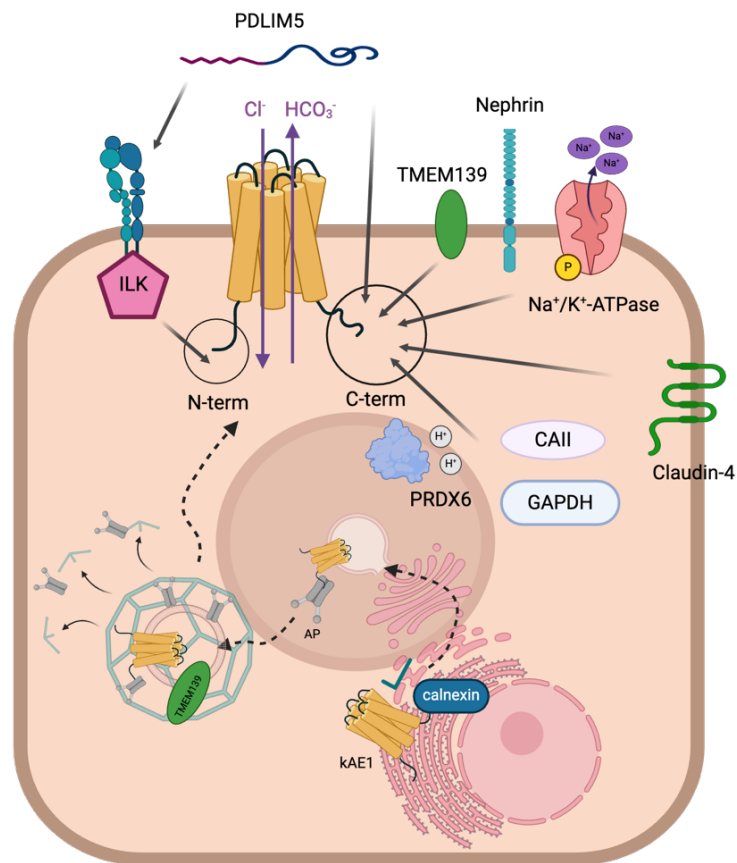


Figure 1.6 A simplified graphic illustrating the diverse protein interactions of kAE1 with key partners, including nephrin, PDLIM5, ILK (Integrin-linked kinase), carbonic anhydrase 2 (CAII), GAPDH, claudin-4, calnexin, peroxiredoxins 6, sodium/potassium ATPase, TMEM139, and adaptor proteins. These interactions encompass various molecular mechanisms such as direct physical binding, chaperone functions, and membrane stabilization, resulting in proper kAE1 function and localization to the cell membrane. The kAE1 domain interacting with claudin-4 is currently unknown and has arbitrarily been represented with the carboxyl-terminus. *This figure was made with BioRender.com and was created for the now published review article: <http://dx.doi.org/10.1139/cjpp-2023-0482>.*

kAE1 Mutations That Cause Distal Renal Tubular Acidosis

- In Humans

Several mutations to kAE1 that are linked to dRTA¹⁵. The most common autosomal dominant dRTA mutation, and one relevant to this thesis project, is the AE1 R589H. This mutation is located on the cytosolic side between transmembrane domains 6 and 7 in the gate domain of kAE1^{6,91,133} (**Figure 1.5**). *In vitro* studies using *Xenopus* oocytes, human embryonic kidney (HEK) 293 cells, and Madin-Darby canine kidney (MDCK) cells have revealed endoplasmic reticulum retention^{16,51} and apical mistargeting^{115,116} of the mutant protein, and a 20-50 % reduction in its anion exchange activity compared to wild-type (WT) kAE1⁵². However, the mutant protein can hetero-oligomerize with WT kAE1⁹¹ thereby resulting in a slightly reduced chloride/bicarbonate exchange at the cell surface. Another common autosomal dominant mutation, also relevant to this thesis, is the AE1 R901X, which causes a cytosolic C-terminal tail truncation and premature stop (**Figure 1.5**). In *Xenopus* oocytes, HEK 293 or MDCK cells, the R901X mutant has normal transport activity, but is retained intracellularly and is also apically mistargeted^{17,87,116}, similarly to the R589H mutant. Together, these *in vitro* results suggest that the R589H and R901X mutations alter kAE1 trafficking and reduce its function.

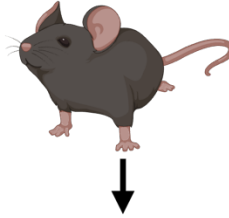
- In Mice

The first notable *in vivo* model is the Ae1 deficient (*Slc4a1*^{-/-}) mouse model. Ae1^{-/-} mice, lacking total Ae1 protein, exhibit severe hematologic defects, reduced survival rates, growth retardation, and severe anemia compared to WT and heterozygous mice¹⁰⁶. These mice display metabolic acidosis, alkaline urine, electrolyte imbalances, and an inability to concentrate urine¹⁰⁶. Functional assessment revealed significantly reduced chloride/bicarbonate exchanger activity in their kidney cells, indicating decreased Ae1 function¹⁰⁶. A second *in vivo model*, and one highly

relevant to this master's project, is the R607H knock-in (KI) mice, which at this date is the only one with a mutation on the *SLC4A1* gene that recapitulates human dRTA symptoms⁷³. These mutant mice exhibit incomplete dRTA without major red blood cell or kidney structural abnormalities at steady state⁷³. Mumtaz et al. found that upon an acid challenge, R607H KI/KI mice had alkaline urine, decreased blood pH and bicarbonate, and increased blood chloride. At steady state, only NBCn1 (TAL protein) was significantly upregulated in homozygous mice, potentially contributing to their milder baseline dRTA phenotype compared to humans. Ae1 in the KI mice was correctly targeted to the basolateral membrane, but its abundance was significantly reduced in the cortex and medulla, seen through decreased Ae1 staining intensity and Ae1 mRNA and protein expression. Ae1 also had normal intrinsic anion transport activity, confirming that the mutant protein functions similarly to WT kAe1. Conversely, apical sorting of the B1- subunit of H⁺-ATPase was severely compromised in the A-ICs. Interestingly, the number of A-ICs was dramatically reduced, with no change to the number of B-ICs and PCs, an effect more pronounced after acid challenge. The remaining A-ICs were enlarged and contained the presence of atypical lysosome-like vesicles, some colocalized with ubiquitin, suggesting signs of dysregulated autophagy⁷³. This latter point, and the decreased abundance of A-ICs, has also been confirmed in human kidney biopsy samples^{22,121}. Brought together, these mice provide insights into dRTA pathogenesis, highlighting alterations in A-IC numbers and the potential involvement of autophagy dysregulation. A summary of the important findings on the R607H KI model can be found in **Figure 1.7**.

The findings from *in vitro* and *in vivo* studies underscore the complexity of dRTA and the need to integrate information from various models to better elucidate the molecular and cellular mechanisms leading dRTA.

**Ae1 R607H KI
mice model**



Baseline

- No major impacts to red blood cells or kidney structure
- Alkaline urine
- Decreased abundance of A - ICs
- Remaining A - ICs were enlarged with increased autophagic structures
- Proper targeting and function of kAE1
- Compromised targeting of B1 subunit H⁺-ATPase
- Increased protein abundance of NBCn1 in TAL

Acid Challenge

- In addition to baseline traits that were exacerbated...
 - Low plasma pH and bicarbonate
 - Alkaline urine
 - High blood chloride

Figure 1.7 Visual summary of findings on the Ae1 R607H Knock-In dRTA mutant mouse model at baseline and following acid challenge. Ae1 R607H KI mice notably displayed alkaline urine, increased NBCn1, and proper targeting and function of Ae1 at baseline. As they display incomplete dRTA, administration of the acid challenge induces metabolic acidosis and high blood chloride. These mice also exhibited a decreased abundance of A-ICs, relative to other CD cells, a phenotype enhanced during an acid challenge. The results summarised here are from the research article by Mumtaz et al⁷³. *This figure was created in BioRender.com.*

HYPOTHESIS AND RATIONALE

As mentioned above, a critical symptom of dRTA is urinary sodium wasting. This phenotype can continue to persist despite sustained correction of acidosis. The mechanisms that lead to this impairment need further investigation, not only to improve treatments for patients with dRTA, but also because it may unveil novel sodium transport pathways that could be actionable in other diseases of acid-base imbalance or sodium homeostasis. Our lab has two dRTA kAe1 KI mouse models, L919X and R607H, that recapitulate classical metabolic acidosis seen in human patients. The R607H KI model is previously published ⁷³, and as described above, evidence from these mice suggests they have a decreased abundance of A-ICs. Therefore, **we hypothesize that these two dRTA mutant mice serve as an effective model for studying the mechanisms behind the persistent urinary ion loss, as observed in human patients.** The three objectives of our work were to 1) comprehensively characterize the previously unpublished mouse line carrying the Ae1 KI L919X mutation, 2) determine whether the two mouse models accurately reflect the urinary ion loss seen in dRTA patients, and 3) elucidate the mechanism behind this urinary sodium loss.

Chapter 2: Materials and Methods

ANIMALS AND ETHICS APPROVAL

All animal protocols were approved by the University of Alberta's Animal Care and Use Committee (AUP #1277) and were in accordance with the National and Institutional animal care guidelines. All mice were maintained on a 12-h light/dark cycle with drinking water and standard rodent chow (PicoLab® Mouse Diet 20 # 5058) available *ad libitum*. Ae1 R607H KI mice (129/SvJ strain) and wild-type (WT) counterparts were generated and described previously⁷³. To generate the L919X KI mice (129/SvJ strain) a 9.1 kb fragment including exons 14-20 of the Ae1 gene was introduced into a pKO-V901 construct containing a phosphoglycerate kinase (Pgk) promoter-driven diphtheria toxin A cassette. A neomycin resistance cassette flanked by 2 loxP sites and preceded by an *EcoRV* site was introduced to replace a *BspHI* site between exons 19 and 20. Site-directed mutagenesis was used to generate the L919X mutation before electroporation of the linearized construct into R1 mouse embryonic stem cells. Clones resistant to Neomycin were submitted to Southern blot using *EcoRV* and an external probe, generating a single 9.1 kb fragment in WT clones or a 6.1 kb fragment in mutated clones. After injection of correctly targeted ES clones into C57BL/6 blastocysts, chimeric mice were bred with a Cre-Deleter mouse strain to eliminate the selection cassette. Heterozygous KI mice in a mixed 129Sv/C57BL/6 background from at least F5 generation were bred to produce the WT and homozygous KI mice (KI/KI). Heterozygous KI mice were bred to produce the WT and homozygous KI mice of each mutant strain. Mice were genotyped by PCR of ear notch biopsies using the following primers for the R607H mice: 5'-TAG CTC CTT CTA CCC CAC CCA-3' and 5'-CCA GAG GTA CAT GGT AAA ACA TTG TC-3', as previously published⁷³ and the following primers for the L919X mice: 5'-GCT TCC GTC TTG GTC TGC TGT G-3' and 5'-TGG ACA AGC CCT GCT GTC CCT A-3', detecting a 301 bp band for WT allele and a 444 bp for the knock-in allele.

METABOLIC CAGE STUDIES WITH SPECIALIZED DIETS

During experimentation, R607H KI/KI or L919X KI/KI and WT littermates, aged 2 - 4 months, with equal distribution of male and female, were placed in metabolic cages (Tecniplast, Buguggiate, Italy) for 72 hours to acclimate. Standard rodent chow and water (PicoLab® Mouse Diet 20 # 5058) were available *ad libitum*. Body weight, urine, and feces weight were collected every 24 hours. Following these 72 hours, mice were fed one of the 3 diets (**Figure 2.1**).

- “Salt-Depletion”: R607H, L919X KI/KI mice and WT littermates were fed a salt-depleted diet (0.01 - 0.02 % sodium, 0.07 % chloride, Teklad Custom Diet #TD.08290, Inotiv, USA) and given water *ad libitum* for 24 hours.
- “Acid Load”: R607H, L919X KI/KI mice, and WT littermates were given 0.28 M NH₄Cl with 0.5 % sucrose in their drinking water, available *ad libitum* for 6 days (fresh water of pH ~ 5.19 was prepared each day).⁷³
- “Salt-Depleted Acid Diet”: R607H, L919X KI/KI and WT littermates were fed a salt-depleted diet for 8 days. On day 9, the mice were fed the same diet but were also provided with acid in their drinking water (0.28 M NH₄Cl with 0.5 % sucrose, available *ad libitum*) for 6 additional days. Total experimental period was 14 days¹⁰⁰.

Body weight, chow and water consumption, urine (under mineral oil), and feces measurements were collected every 24 hours. On the final experimental day, mice were anesthetized with a 50 mg/kg dose of pentobarbital. Blood was collected in lithium heparin-coated tubes via periorbital bleeding and centrifuged for 10 minutes at 4°C to collect serum which was then stored at -80°C. Whole kidneys (after complete perfusion) were dissected into 4 halves and each half was processed for either RNA extraction, western blot, immunofluorescence, or immunohistochemistry, and then stored at -80°C.

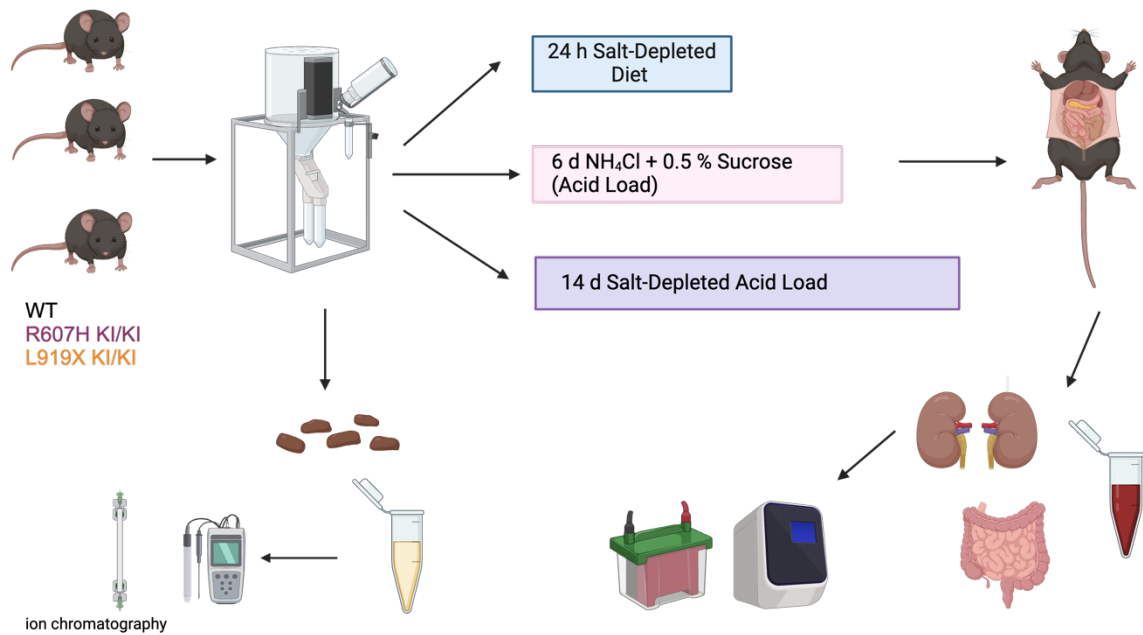


Figure 2.1 Metabolic cage experiment protocol with specialized diets. Animals were placed in metabolic cages for 72 hours and given water and chow *ad libitum* during the acclimatization process. Then, one of three dietary challenges were started. Body weight, urine and feces measurements were taken on Day 0 and every 24 hours thereafter. Blood was collected via periorbital bleeding while the animal was under anesthesia. Post-euthanizing, gut and kidney tissues were collected. The ileum, jejunum, and duodenum were snap frozen and then stored at -80°C . The kidneys were dissected into four halves and processed for immunoblots, mRNA isolation, immunofluorescence, and immunohistochemistry, and then stored at -80°C . *This figure was created with BioRender.com.*

URINE AND SERUM ANALYSIS

Freshly collected blood was analyzed for electrolytes (Na^+ , K^+ , Cl^-), glucose, urea nitrogen (BUN), hematocrit (Hct) and hemoglobin (Hb), and pH using an i-STAT1 Analyzer (Abaxis, Union City, CA, USA) with the i-STAT Chem8+ cartridge chip (Abott Laboratories, USA). Urine pH was measured using pH microelectrode (PerpHect® Ross® Micro Combination pH electrode, ThermoScientific, Beverly, MA, USA attached to a Accumet AR10 pH meter, Fischer Scientific). Urine osmolality was measured using the Advanced Instruments Osmo1 Single-Sample Micro-Osmometer (Thermo Fisher Scientific), diluting samples at 1:10 or 1:100 with filtered ddH₂O. Urine electrolytes were measured by ion chromatography (Dionex Aquion Ion Chromatography System, Thermo Fisher Scientific Inc., Mississauga, ON, Canada) with autosampler. Urine samples were diluted 1:100 or 1:250 with ddH₂O and with 4.5 mM Na₂CO₃/1.5 mM NaHCO₃ in ddH₂O for anion eluent, 20 mM Methanesulfonic acid in ddH₂O for cation eluent composition. Urinary creatinine concentration was measured using Parameter creatinine kit (R&D systems, Minneapolis, USA) or with ion chromatography. Chromeleon 7 Chromatography Data System software (Thermo Scientific) was used to analyze results. Urine anions were normalized to urinary creatinine concentration. Creatinine was chosen in order to normalise ion excretion to kidney function.

RNA ISOLATION AND REVERSE TRANSCRIPTASE QUANTITATIVE POLYMERASE CHAIN REACTION

Immediately after collection, one half kidney was incubated in RNAlater (ThermoFisher) for 8 hours at room temperature before storing in -80°C. Total RNA was extracted using TRIzol reagent (Invitrogen, Carlsbad, CA, USA) as previously described ⁴¹. RNA quantification was performed using NanoDrop (NanoDrop 2000C, Thermo Fisher Scientific, Waltham, MA). cDNA

was reverse transcribed with SuperScript™ II (Invitrogen) as per the manufacturer's instructions (RT-PCR). The cDNA was pooled to create a serially diluted standard curve. Real - time/quantitative PCR (qPCR) was performed in triplicate for each cDNA sample using TaqMan PCR master mix in a QuantStudio 6 Pro RT (real time) PCR system (ThermoFisher Scientific). Standard curve analysis was performed using a Quant Studio Design and Analysis Software version 2.4.3. Samples were quantified using the $2^{-\Delta\Delta C_t}$ method ⁶⁷. Expression levels of mRNA from specific genes were normalized to housekeeping ribosomal protein lateral stalk subunit P0 (RPLP0) gene. RPLP0 gene was selected as the housekeeping gene due to its comparable expression levels in both KI and WT mice, and its stability across all PCR runs. Primers for the genes of interest are listed in **Table 2.1**.

Table 2.1: Primers and Probes Used for qRT-PCR on Mouse Genes

Name	Forward	Reverse	Probe
Ae4 NM_N172830	5'- CTCTGTGTCTTTGA GCTTTGC-3'	5'- TCTGCCTATGGT TGCTTCTG-3'	5'-/56- FAM/TGTTTCCTC/ZEN/ CTGTGCCTGGGTATTG /3IABkFQ/-3'
alpha-ENaC NM_011324.2	5'- CAGTGATGTCCCTG TCAAGAA-3'	5'- CTTGGGCTTAG GGTAGAAGATG -3'	5'- /56-FAM/TGA TCA AGA /ZEN/AGT GTGGCT GTG CCT /3IABkFQ/ -3'
B1-H ⁺ -ATPase NM_134157.1	5'- CTTCTCACACTGGT AGGCAAG-	5'- AGTCAGATTTC GAGCAGAATGG -3'	5'-/56- FAM/CCGCTCAAT/ZEN /CGTAGGGTCATTGGC/ 3IABkFQ/-3'
Claudin-10b NM_N021386.1	5'- GCAGCGATCATTAG TCCTCTAC-3'	5'- CCACAGCCACT TATTTTGCC-3'	5-/56-FAM/A ATCGGTA A/ZEN/CGCAGATCTCC ACAGG/3IABkFQ/-3'
Claudin-4 NM_N009903.1	5- 'CAGGACTGCCAAG GAGATTC-3'	5- 'AACACTTTCTC AGCCCTCTG-3'	5-'/56- FAM/CATAGACGC/ZE N/CATCGCTCAGCCTC/ 3IABkFQ/-3'
Claudin-3 NM_N009902.1	5- 'GGTTCATCGACTGC TGGTAG-3'	5- 'CACCAAGATCC TCTATTCTGCG- 3'	5-'/56- FAM/CCCCTCAGA/ZEN /CGTAGTCCTTGCG/3 A BkFQ/-3'
Claudin-8 NM_N018778.1	5- 'CCACTGAGGCATG ATAGTCAC-3'	5- 'AGCTGGATACA ATTTGGGAGG-3'	5-/56- FAM/TGCAGCCAT/ZEN /TTGAAGAGCGTAGGT /3IABkFQ/-3'

Claudin-7 NM_N016887.1	5'- 'TCTTCGCTTTGTCA TCTCCC-3'	5'- AAATGTACGAC TCGGTGCTC-3'	5'-/56- FAM/TAATGGTGG/ZEN /TGTCCCTGGTGTGG/ 3IABkFQ/-3'
gamma-ENaC NM_N011326.1	5'- GTCAGAGGTGTCAT TTGAGCA-3'	5'- GAGAACGAGAA GGGAAAGGC-3'	5'-/56- FAM/TCGGAAGCG/ZE N/GAAAATCAGGGGA A/3IABKFQ/-3'
kAe1 NM_009902.4	5'- AAGAGGTCAAGGA ACAGCG-3'	5'- GTACAGGAAGA TGCCGAAGAG- 3'	5-/56- FAM/CCCACAAGC/ZE N/ACAGAGACCAGGA G/3IABkFQ/-3'
NCC NM_019415	5'- CAGATCAACAGGAT GGACGAAG-3'	5'- GCAATCATGTC CTCAAACCG-3'	5'-/56- FAM/TCCCGACAT/ZEN /CA ACCAGA AGCCC/3IABkFQ/-3'
NDCBE NM_021530.2	5'- ATGGGAAGATGGT GAGGAAC-3'	5'- ACGTGCTCTTTT GGTCCTG-3'	5'-/56- FAM/AAGGTGCTG/ZE N/GAGACGATGAAGG G/3IABKFQ/-3'
NHE3 NM_N0010810 60.1	5'- CCAAACAGCAAGA AATCCAGG-3'	5'- TCCCTCTATGGT GTCTTCCTC-3'	5'-/56-FAM/CCA ATTTC/ZEN/AGTTCAC CCATCA AGCCAC/3IABKFQ/-3'
NKCC2 NM_183354	5'- CAAGGAACATTACC AAGCC-3'	5'- CACCAGTTTGA TTGAACTCC-3*	5'-/56- FAM/CAAGAAAGA/ZE N/CGGCAACATCAGCA GC/3IABKFQ/-3'
Pendrin NM_011867	5'- TGATGGAGGCAGA GATGAATG-3'	5'- CAGAAAACACT GAGAGACTG-3'	5-/56- FAM/ATG TTCAGG/ZEN

			/ATGAGGCCATGCGTA G/3IABkFQ/-3'
Renin	TaqMan Gene Expression Assay (Applied Biosystems) REF# 4331182		
RPLP0 Mm.PT.58.4389 4205	5'-TTATA ACCCTGA AGGCTCGAC-3'	5'- CGCTTGTACCC ATTGATGATG-3'	5'-/56- FAM/AGGCCCTGC/ZEN /ACTCTCGCTT/3IABkF Q/-3'

PROTEIN EXTRACTION AND IMMUNOBLOTTING

A quarter of a freshly dissected kidney was decapsulated and mechanically homogenized in ice-cold RIPA (2mM EDTA, 2 % Deoxycholate, 0.3 M NaCl, 20 mM Tris/HCL pH 7.5, 2 % Triton X-100, 0.2 % SDS, pH 7.4, completed EDTA-free protease inhibitors, and PhoSTOP phosphatase inhibitors (Roche)) or Knepper lysis buffer (0.3M Sucrose, 25mM Imidazole, 1mM EDTA, 8.5uM Leupeptin, 1mM PMSF)⁵⁵ vortexed every 15 mins over 1 hour, and centrifuged at 4°C, 14000 rpm for 15 minutes. Protein concentration was measured using a Bicinchoninic Acid Protein Assay as per manufacturer instructions (ThermoScientific, USA). Immunoblot experiments were performed with 8 %, 10 %, or 12 % SDS-PAGE gels, transferred to a PVDF membrane, and blocked with 3 % milk in TBST (5mM Tris base, 15 mM NaCl, 0.1% Tween 20). Membranes were incubated in primary antibodies overnight at 4°C followed by incubation in secondary antibodies conjugated to horseradish peroxidase in a solution of 1% Milk + TBST. The primary and secondary antibodies used are listed in **Table 2.2**. Proteins were visualized using the Clarity Western ECL kit (Bio-Rad) and images were captured by ChemiDoc touch imaging systems (Bio-Rad, CA,USA). Quantification and densitometric analysis were performed by ImageJ (National Institutes of Health, USA).

COOMASSIE BLUE STAINING FOR RELATIVE QUANTIFICATION OF URINE ALBUMIN

A Bicinchoninic Acid Protein Assay was performed according to the manufacturer's guidelines (ThermoScientific, USA) on urine samples obtained from both WT and dRTA mutant mice, following the "Salt-Depleted Acid Diet". Subsequently, 2 µL of the urine samples were diluted in 2x Laemmli Buffer (BioRad) and loaded onto an 8 % SDS-PAGE gel, which was subsequently fixed in a solution containing 7 % glacial acetic acid (Fisher) and 40 % methanol

(Sigma-Aldrich). Following gel fixation, the Brilliant Blue G - Colloidal Concentrate protocol (Millipore Sigma, Product No. B2025) was followed according to the manufacturer's instructions for gel staining. The resulting Coomassie-stained gels were visualized using a White Sample Tray within the ChemiDoc touch imaging systems (Bio-Rad, CA, USA). Subsequent quantification and densitometric analysis of the gel bands were performed using ImageJ software (National Institutes of Health, USA).

Table 2.2: Primary Antibodies Used on Mouse Kidney Tissues.

Name	Type	Reference	Dilution	Special Notes
Rb anti-Claudin-10 (~ 17 kDa)	Primary	Antibodies.com	1:1000	
Rb anti-Claudin-4 (~ 20 kDa)	Primary	Invitrogen	1:1000	
Rb anti-ENaC gamma (~ 75- 90 kDa)	Primary	StressMarq Biosciences Inc	1:5000	
Rb anti-NBCn1-N (~ > 180 kDa)	Primary	Gift from Dr. Jeppe Prætorius	1:1000	Use 5% Milk for blocking. Use PBS-T for washes. Use 1% BSA for antibody dilution.
Direct-Blot HRP anti- β Actin (~ 42 kDa)	Primary	BioLegend	1:10000	

Please see above text for the incubation conditions unless stated in the special notes.

TAIL-CUFF BLOOD PRESSURE MEASUREMENTS

Blood pressure measurements were acquired using the tail-cuff blood pressure instrument BP - 2000 SERIES II Blood Pressure Analysis System™ (Visitech Systems, USA). Prior to data collection, conscious WT and dRTA mutant mice underwent a 3 to 5 days training regimen within the apparatus to ensure familiarization with the experimental setup and minimize stress-induced variability. The mice were gently restrained with their tails secured in a computerized tail-cuff system. Each measurement session consisted of three sets, each comprising 10 rounds of preliminary measurements for acclimatization and then 20 consecutive rounds of blood pressure readings.

STATISTICAL ANALYSIS

All data are presented as mean \pm SEM and statistical analysis was completed using GraphPad Prism software (Ver 7. 0e). Normality was checked for all data sets (using Shapiro-Wilk test) and outliers (as determined by Prism) were removed. Analysis was performed using unpaired Student's t-test or Mann-Whitney test, or Two-Way ANOVA (with Full Fit Model) where appropriate. A P-value of less than 0.05 was considered statistically significant.

Chapter 3: Results

CHARACTERIZATION OF dRTA MUTANT MICE AT STEADY STATE

R607H KI/KI and L919X KI/KI mice have decreased kAe1 mRNA abundance and excrete alkaline urine with less urinary ammonium.

Dr. Christian Hubner's laboratory generated mice carrying the orthologous mouse Ae1 L919X mutation (**Appendix A: Figure 3.34, Figure 3.35**). Homozygous mice were viable, developed normally and were fertile. Neither gross kidney malformation nor nephrocalcinosis were observed in these mice (**Appendix A**), similarly to the Ae1 R607H mutant mice⁷³. Before conducting experiments to understand the sodium wasting phenotype that occurs during dRTA, we first sought to confirm that our two mouse models have dRTA. To do this, we measured the mRNA abundance of Ae1 in perfused kidney homogenates and measured the pH and ion concentrations of their plasma and urine at steady state. Both R607H KI/KI and L919X KI/KI mice had significantly less kAe1 gene expression compared to WT mice (**Figure 3.1 A, B, Appendix A**). This confirmed the decreased abundance of A-ICs in our mice as previously reported⁷³. Both KI/KI mutant mice strains had alkaline urine pH compared to WT counterparts (**Figure 3.2 A, D**). In alignment, both mutant mice also excreted significantly less urinary ammonium compared to WT mice (**Figure 3.2 B, E**). As a characteristic marker of dRTA is the inability to properly acidify urine^{73,92,123} this analysis confirms the correct phenotype of the two mouse models (**Figure 3.2**).

We also completed a primary characterization of physiological parameters of these mice at steady state. We observed that R607H KI/KI mice had no significant differences in body weight, chow or water consumption, and feces and urine excretion compared to WT mice (**Table 3.1**). In contrast, the L919X KI/KI mice weighed significantly more and excreted significantly less feces, although their chow and water consumption, and urine excretion volume was no different to WT mice (**Table 3.1**).

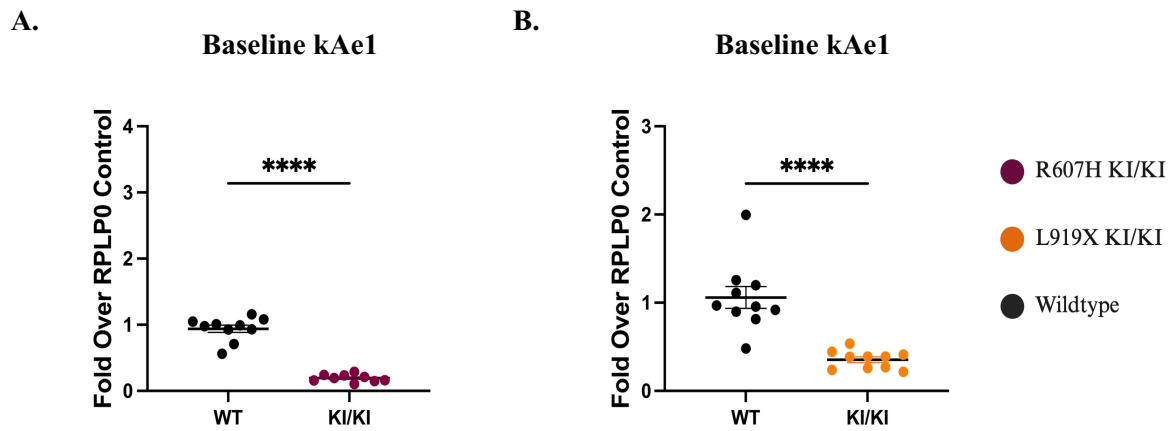


Figure 3.1 mRNA levels of Ae1 are lower in dRTA mutant mice compared to WT mice at baseline. Perfused whole kidney tissue mRNA was isolated from all groups, and qRT-PCR confirmed reduced Ae1 abundance in agreement with decreased A-ICs in the mutant mice. PCR results were normalized to RPLP0 mRNA. **A)** Shows significantly decreased Ae1 expression in R607H KI/KI mice (n=10 WT, n=9 KI/KI), while **B)** indicates a similar lower expression in L919X KI/KI mice (n=11 WT, n=11 KI/KI). Data is presented as mean \pm SEM and analyzed using unpaired Student's t-test or Mann-Whitney test. *PCR and analysis was conducted by Saron Gebremariam, and graphs were created by Priyanka Mungara.*

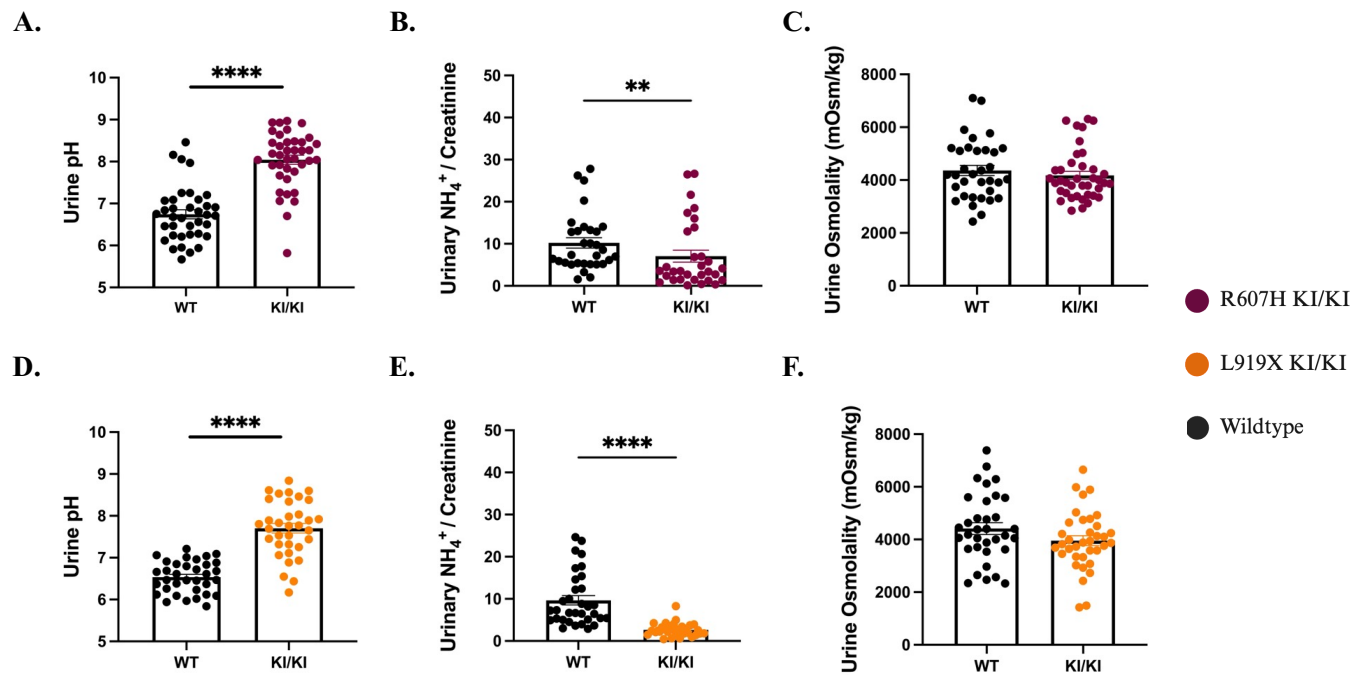


Figure 3.2 Urinary pH is higher while urine ammonium excretion is lower in dRTA mutant mice than WT counterparts at baseline. Steady state urine was collected after 3 days of acclimatization to metabolic cages. pH was measured immediately after collection under mineral oil, while urine for ion concentration and osmolality was frozen, thawed, and diluted with water prior to analysis. **A)** R607H KI/KI mice exhibited alkaline urine pH and **B)** reduced ammonium excretion, consistent with alkaline pH (n = 37 WT, n = 39 KI/KI). **C)** No differences in urine osmolality were observed between WT and mutant mice. **D)** L919X KI/KI mice showed elevated urine pH, **E)** decreased ammonium excretion, and **F)** no variance in urine osmolality compared to WT mice (n = 34 WT, n = 34 KI/KI). Urinary ion concentrations were normalized to urinary creatinine and presented as a ratio. Data is presented as mean ± SEM, **P < 0.01, ****P < 0.0001 using unpaired Student's t-test or Mann-Whitney test.

Table 3.1 Metabolic Cage Parameters of Ae1 R607H KI/KI and L919X KI/KI Mice at Steady State

Parameter	Units	WT (n=37)	R607H KI/KI (n=41)	p-value
		M: n = 17	M: n = 21	
		F: n = 20	F: n = 20	
Body Weight	g	25.38 ± 0.64	26.51 ± 0.60	0.2003
Food Consumption	g / BW / 24	0.1771 ± 0.01	0.1654 ± 0.12	0.2771
Water Consumption	g / BW / 24	0.271 ± 0.02	0.278 ± 0.02	0.7058
Feces	g	0.0788 ± 0.01	0.066 ± 0.01	0.1107
Urine Volume	mL/day	1.366 ± 0.13	1.382 ± 0.13	0.9115

Parameter	Units	WT (n=34)	L919X KI/KI (n=36)	p-value
		M: n = 16	M: n = 21	
		F: n = 18	F: n = 15	
Body Weight	g	24.19 ± 0.46	26.58 ± 0.41	0.0002
Food Consumption	g / BW / 24	0.1929 ± 0.01	0.1652 ± 0.01	0.1171
Water Consumption	g / BW / 24	0.303 ± 0.02	0.251 ± 0.02	0.1675
Feces	g	0.095 ± 0.01	0.068 ± 0.01	0.0036
Urine Volume	mL/day	1.345 ± 0.15	1.072 ± 0.10	0.4599

Data is presented as mean ± SEM. Student's T-Test or Mann-Whitney test used where appropriate. Significant data is bolded.

R607H KI/KI and L919X KI/KI mice have comparable plasma and urine ion concentrations to WT mice.

We next measured the concentrations of sodium, potassium, and chloride in the urine of WT or mutant mice at steady state. R607H KI/KI and L919X KI/KI mice had no significant differences in urinary sodium, chloride, or potassium excretion compared to WT counterparts (**Figure 3.3 A, B, D, E**). In alignment, there was no differences in urine osmolality between WT and mutant animals of both strains (**Figure 3.2 C, F**). While there were no notable differences in plasma ion concentrations or pH between the L919X KI/KI mice and their WT counterparts (**Table 3.3**), R607H KI/KI mice had significantly increased plasma potassium and blood urea nitrogen levels compared to WT mice (**Table 3.2**). Although this specific plasma potassium phenotype seen in the R607H KI/KI mice is not commonly seen in human dRTA patients ^{92,123}, these results overall provide evidence that the dRTA mutant mice have an ability to regulate ion homeostasis (of sodium, chloride, and potassium) similarly to WT mice at steady state.

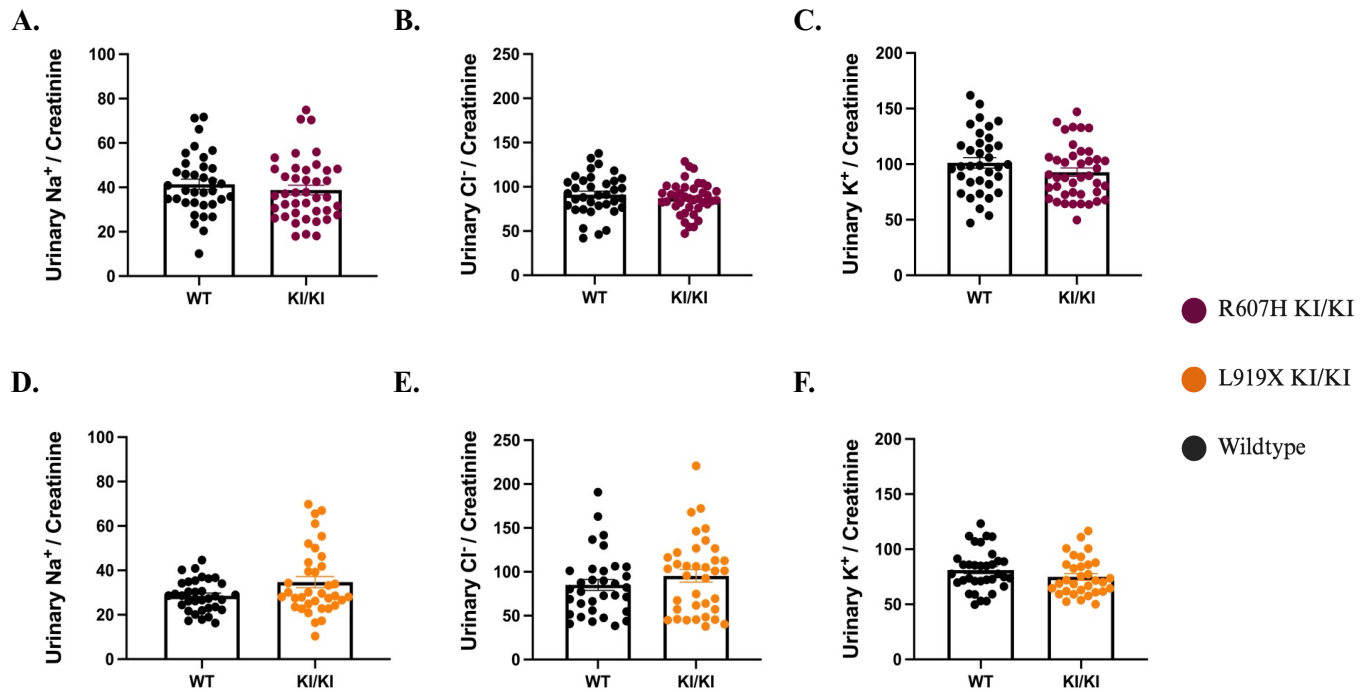


Figure 3.3 Comparison of urinary sodium, potassium, and chloride excretion between dRTA mutant mice and WT counterparts. R607H KI/KI mice showed similar **A)** sodium, **B)** chloride, and **C)** potassium excretion compared to WT ($n = 37$ WT, $n = 41$ KI/KI). **D)** L919X KI/KI mice also exhibited comparable **D)** sodium, **E)** chloride, and **F)** potassium excretion to WT counterparts ($n = 34$ WT, $n = 36$ KI/KI). Urinary ion concentrations were normalized to urinary creatinine and presented as a ratio. Data is presented as mean \pm SEM and analyzed using unpaired Student's t-test or Mann-Whitney test.

Table 3.2 Baseline Plasma Characterization of WT and R607H AE1 KI/KI Mice

Parameter	Units	WT (n=11)	R607H AE1 KI/KI (n=9)	p-value
Na ⁺	mM	146.4 ± 0.50	147.1 ± 0.59	0.3148
Cl ⁻	mM	118.2 ± 1.11	118.5 ± 0.62	0.1409
K⁺	mM	4.5 ± 0.14	4.920 ± 0.08*	0.0207
HCO ₃ ⁻	mM	18.66 ± 0.63	19.07 ± 0.46	0.6142
pH		7.256 ± 0.01	7.258 ± 0.01	0.9102
TCO ₂	mmHg	19.91 ± 0.65	20.20 ± 0.53	0.7370
BUN	mg/dl	21.09 ± 1.35	23.60 ± 0.92*	0.0438
Glucose	mg/dl	196.3 ± 7.07	197.3 ± 12.31	0.9417
HCT	%	37.73 ± 1.22	38.60 ± 0.34	0.5178
pCO ₂	mmHg	42.05 ± 1.47	42.72 ± 1.41	0.7417
AnGAP	mM	13.27 ± 1.54	14.60 ± 0.60	0.9863
Hb	g/dl	12.82 ± 0.41	13.14 ± 0.12	0.4826
BE _{ecf}	mM	-8.545 ± 0.73	-8.100 ± 0.59	0.5666

Data is presented as mean ± SEM. Student's T-Test or Mann-Whitney test used where appropriate. Significant data is bolded.

Table 3.3 Baseline Plasma Characterization of WT and L919X AE1 KI/KI Mice

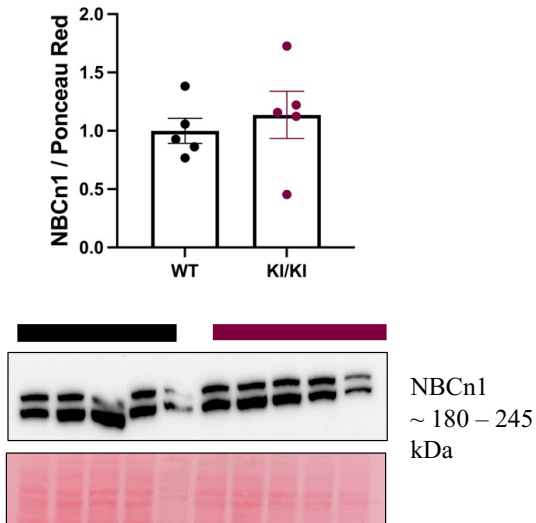
Parameter	Units	WT (n=10)	L919X AE1 KI/KI (=10)	p-value
Na ⁺	mM	147.5 ± 0.56	146.9 ± 0.62	0.4327
Cl ⁻	mM	118.8 ± 0.96	119.6 ± 1.54	0.6644
K ⁺	mM	4.633 ± 0.17	4.610 ± 0.20	0.7029
HCO ₃ ⁻	mM	18.38 ± 0.56	19.95 ± 0.51	0.0930
pH		7.289 ± 0.002	7.249 ± 0.009	0.1186
TCO ₂	mmHg	19.50 ± 0.75	21.30 ± 0.52	0.0636
BUN	mg/dl	22.70 ± 1.38	19.80 ± 0.99	0.1050
Glucose	mg/dl	181 ± 13.11	198.3 ± 10.58	0.3181
HCT	%	36.80 ± 0.55	36 ± 0.79	0.4174
pCO ₂	mmHg	38.99 ± 2.86	45.75 ± 1.60	0.0525
AnGAP	mM	14.6 ± 0.62	13.22 ± 1.33	0.1197
Hb	g/dl	12.53 ± 0.19	12.23 ± 0.27	0.3729
BEecf	mM	-8.100 ± 0.78	-7.100 ± 0.50	0.2963

Data is presented as mean ± SEM. Student's T-Test or Mann-Whitney test used where appropriate.

R607H KI/KI and L919X KI/KI mice show a slight trend for increased NBCn1 protein abundance at steady state.

A previous report on the R607H KI/KI mice showed an increase in NBCn1 protein abundance at steady state ⁷³. NBCn1 functions as a basolateral sodium/bicarbonate cotransporter within the medullary TAL, facilitating ammonium and acid excretion in response to chronic metabolic acidosis ⁷⁹. The authors of that report predicted that this adaptation provided these mice a milder dRTA-like phenotype at steady state ⁷³. To determine whether our mice manifest a similar increase in NBCn1, preliminary immunoblots were conducted to evaluate NBCn1 protein expression at baseline (**Figure 3.4 A, B**). Although a comprehensive blot analysis is pending completion, our findings suggest a trend for increased NBCn1 protein levels in both R607H KI/KI and L919X KI/KI mice compared to WT at baseline (**Figure 3.4 A, B**). This is consistent with previous observations in R607H KI/KI mice ⁷³ and suggests a similar trend in L919X KI/KI mice.

A.



B.

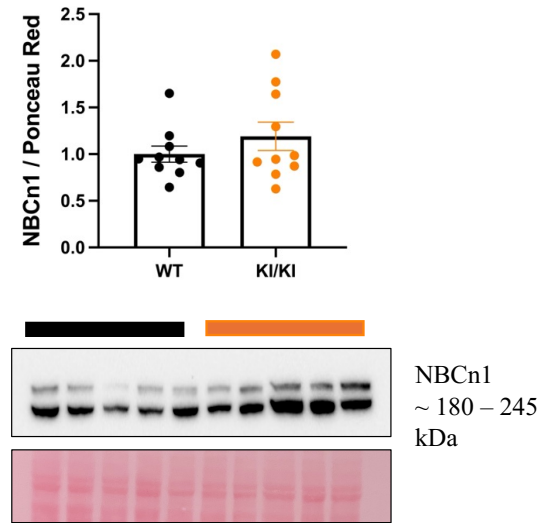


Figure 3.4 Preliminary examination of NBCn1 protein abundance suggests a trend for higher NBCn1 protein abundance in dRTA mutant mice compared to WT mice. A) R607H KI/KI mice exhibit a slight trend toward increased NBCn1 compared to WT mice (n = 5 WT, n = 5 KI/KI). B) L919X KI/KI mice also display a trend for increased NBCn1 compared to WT mice under steady state conditions (n = 10 WT, n = 10 KI/KI). NBCn1 protein bands were normalized to whole lane ponceau red. Data is presented as mean \pm SEM and analyzed using Student's T-Test or Mann-Whitney test as appropriate.

DIETARY CHALLENGE 1: 24 HOURS OF SALT-DEPLETED DIET

After 24 hours of salt-depletion, dRTA mutant and WT mice exhibit decreased water and chow consumption, decreased waste excretion, with no change to body weight.

Following the baseline characterization of the two mouse models, we next assessed whether the R607H KI/KI and L919X KI/KI dRTA mutant mice are suitable models to study the sodium-losing phenotype observed in dRTA patients. To do this, we measured physiological parameters, blood, and urine compositions of both mutant mice strains and WT counterparts following an acute 24-hour salt-restriction diet (**Figure 2.1**).

R607H KI/KI and L919X KI/KI mice had comparable body weights to their WT counterparts, prior to and following the salt-depletion (**Figure 3.5 A, Figure 3.6 A**). L919X KI/KI and WT mice significantly reduced their chow and water consumption post-salt depletion, with no genotype-based differences (**Figure 3.5 B, C**). This trend was mirrored in R607H KI/KI and WT mice, but with no significant differences between genotypes at baseline (**Figure 3.6 B, C**). L919X KI/KI and WT mice both decreased urine volume and fecal mass following the diet, albeit with lower baseline fecal mass in L919X KI/KI mice (**Figure 3.5 D and E**). R607H KI/KI and WT mice exhibited consistent reductions over the 24-hour period, without genotype differences (**Figure 3.6 D and E**)

Overall, this data indicates that both WT and KI/KI mice were healthy following the diet and responded to the diet with decreased water and chow consumption and decreased waste excretion, without reduction in body weight.

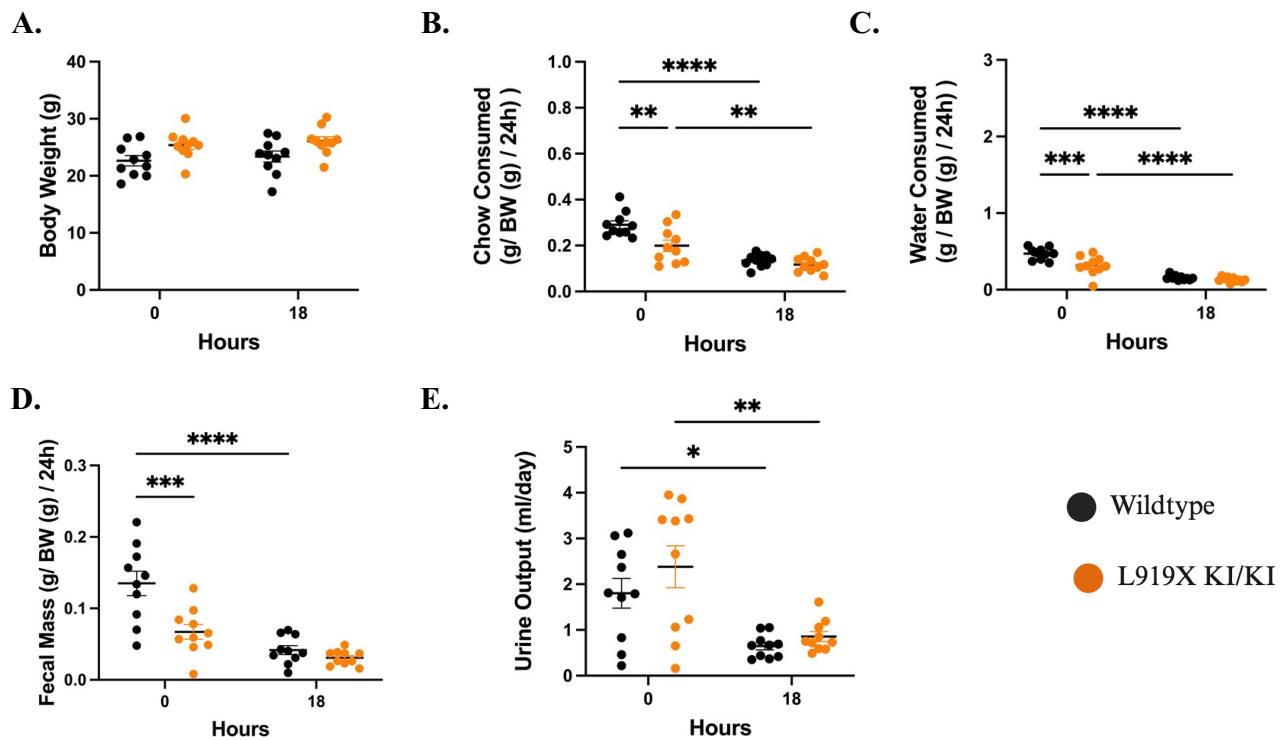


Figure 3.5 Both L919X KI/KI mice and WT mice reduce their chow and water consumption, and fecal mass after 18 hours of salt-restriction. A) There were no differences in body weight pre- and post-diet between WT and mutant mice (n = 10 WT, n = 10 KI/KI). **B)** Both genotypes decrease chow consumption, and **C)** water consumption following the diet, with L919X KI/KI mice consuming less at baseline. **D)** Fecal mass excreted and **E)** urine volume voided also decreased similarly in both genotypes, with less feces produced in the mutant at baseline. The 18-hour time point was selected to represent the phenotype of the mice following the diet. There were 5 WT males, 5 WT females, 5 KI/KI males, and 5 KI/KI females in this data set. Data is presented as mean \pm SEM, **P < 0.01, ***P < 0.001, ****P < 0.0001 using 2-way ANOVA with Tukey's multiple comparison test. *Only significant bars comparing pre- and post-diet and between genotypes at each time point are shown for clarity.*

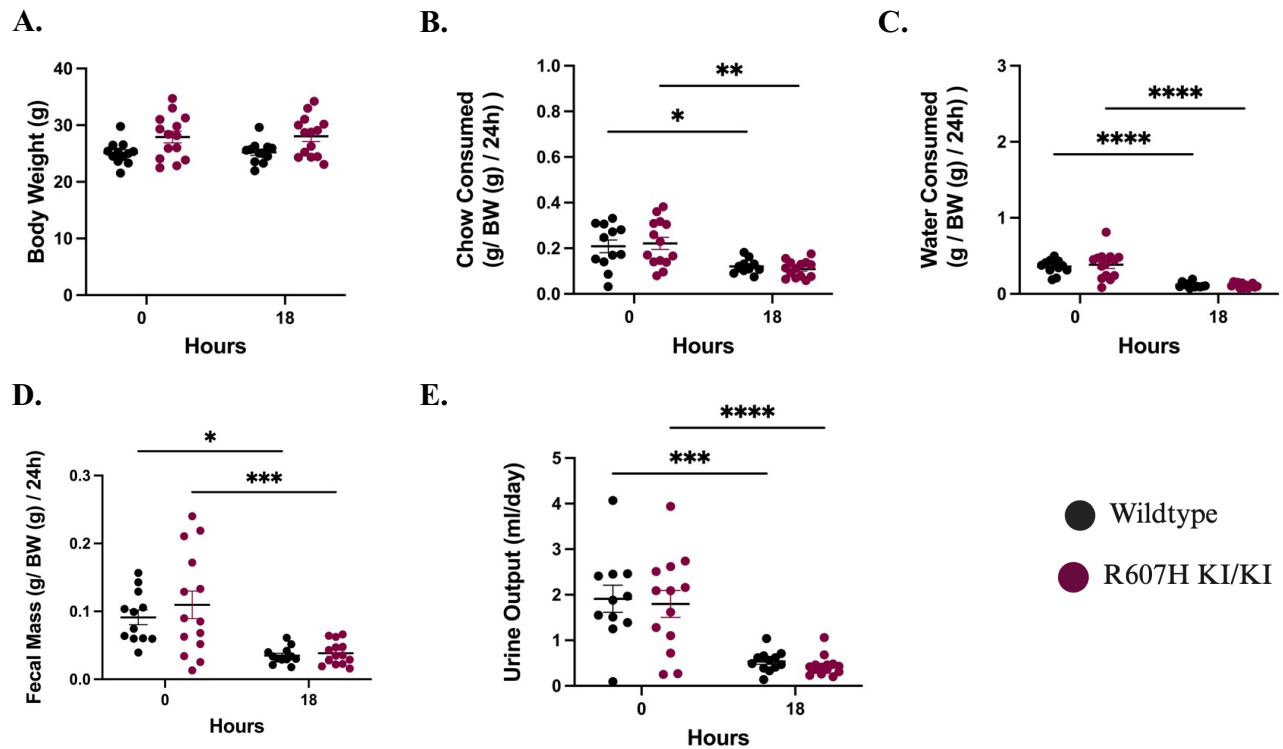


Figure 3.6 Both R607H KI/KI mice and WT mice reduce their chow and water consumption, and fecal mass after 18 hours of salt-restriction. **A)** No differences in body weight were found pre- and post-diet between WT and mutant mice ($n = 12$ WT, $n = 14$ KI/KI). **B)** Both genotypes show decreased chow consumption and **C)** water consumption declines following the diet. **D)** Fecal mass excreted and **E)** urine volume voided 18 hours after the diet also decreased similarly in both genotypes. These results mirror those observed in L919X KI/KI mutant mice (**Figure 3.5**). The 18-hour time point was selected to represent the phenotype of the mice following the diet. There were 5 WT males, 7 WT females, 7 KI/KI males, and 7 KI/KI females in this data set. Data is presented as mean \pm SEM, * $P < 0.05$, ** $P < 0.01$, *** $P < 0.001$, **** $P < 0.0001$ analyzed using 2-way ANOVA with Tukey's multiple comparison test. *Only significant bars comparing pre- and post-diet and between genotypes at each time point are shown for clarity.*

Acute salt-restriction leads to high plasma potassium in R607H KI/KI mice only.

On the acute salt-depletion, no differences in plasma ion concentrations were observed between R607H KI/KI and WT mice although these mutant mice still exhibited significantly increased plasma potassium compared to WT littermates (**Table 3.4**). Notably, the plasma potassium values were not significantly different from baseline values in these mice (**Table 3.2**). In contrast to this mouse model, no significant differences in plasma ion concentrations were found between L919X KI/KI mice and WT counterparts, including plasma sodium, potassium, and chloride (**Table 3.5**). dRTA patients normally present with hypokalemic phenotype ^{1,123}. Therefore, while these results contradicts findings from dRTA patients, they could potentially point to an abnormality in renal potassium handling and the CDs of mutant mice.

Table 3.4. Plasma Characterization of WT and R607H AE1 KI/KI Mice Following 24 hours of Salt -Restriction

Parameter	Units	WT (n=12)	R607H AE1 KI/KI (n=14)	p-value
Na ⁺	mM	146.3 ± 0.89	148.1 ± 0.28	0.8166
Cl ⁻	mM	121.5 ± 2.06	122.9 ± 0.77	0.5196
K⁺	mM	4.475 ± 0.10	4.843 ± 0.10	0.0162
HCO ₃ ⁻	mM	19.04 ± 0.97	18.39 ± 0.54	0.5437
pH		7.203 ± 0.02	7.215 ± 0.01	0.6389
TCO ₂	mmHg	20.50 ± 1.00	19.86 ± 0.59	0.9305
BUN	mg/dl	23.75 ± 1.47	25.00 ± 1.27	0.5236
Glucose	mg/dl	154.5 ± 11.59	182.6 ± 9.27	0.0667
HCT	%	37.50 ± 2.18	37.86 ± 0.71	0.1096
pCO ₂	mmHg	48.33 ± 2.36	45.75 ± 1.90	0.3983
AnGAP	mM	10.25 ± 2.39	11.64 ± 0.61	0.1453
Hb	g/dl	12.76 ± 0.74	12.86 ± 0.25	0.0994
BEecf	mM	-9.000 ± 1.21	-9.357 ± 0.61	0.7847

Data is presented as mean ± SEM. Student's T-Test or Mann-Whitney test used where appropriate. Significant data is bolded.

Table 3.5. Plasma Characterization of WT and L919X AE1 KI/KI Mice Following 24 hours of Salt-Restriction

Parameter	Units	WT (n=10)	L919X AE1 KI/KI (n=10)	p-value
Na ⁺	mM	147.9 ± 0.69	147.7 ± 0.58	0.8268
Cl ⁻	mM	117.6 ± 0.90	120.9 ± 1.33	0.0543
K ⁺	mM	4.980 ± 0.16	5.180 ± 0.46	0.5661
HCO ₃ ⁻	mM	20.59 ± 0.61	20.40 ± 0.83	0.8554
pH		7.240 ± 0.02	7.248 ± 0.03	0.8469
TCO ₂	mmHg	22.20 ± 0.59	21.80 ± 0.85	0.7048
BUN	mg/dl	30.10 ± 4.37	23.30 ± 0.99	0.1249
Glucose	mg/dl	164.5 ± 12.69	157.1 ± 9.72	0.6490
HCT	%	40.70 ± 0.67	38.90 ± 0.69	0.1152
pCO ₂	mmHg	47.95 ± 1.13	47.74 ± 3.41	0.9540
AnGAP	mM	14.90 ± 0.80	11.89 ± 1.37	0.0677
Hb	g/dl	13.84 ± 0.23	13.22 ± 0.24	0.0741
BEecf	mM	-6.900 ± 0.97	-6.800 ± 1.07	0.9457

Data is presented as mean ± SEM. Student's T-Test or Mann-Whitney test used where appropriate.

Following salt-restriction, both dRTA mutant mice have an alkaline urine pH and decreased urinary potassium excretion compared to WT mice.

Next, we analyzed the pH and ion composition (levels of sodium, chloride, and potassium) of the excreted urine from WT and mutant mice. Given the tightly coupled exchange of protons and sodium along the nephron ¹²⁹ we anticipated a reduction in urinary pH, particularly in WT mice compared to mutant animals after salt-depletion. Consistently, despite overall urinary acidification in all genotypes over the 24 h time course (**Figure 3.7 B, D**), both R607H and L919X KI/KI mice exhibited more alkaline urine throughout the experiment compared to WT counterparts (**Figure 3.7 A, C**).

Both dRTA mutant strains and WT counterparts revealed an appropriately reduced urinary sodium and chloride excretion (**Figure 3.8 A, B, Figure 3.9 A, B**), with no significant difference between the genotypes (**Figure 3.8 D, E, Figure 3.9 D, E**). However, in response to the sodium restriction, L919X KI/KI mice excreted significantly less urinary potassium (**Figure 3.9 C, F**), with a similar trend in R607H KI/KI mice than WT counterparts (**Figure 3.8 C, F**). This confirmed a different potassium handling phenotype in the dRTA mutant mice compared with WT mice, highlighting a CD abnormality. Despite the change in urinary ions, mutant mice strains revealed no significant differences in urine osmolality compared to WT mice over the 24 hours (**Figure 3.10**).

Overall, this data confirms the L919X KI/KI and R607H KI/KI as appropriate dRTA model, due to their inability to acidify urine. The salt-restriction also revealed an abnormal potassium handling in dRTA mutant mice.

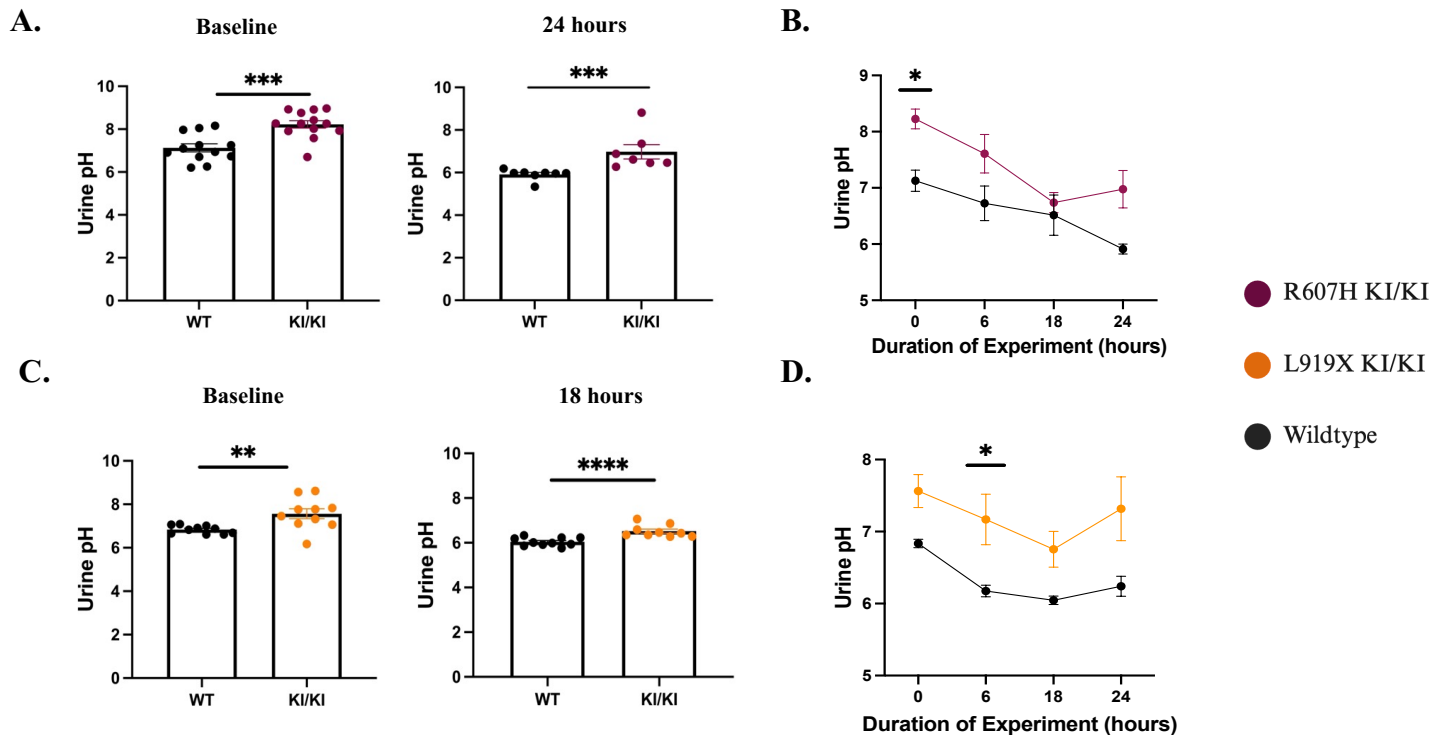


Figure 3.7 Urinary pH is alkaline before and after a 24-hour salt-restriction diet in dRTA mutant mice compared to WT mice. A) R607H KI/KI mice displayed alkaline urine pH both initially and after the diet (n = 12 WT, n = 14 KI/KI). **B)** Both genotypes reduced urine pH, but R607H KI/KI mice maintained alkaline urine. **C)** L919X KI/KI mice also had alkaline urine initially and 18 hours post-diet, n = 10 WT, n = 10 KI/KI. Specifically, here, the 18-hour time point is shown due to the reduced sample size available for measurement at 24-hour time point. **D)** Both genotypes could acidify urine over time, although mutant mice remained significantly more alkaline. Data presented as mean \pm SEM, *P < 0.05, **P < 0.01, ***P < 0.001, ****P < 0.0001 using unpaired Student's t-test, Mann-Whitney test, or 2-way ANOVA with Tukey's multiple comparison test.

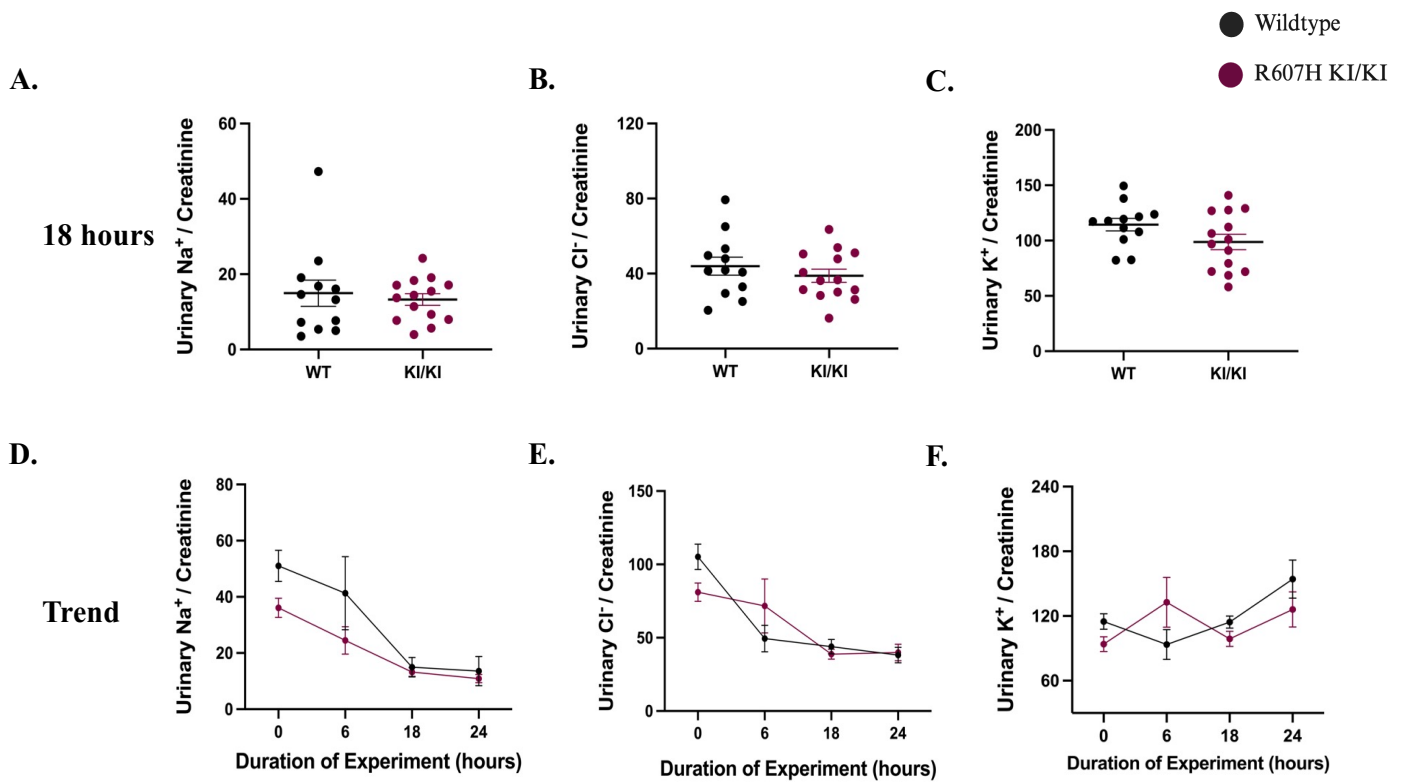


Figure 3.8 There is no significant difference in urinary sodium, potassium, and chloride excretion in R607H KI/KI mice compared to WT mice. At 18 hours into salt-restriction: **A)** R607H KI/KI mice show comparable sodium and **B)** chloride excretion levels compared to WT mice (n = 12 WT, n = 14 KI/KI). **C)** There was a trend for decreased potassium excretion in mutant animals compared to WT. **D)** Sodium and **E)** chloride excretion appropriately decline in both genotypes. **F)** Potassium excretion sharply increases in WT mice but remains low in KI/KI mice. Data presented as mean \pm SEM, analyzed using unpaired Student's t-test, Mann-Whitney test, or 2-way ANOVA with Tukey's multiple comparison test.

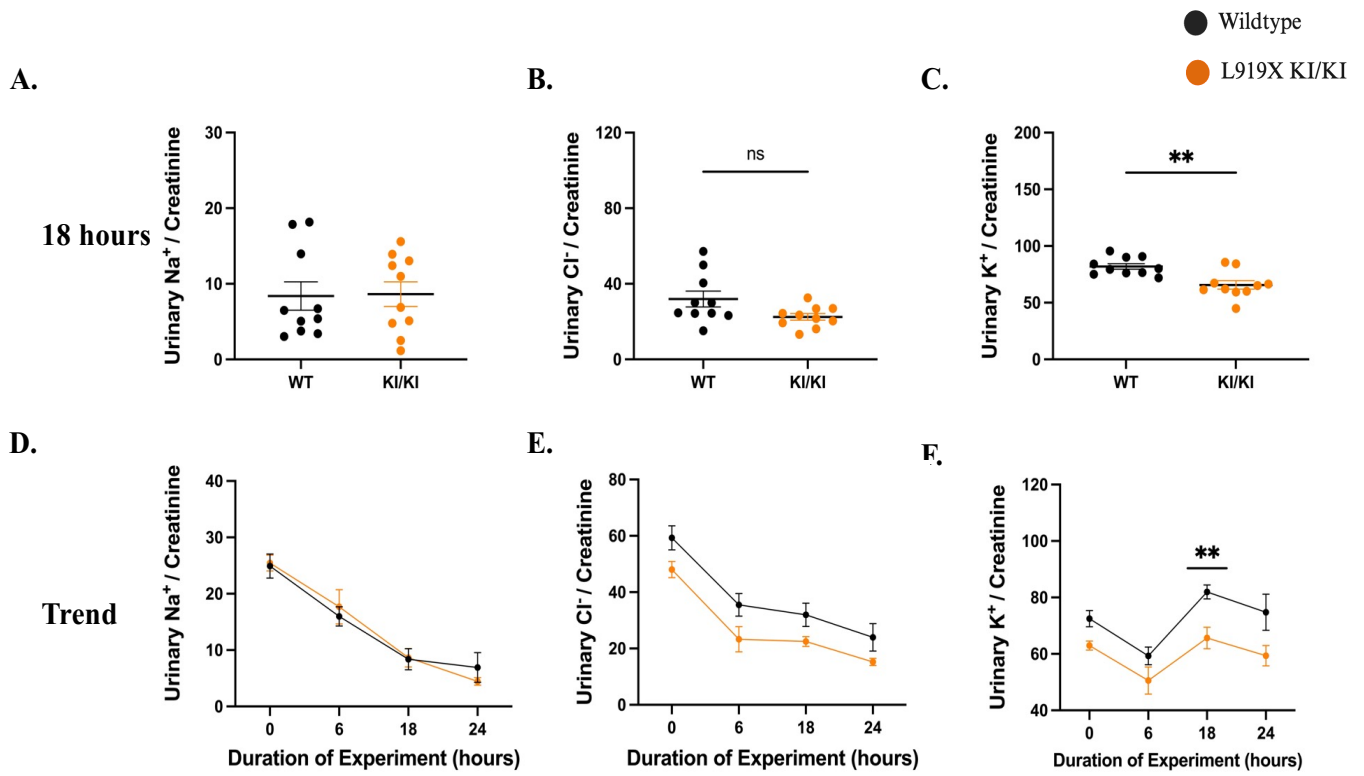
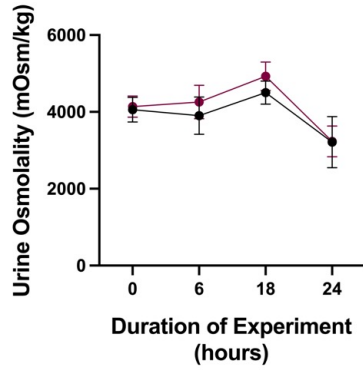


Figure 3.9 L919X KI/KI mice excrete less urinary potassium than WT mice without differences in sodium and chloride excretion. After 18 hours of salt-restriction: **A)** L919X KI/KI mice exhibit comparable sodium excretion and **B)** chloride levels compared to WT (n = 10 WT, n = 10 KI/KI). **C)** Potassium excretion was significantly decreased in the mutant mice compared to WT. **D)** Sodium and **E)** chloride excretion decline appropriately in both genotypes. **F)** Potassium excretion sharply increases in WT mice but remains significantly low in KI/KI mice, like R607H KI/KI mice. Data presented as mean \pm SEM, **, **P < 0.01 using unpaired Student's t-test, Mann-Whitney test, or 2-way ANOVA with Tukey's multiple comparison test.

A.



B.

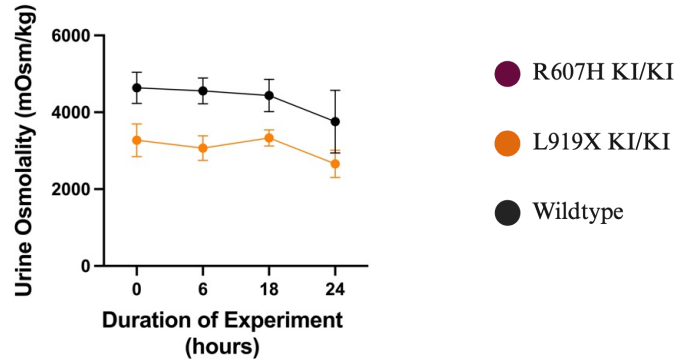


Figure 3.10. Urine osmolality in the R607H KI/KI and L919X KI/KI mice is not significantly different compared to WT, following the 24-hour salt-restriction diet. Urine was frozen and thawed and diluted with water prior to osmolality analysis. **A)** R607H KI/KI and WT counterparts did not differ in urine osmolality (n = 12 WT, n = 14 KI/KI). **B)** L919X KI/KI also did not display different urine osmolality compared to WT, although there was a trend for lower urine osmolality compared to WT counterparts throughout the experiment (n = 10 WT, n = 10 KI/KI). All data is presented as mean \pm SEM compared with a 2-way ANOVA, Tukey's multiple comparison test.

DIETARY CHALLENGE 2: 6 DAYS OF ACID LOAD

Acid load decreases urine output and feces excretion in dRTA mutant mice compared to WT.

While no clear sodium-wasting phenotype was revealed in our dRTA mutant mice following acute salt-depletion, evidence of disrupted CD function was emerging. This prompted us to investigate this phenotype through a second challenge: an acid load. As our dRTA mutant mice have incomplete dRTA⁷³, the acid load would intensify the dRTA phenotype^{1,117,123} which we predicted may reveal a urinary ion imbalance. Therefore, WT mice and both dRTA mutant mice were fed a 6-day challenge of 0.28 M NH₄Cl + 0.5 % sucrose in drinking water available *ad libitum* (**Figure 2.1**).

R607H KI/KI and L919X KI/KI mice had comparable body weights, chow, and water consumption to their WT counterparts, prior to and following the acid challenge (**Figure 3.11 A-C**, **Figure 3.12 A-C**). The R607H KI/KI mice excreted significantly less urine volume compared to WT mice on Day 6 of acid load (**Figure 3.11 D**), but no significant differences were observed in feces production after the diet (**Figure 3.11 E**). L919X KI/KI mutant mice produced significantly less urine volume from baseline and compared to WT mice on day 6 of the challenge. They also significantly reduced feces production from steady state (**Figure 3.12 D, E**).

Overall, this data indicates that both WT and KI/KI groups responded to the acid challenge with decreased waste excretion, which is in line with decreased water consumption likely due to the acid load.

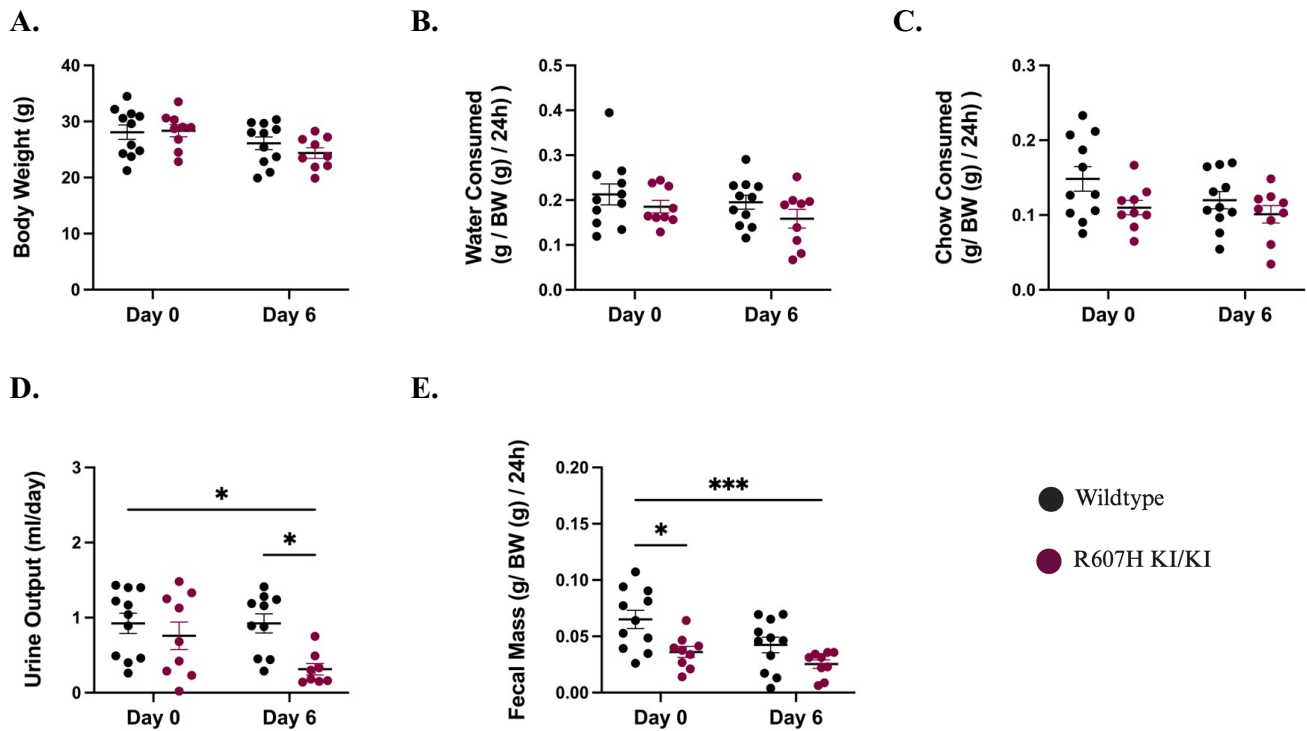


Figure 3.11 R607H KI/KI mice reduce their urine output and trend for reduced fecal mass compared to WT mice on a 6-day acid challenge. **A)** There were no difference in body weight pre- and post- acid diet between WT and mutant mice (n=11 WT, n=9 KI/KI). **B)** Water and **C)** chow consumption also show no differences between genotypes. **D)** Urine volume voided is decreased in mutant animals compared to WT on Day 6. **E)** Fecal mass excreted is decreased in mutant mice compared to WT at baseline, but no difference between genotypes is observed by Day 6. There were 5 WT males, 6 WT females, 4 KI/KI males, and 5 KI/KI females in this data set. Data presented as mean \pm SEM, *P < 0.05 using 2-way ANOVA with Tukey's multiple comparison test. Note: *Only significant comparisons are shown for clarity, comparing pre- and post-diet and between genotypes at each time point.*

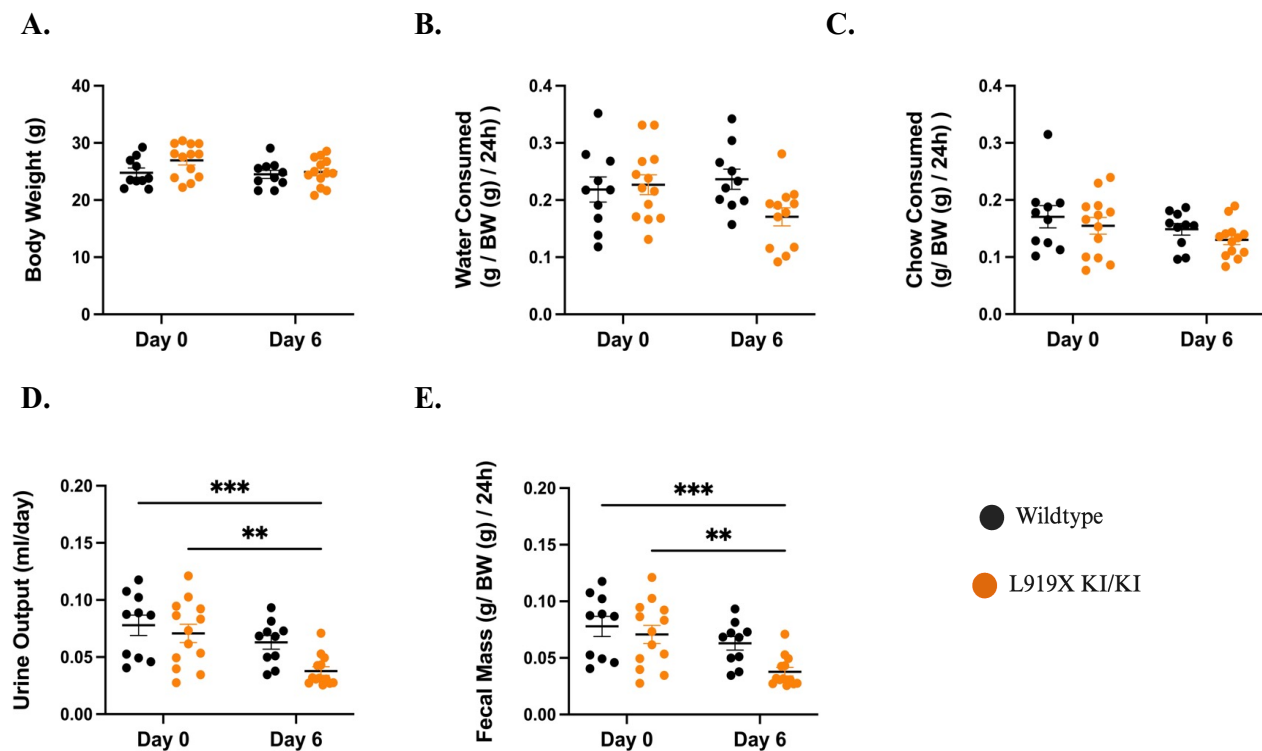


Figure 3.12 L919X KI/KI mice reduce their urine output compared to WT mice and their fecal mass compared to baseline on a 6- day acid challenge. (A) There were no differences in body weight pre- and post- acid diet (n= 10 WT, n= 13 KI/KI). **(B)** Water consumption and **(C)** chow consumption also showed no difference between genotypes. **(D)** Urine volume voided was decreased in the mutant animals compared to pre-challenge state and was decreased compared to WT on Day 6. **(E)** Fecal mass excreted was also decrease in the mutant animals compared to pre-challenge state. There were 5 WT males, 5 WT females, 7 KI/KI males, and 6 KI/KI females in this data set. Data is presented as mean \pm SEM *P < 0.05, **P < 0.01 using a 2-way ANOVA, Tukey’s multiple comparison test. *Please note, not all significant bars are shown for clarity, only comparing pre- and post-diet and between genotypes at each time point.*

R607H KI/KI and L919X KI/KI dRTA mutant mice have high plasma sodium and chloride following the acid challenge.

Following the analysis of metabolic cage parameters, we moved to analyze the ion concentrations and pH of plasma in our mice for evidence of ion imbalance (**Table 3.6, Table 3.7**). Interestingly, both dRTA mutant animals had high plasma sodium and chloride compared to WT mice following the acid load (**Table 3.6, Table 3.7**). This phenotype has not been previously reported in human dRTA patients^{1, 123}. However, while not significant, both WT and mutant mice showed some reduction in water consumption during this challenge. Therefore, hypernatremia and hyperchloremia may be a secondary cause of dehydration. Regardless, these mice display interesting and disrupted balance in plasma ions that will require further investigation. In addition to this phenotype, the L919X KI/KI mice displayed a more acidic plasma pH ($p = 0.0506$) (**Table 3.7**) indicating that the acid challenge induced acidosis (suggestive of an incomplete dRTA phenotype). This however was not pronounced in the R607H KI/KI mice (**Table 3.6**).

Table 3.6. Plasma Characterization of WT and R607H AE1 KI/KI Mice Following 6 Days Acid Challenge

Parameter	Units	WT (n=10)	R607H AE1 KI/KI (n = 13)	p-value
Na ⁺	mM	152.1 ± 0.87	157.8 ± 2.83	0.0472
Cl ⁻	mM	123.3 ± 2.07	130.6 ± 2.79	0.0480
K ⁺	mM	5.127 ± 0.16	5.111 ± 0.42	0.3997
HCO ₃ ⁻	mM	21.72 ± 1.48	18.90 ± 1.25	0.1733
pH		7.272 ± 0.04	7.239 ± 0.03	0.5300
TCO ₂	mmHg	23.00 ± 1.54	20.11 ± 1.20	0.1705
BUN	mg/dl	22.36 ± 1.88	31.89 ± 5.52	0.1670
Glucose	mg/dl	157.1 ± 10.65	152.3 ± 9.16	0.7450
HCT	%	39.18 ± 0.83	38.56 ± 1.06	0.6415
pCO ₂	mmHg	44.84 ± 3.66	43.82 ± 2.52	0.8285
AnGAP	mM	12.00 ± 0.67	12.14 ± 0.55	0.8793
Hb	g/dl	13.33 ± 0.28	13.11 ± 0.36	0.6366
BEecf	mM	-5.091 ± 1.95	-8.444 ± 1.64	0.1153

Data is presented as mean ± SEM. Student's T-Test or Mann-Whitney test used where appropriate. Significant data is bolded.

Table 3.7. Plasma Characterization of WT and L919X AE1 KI/KI Mice Following 6 Days Acid Challenge

Parameter	Units	WT (n=11)	L919X AE1 KI/KI (n = 9)	p-value
Na ⁺	mM	150.0 ± 0.88	157.6 ± 0.90	< 0.0001
Cl ⁻	mM	125.6 ± 0.88	135.2 ± 1.09	< 0.0001
K ⁺	mM	4.556 ± 0.11	4.462 ± 0.14	0.6267
HCO ₃ ⁻	mM	16.39 ± 0.95	15.32 ± 0.73	0.3839
pH		7.183 ± 0.02	7.132 ± 0.02	0.0506
TCO ₂	mmHg	17.78 ± 0.98	16.77 ± 0.81	0.3794
BUN	mg/dl	28.67 ± 1.90	36.39 ± 1.48	0.0040
Glucose	mg/dl	162.9 ± 10.62	133.5 ± 5.02	0.0120
HCT	%	37.67 ± 0.93	37.15 ± 0.50	0.6057
pCO ₂	mmHg	43.47 ± 2.03	45.78 ± 2.24	0.5015
AnGAP	mM	12.56 ± 1.06	11.60 ± 0.67	0.1819
Hb	g/dl	12.81 ± 0.32	12.63 ± 0.18	0.5969
BEecf	mM	-12.00 ± 1.21	-11.38 ± 2.43	0.6101

Data is presented as mean ± SEM. Student's T-Test or Mann-Whitney test used where appropriate. Significant data is bolded.

After an acid challenge, both dRTA mutant mice have alkaline urine pH and the L919X KI/KI mice show a urinary sodium loss.

Both L919X KI/KI and R607H KI/KI mice continued to exhibit an alkaline urine, when compared with WT counterparts following the diet (**Figure 3.13 A, C**), again affirming the dRTA phenotype in our mice ^{73, 123}. However, mutant mice did show a strong ability to acidify their urine although not to the same extent as WT littermates (**Figure 3.13 B, D**).

The acid challenge had no impact on urinary sodium, potassium, and chloride concentrations in the R607H KI/KI mice and WT counterparts, despite the hypernatremia and hyperchloremia (**Table 3.6, Figure 3.14 A - C**). Despite this, the R607H KI/KI mice had increased urinary osmolality compared to baseline and to WT mice (**Figure 3.15 A**). The L919X KI/KI mice also had no changes in urinary chloride and potassium excretion compared to steady state or to WT mice (**Figure 3.14 E, F**), but the L919X KI/KI mice showed significant urinary sodium loss compared to steady state (**Figure 3.14 D**), again despite hypernatremia and hyperchloremia (**Table 3.7**). In alignment, the L919X KI/KI mice had higher urine osmolality following the acid challenge, while the WT mice had no change (**Figure 3.15 B**). Notably, the jump in chloride excretion seen in both WT and both mutant strains reflects the chloride loading due to the NH₄Cl challenge.

In summary, urine analysis from the L919X KI/KI and R607H KI/KI mice confirmed alkaline urine consistent with dRTA, with L919X KI/KI mice showing increased urinary sodium loss and elevated urine osmolality post-acid challenge compared to WT counterparts.

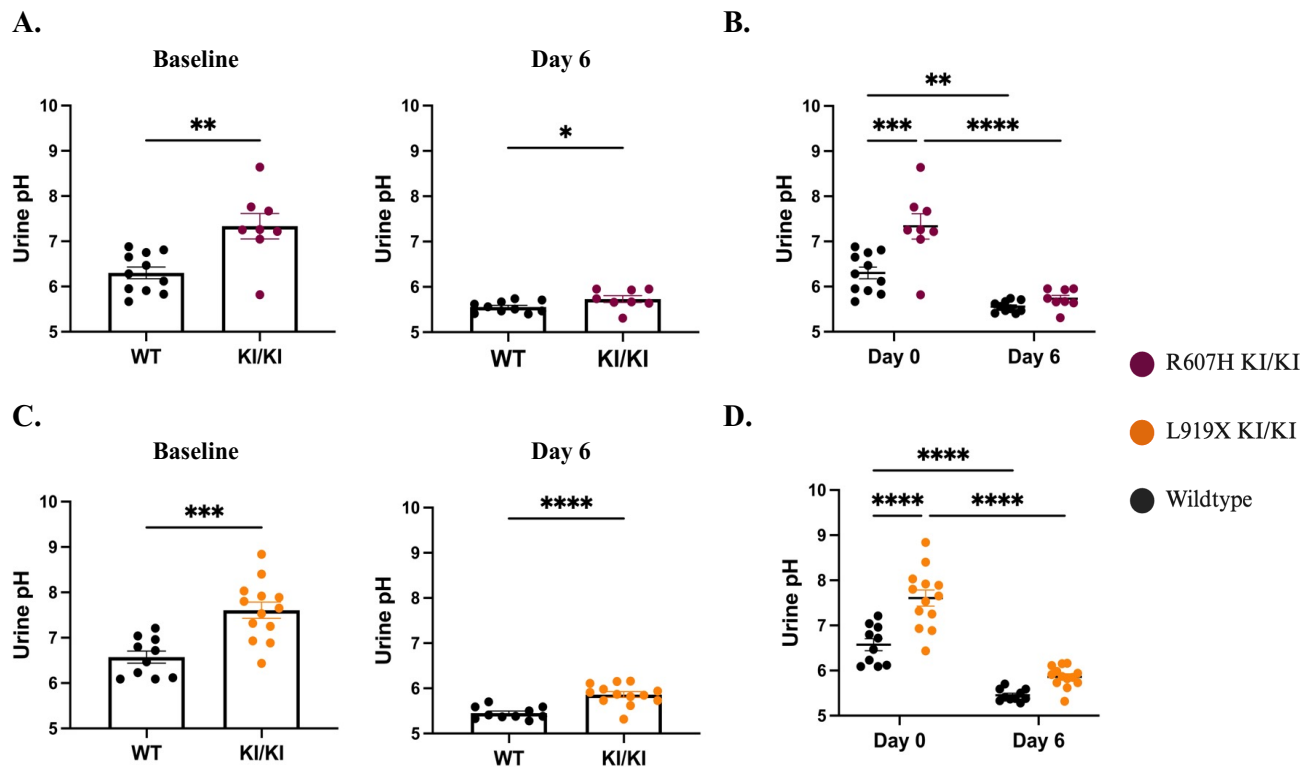


Figure 3.13 Urinary pH remains alkaline in dRTA mutant mice compared to WT before and after a 6-day acid challenge. **A)** R607H KI/KI mice maintained an alkaline urine pH both at baseline and post-diet. **B)** Overall, both genotypes showed an ability for urine acidification. **C)** L919X KI/KI mice also exhibited alkaline urine pH before and after the acid challenge. **D)** Throughout the experiment, both WT and mutant genotypes demonstrated the ability to acidify urine. Data represent mean \pm SEM, * $P < 0.05$, ** $P < 0.01$, *** $P < 0.001$, **** $P < 0.0001$ using unpaired Student's *t*-test, Mann-Whitney test, or 2-way ANOVA with Tukey's multiple comparison test. *Only significant comparisons between pre- and post-diet and between genotypes at each time point are shown for clarity.*

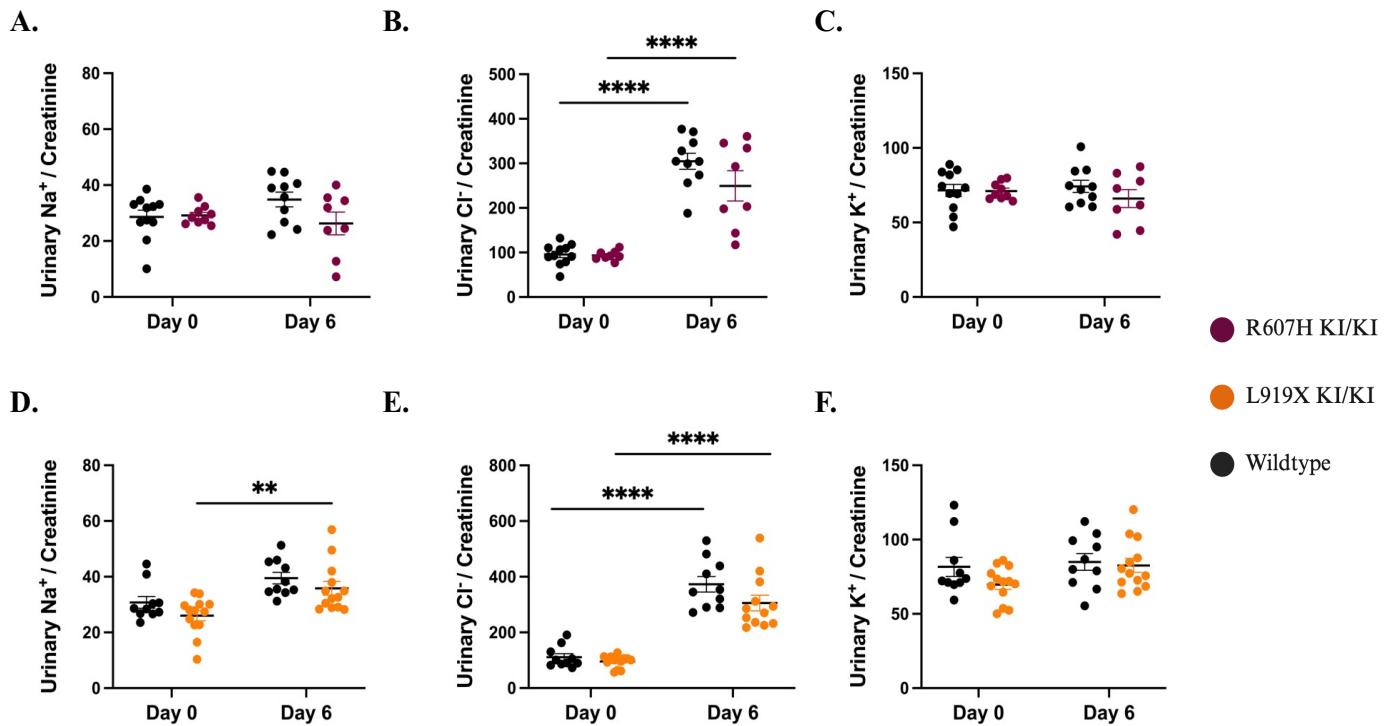


Figure 3.14 L919X KI/KI mice significantly increase their urinary sodium excretion after the acid diet. R607H KI/KI mice exhibited similar excretion levels of **A)** sodium, **B)** chloride, and **C)** potassium as WT mice. **D)** L919X KI/KI mice showed increased sodium excretion compared to steady state, indicating urinary sodium loss due to the acid challenge. However, **E)** chloride and **F)** potassium excretion remained comparable between L919X KI/KI and WT mice. Urine ion data was normalized to urinary creatinine and are presented as mean \pm SEM, **P < 0.01, ****P < 0.0001 using 2-way ANOVA with Tukey's multiple comparison test. *Significant bars are depicted for pre- and post-diet and between genotypes at each time point for clarity.*

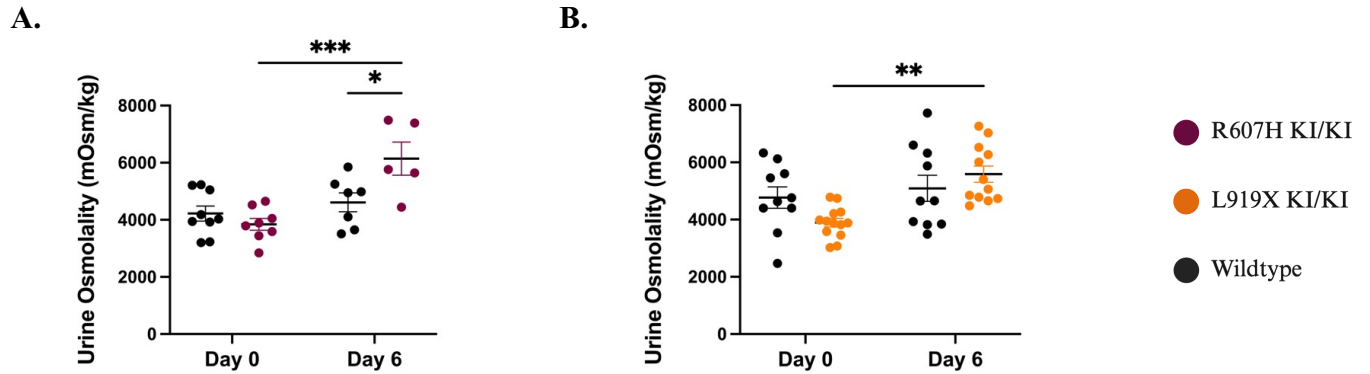


Figure 3.15 R607H KI/KI have a more concentrated urine than WT littermates following the acid diet. Urine samples were frozen, thawed, and diluted with water before osmolality analysis. **A)** While R607H KI/KI and WT mice showed similar urine osmolality at baseline, mutant mice exhibited a significant increase post-diet and from steady state. **B)** Similarly, L919X KI/KI mice did not differ in baseline urine osmolality compared to WT but showed a significant increase compared to steady state. Data are presented as mean \pm SEM, **P < 0.01, ***P < 0.001 using 2-way ANOVA with Tukey's multiple comparison test.

L919X KI/KI mice given an acid load have increased claudin-10b expression compared to WT mice.

Given the urinary sodium waste in L919X KI/KI mice after the acid diet, we were prompted to next determine if there were changes in acid-base and salt transporters in the nephrons of these mice. Our investigation started with gene expression of CD markers (**Figure 3.16**). Specifically, qRT-PCR was performed to identify gene expression of Ae1, B1-H⁺-ATPase, Ae4, pendrin, NDCBE, and claudin-4. Ae1 was significantly decreased in L919X KI/KI mice as expected (**Figure 3.16 A**), suggesting a decreased abundance of A-ICs ⁷³. There was a trend for decreased B1-H⁺-ATPase, pendrin, and Ae4 (**Figure 3.16 B, D, E**) but a trend for increased claudin-4 and NDCBE gene expression (**Figure 3.16 C, F**). No significant differences in gene expression of ENaC (trend for increase in gamma ENaC), ROMK, or distal convoluted tubule marker, NCC was seen (**Figure 3.17 E - H**).

Given the lack of significant differences found in the CD, our next area of investigation focused on a prior nephron segment also responsible for urine acidification and electrolyte balance, the TAL ^{72,78,129,132} (**Figure 3.17 A - C**). We investigated gene expression of NKCC2, NHE3, and claudin-10b. There was no change in NHE3, a trend for a decrease in NKCC2 gene expression, and a significant increase in claudin-10b. Claudin-10b is a critical component of the TAL tight junction allowing paracellular sodium transport ⁸⁹.

Altogether, these results confirmed a decreased abundance of A-ICs in the L919X KI/KI mice and highlight potential paracellular pathway upregulation during dRTA pathogenesis in these mice.

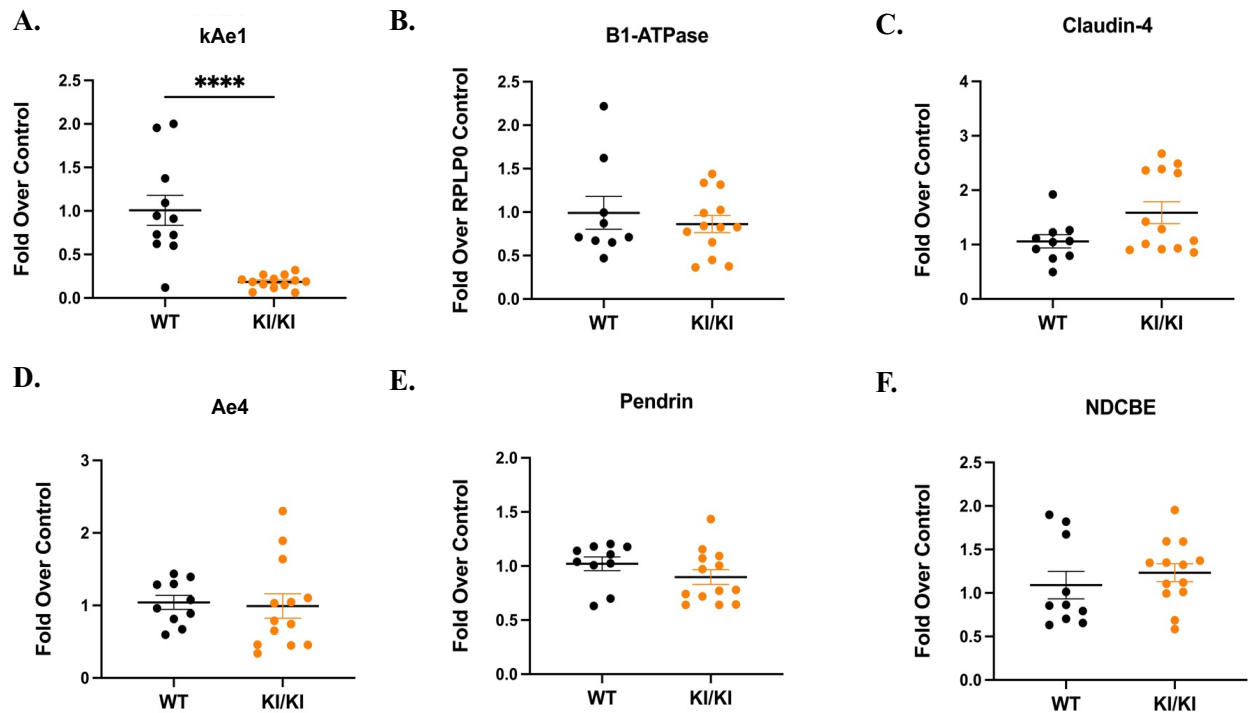


Figure 3.16 Gene expression of IC marker Ae1 is decreased in L919X KI/KI mice compared to WT mice. **A)** mRNA abundance of Ae1 was significantly decreased in KI/KI mice compared to WT mice (n = 10 WT, n = 13 KI/KI). mRNA levels of **B)** B1 - H⁺-ATPase, **C)** claudin-4, **D)** Ae4, **E)** pendrin, and **F)** NDCBE did not significantly differ between WT and KI/KI mice. Results are normalized to RPLP0 mRNA abundance. Data are presented as mean ± SEM, ****P < 0.001 using unpaired Student's t-test or Mann-Whitney test. Black dots represent WT animals, and orange dots represent L919X KI/KI mice.

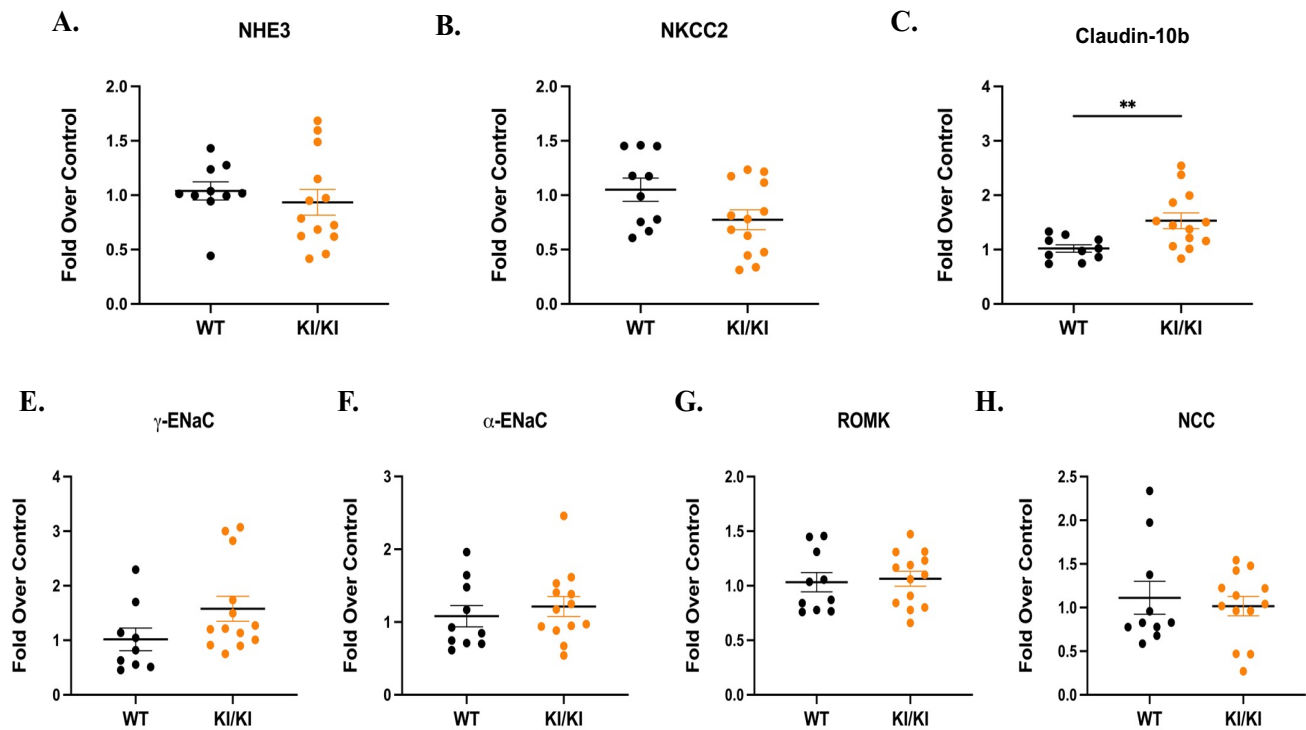


Figure 3.17 Gene expression of tight junction protein claudin-10b is higher in L919X KI/KI mice compared to WT mice. mRNA abundance of **A)** NHE3 and **B)** NKCC2 did not significantly differ between genotypes. **C)** Claudin-10b gene expression was significantly increased in KI/KI mice compared to WT. Both **E - F)** ENaC subunits, **G)** ROMK, and **H)** NCC showed no significant differences between WT and KI/KI mice. Results are normalized to RPLP0 mRNA abundance. Data are presented as mean \pm SEM, ******P < 0.01 using unpaired Student's t-test or Mann-Whitney test. Black dots represent WT animals, and orange dots represent L919X KI/KI mice.

DIETARY CHALLENGE 3: SALT-DEPLETED ACID LOAD

Following the 14-day salt-depleted acid load, dRTA mutant lose significant body weight, decrease their water consumption, and excrete less urine and feces.

Results from the previous dietary challenges suggested that the dRTA mutant mice have abnormal CD function and improper renal ion handling. To further challenge the mice and assess whether they are a suitable model to study a urinary sodium losing phenotype, we fed WT and dRTA mutant mice a salt-depleted acid diet (**Figure 2.1**). This diet was designed to recreate a study by Sebastien et al. revealing a urinary sodium wasting phenotype in dRTA patients on a salt-restricted diet for 8 - 10 days¹⁰⁰. Similarly, to our previous diet challenges, our analysis focused on physiological parameters, blood, and urine composition, following by whole kidney analysis.

After the salt-depleted acid load, both R607H KI/KI and L919X KI/KI mice lost significant weight (**Figure 3.18 A, Figure 3.19 A**) and both genotypes of each mutant strain drank significantly less water (**Figure 3.18 B, Figure 3.19 B**). In agreement, WT and L919X KI/KI mice produced significantly less urine volume and feces by Day 14 of the experiment (**Figure 3.18 D, E, Figure 3.19 D, E**). This trend was mirrored in R607H KI/KI and WT mice, but R607H KI/KI mice excreted significantly less urine volume compared to WT mice at Day 14 (**Figure 3.19 E**). Interestingly, chow consumption did not change pre- to post-diet in either mouse strain or WT mice (**Figure 3.18 C, Figure 3.19 C**).

Altogether, this data highlights the stress caused by the diet on both dRTA mutant animals and WT counterparts, specifically potential dehydration in both groups due to decreased water consumption.

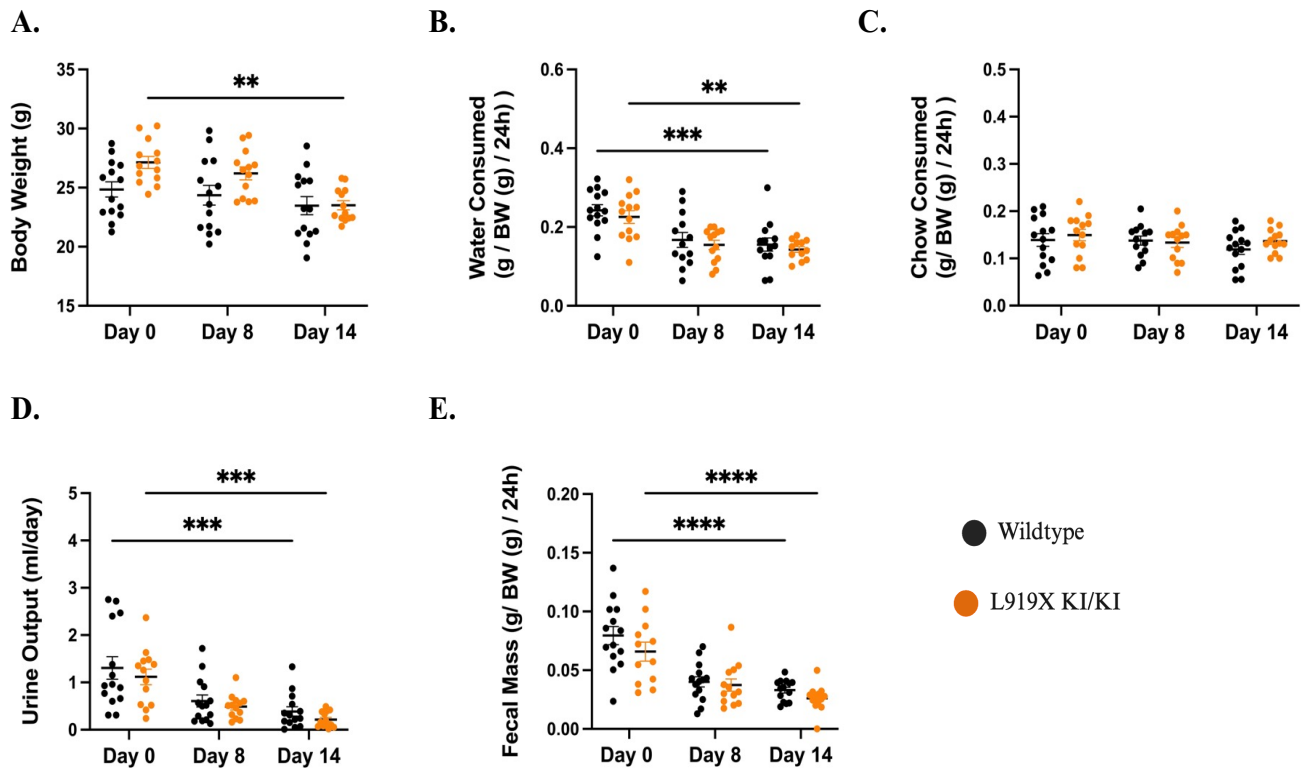


Figure 3.18 Both L919X KI/KI mice and WT mice drink less, produce less urine and feces over a 14-day salt-depleted acid load. **A)** Mutant mice exhibited a significant reduction in body weight compared to baseline (n=14 for both genotypes). **B)** Water consumption significantly decreased by Day 14 for both WT and mutant mice while **C)** chow consumption did not defer. **D)** Urine volume voided and **E)** fecal mass excreted also significantly decreased by Day 14 for both groups. There were 6 WT males, 8 WT females, 9 KI/KI males, and 4 KI/KI females in this data set. Data presented as mean \pm SEM, **P < 0.01, ***P < 0.001, ****P < 0.0001 with a 2-way ANOVA, Tukey's multiple comparison test. *Only significant comparisons between pre- and post-diet and between genotypes at each time point are shown for clarity.*

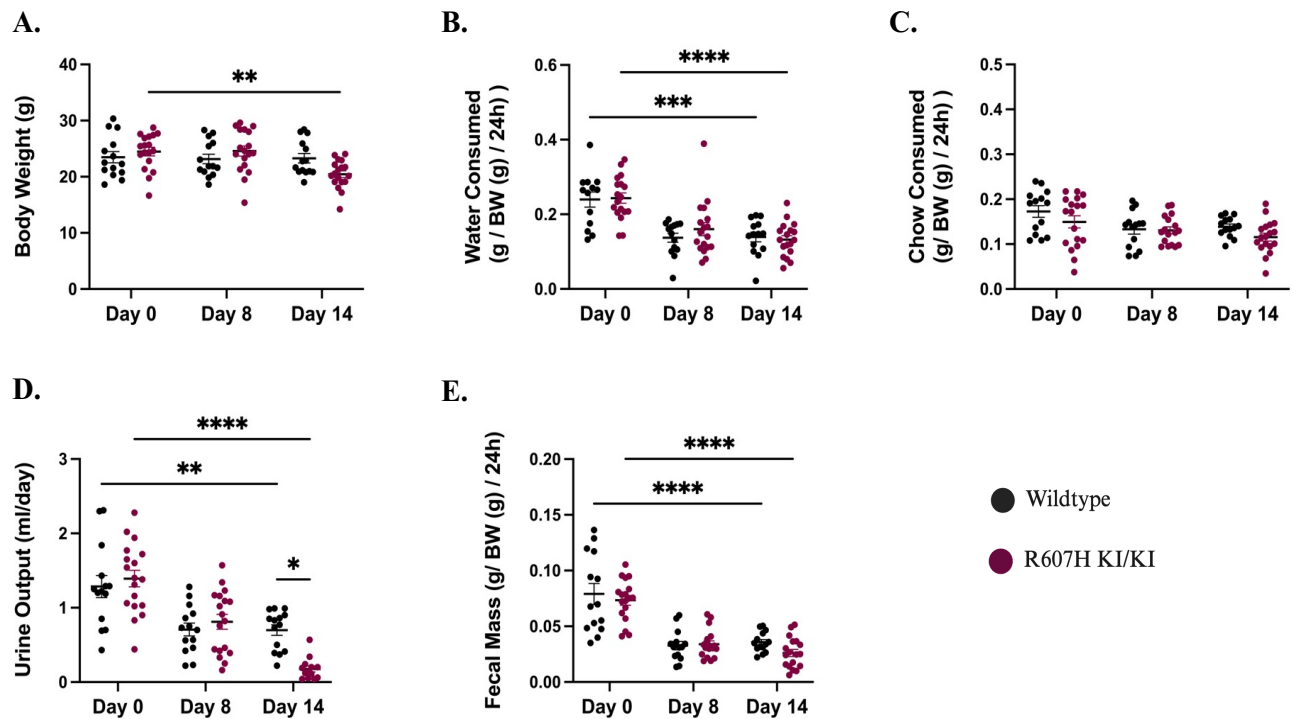


Figure 3.19 R607H KI/KI mice produce less urine than WT mice after a 14-day salt-depleted acid load, although both genotypes reduce their water consumed and fecal mass produced.

A) Mutant mice displayed a significant reduction in body weight compared to baseline (n=14 for WT, n=18 for KI/KI). **B)** Water consumption significantly decreased by Day 14 for both WT and mutant mice while **C)** chow consumption remained stable throughout the diet for both genotypes. **D)** Urine volume voided and **E)** fecal mass excreted also significantly decreased by Day 14 for both groups, with mutant mice producing significantly less urine volume than WT at Day 14. There were 7 WT males, 7 WT females, 10 KI/KI males, and 8 KI/KI females in this data set. Data presented as mean \pm SEM, **P < 0.01, ***P < 0.001, ****P < 0.0001 with a 2-way ANOVA, Tukey's multiple comparison test. *Only significant comparisons between pre- and post-diet and between genotypes at each time point are shown for clarity.*

Salt- depleted acid load reveals hypernatremia and hyperchloremia, coupled with increased renal renin in the dRTA mutant mice.

Following the diet challenge (Day 14), R607H KI/KI mice showed signs of metabolic acidosis through significantly decreased plasma pH and plasma bicarbonate (**Figure 3.20 A**), while L919X KI/KI mice only showed a trend for acidosis ($p = 0.068$) (**Figure 3.21 A**). Notably, and similar to the acid challenge alone, both KI/KI mutant mice had hypernatremia and hyperchloremia compared to WT littermates (**Figure 3.20, Figure 3.21**). Having observed this result in two diet challenges, we predicted whether the renin-angiotensin-aldosterone axis (RAAS) or dehydration was involved. Indeed, both dRTA mutant mice showed higher renal renin mRNA abundance compared to WT (**Figure 3.20 B, Figure 3.21 B**). Blood pressure measurements were taken at baseline, Day 8, and Day 14 of this diet challenge (**Figure 3.22**). R607H KI/KI mice showed a trend for increased systolic blood pressure (not significant) on Day 14 compared to WT (**Figure 3.22 A**), with an opposite trend for diastolic blood pressure (not significant) (**Figure 3.22 B**). Only preliminary measurements have been made for L919X KI/KI mice, shown in **Figure 3.22 C, D**, so nothing can be concluded yet. Exploring plasma renin levels instead might yield a different outcome as the elevation in renal renin could be a compensatory response to reduced salt delivery to the distal nephron. To investigate evidence of dehydration, we quantified water consumption (**Figure 3.18 B, Figure 3.19 B**), urine osmolality (**Figure 3.23**), and plasma hemoglobin and hematocrit levels (**Figure 3.20 A, Figure 3.21 A**) in both KI/KI strains compared to WT counterparts. Only R607H KI/KI mice had increased hemoglobin compared to WT mice (**Figure 3.20 A**). Ultimately, these results point to some evidence of dehydration, particularly in the R607H KI/KI mice.

A.

Parameter	Units	WT (n=14)	R607H AE1 KI/KI (n = 18)	p-value
Na ⁺	mM	145.2 ± 0.88	156.4 ± 0.90	< 0.0001
Cl ⁻	mM	126.8 ± 1.96	138.6 ± 0.54	< 0.0001
K ⁺	mM	4.557 ± 0.23	4.406 ± 0.19	0.6069
HCO ₃ ⁻	mM	14.15 ± 0.92	11.64 ± 0.78	0.0448
pH		7.192 ± 0.03	7.085 ± 0.02	0.0016
TCO ₂	mmHg	15.29 ± 0.96	12.83 ± 0.80	0.0572
BUN	mg/dl	22.50 ± 1.73	34.17 ± 3.62	0.0026
Glucose	mg/dl	163.2 ± 11.93	118.8 ± 7.28	0.0024
HCT	%	34.00 ± 2.18	32.56 ± 2.23	0.8434
pCO ₂	mmHg	46.21 ± 1.43	38.56 ± 2.40	0.4397
AnGAP	mM	10.08 ± 2.07	13.43 ± 1.46	0.6004
Hb	g/dl	11.56 ± 0.74	13.55 ± 0.19	0.0489
BEecf	mM	-14.07 ± 1.27	-18.22 ± 0.97	0.0129

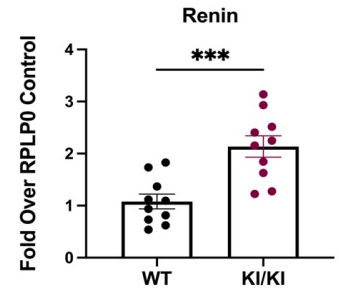
B.

Figure 3.20 After the salt-depleted acid load, R607H KI/KI mice are acidotic, hypernatremic, hyperchloremic, and their kidneys have elevated renin gene expression compared to WT mice. **(A)** The R607H KI/KI mice have hypernatremia, hyperchloremia, and have low plasma pH and bicarbonate after this diet challenge. **(B)** On Day 14, renin mRNA abundance is significantly higher in the mutant animals compared to WT. mRNA abundance was normalized to RPLP0 mRNA. All data is presented as mean ± SEM, ***P < 0.001, with an unpaired Student's t-test or Mann-Whitney test.

A.

Parameter	Units	WT (n=14)	L919X AE1 KI/KI (n = 14)	p-value
Na ⁺	mM	149.4 ± 0.64	156.4 ± 1.15	< 0.0001
Cl ⁻	mM	126.9 ± 2.09	135.1 ± 0.90	0.0140
K ⁺	mM	4.777 ± 0.15	4.669 ± 0.17	0.6430
HCO ₃ ⁻	mM	15.63 ± 0.94	13.88 ± 0.47	0.1164
pH		7.170 ± 0.03	7.131 ± 0.01	0.0683
TCO ₂	mmHg	17.62 ± 0.79	15.15 ± 0.50	0.0147
BUN	mg/dl	23.75 ± 0.95	33.62 ± 1.72	< 0.0001
Glucose	mg/dl	148.9 ± 12.93	131.92 ± 5.05	0.2452
HCT	%	37.38 ± 1.27	37.46 ± 1.26	0.9713
pCO ₂	mmHg	42.84 ± 2.58	41.72 ± 1.63	0.7216
AnGAP	mM	13.33 ± 1.69	13.09 ± 0.95	0.9042
Hb	g/dl	12.70 ± 0.43	12.74 ± 0.43	0.9713
BEecf	mM	-12.93 ± 1.29	-15.31 ± 0.60	0.1169

B.

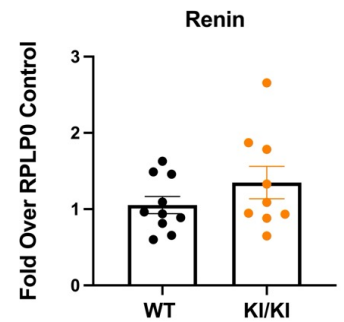


Figure 3.21 L919X KI/KI mice are hypernatremic, hyperchloremia, have elevated BUN, reduced TCO₂ and trend for higher renal renin mRNA abundance compared to WT mice.

(A) The L919X KI/KI mice have hypernatremia, hyperchloremia, but only show a trend for low plasma pH after this diet challenge. (B) On Day 14, the mutant mice exhibits a trend for higher renin mRNA abundance compared to WT (n = 10 WT, n = 9 KI/KI). mRNA abundance was normalized to RPLP0 mRNA. All data is presented as mean ± SEM compared with an unpaired Student's t-test or Mann-Whitney test.

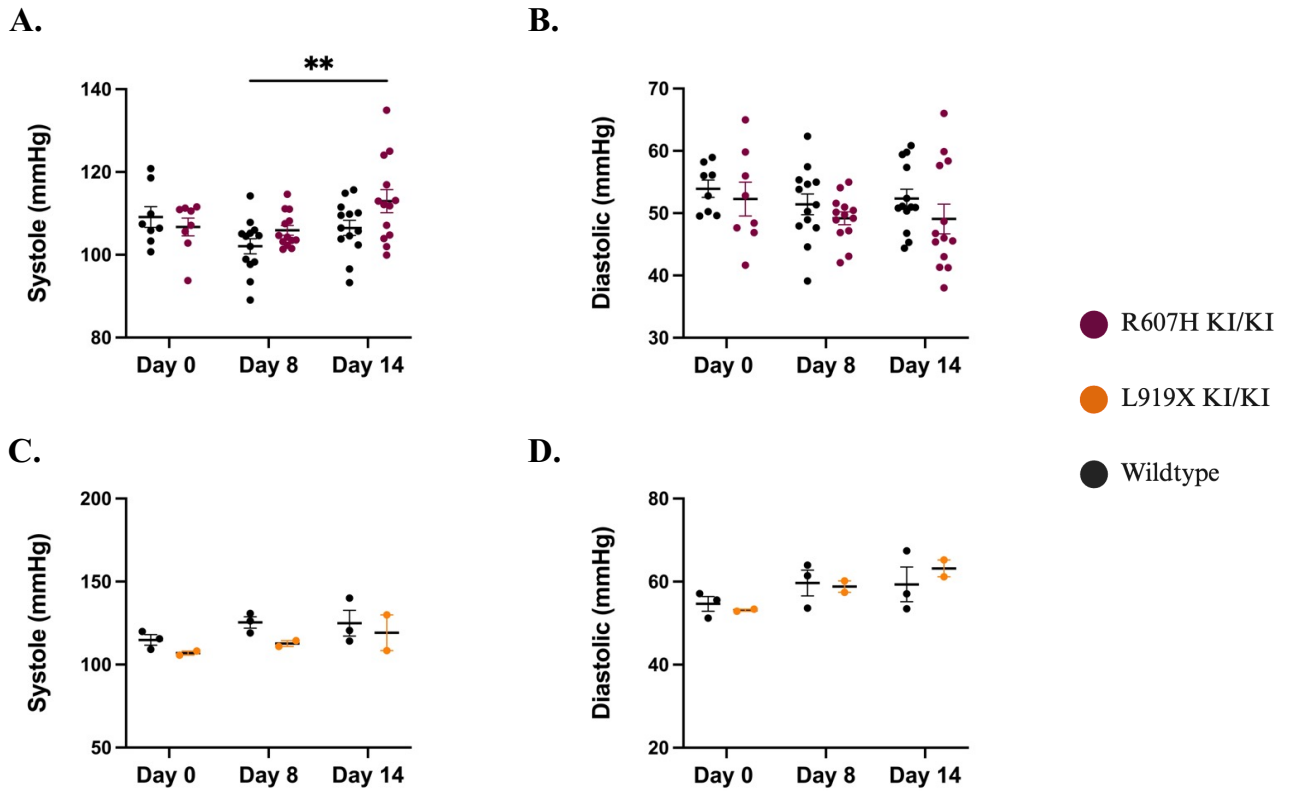
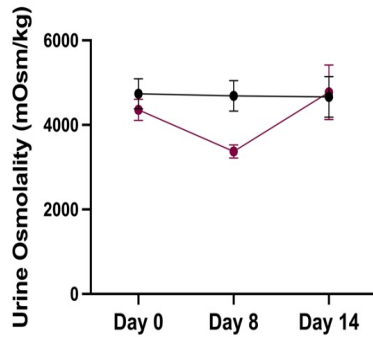


Figure 3.22 R607H KI/KI have a higher systolic blood pressure at Day 14 compared to WT mice at Day 8. **A)** The R607H KI/KI mice showed a trend for increased systolic blood pressure on Day 14 (n = 14 WT, n = 13 KI/KI). **B)** but showed the opposite trend for diastolic blood pressure. L919X KI/KI **C)** systolic and **D)** diastole results are currently preliminary (n = 3 WT and n = 2 KI/KI). Data is presented as mean \pm SEM **P < 0.01, using a 2-way ANOVA, Tukey's multiple comparison test.

A.



B.

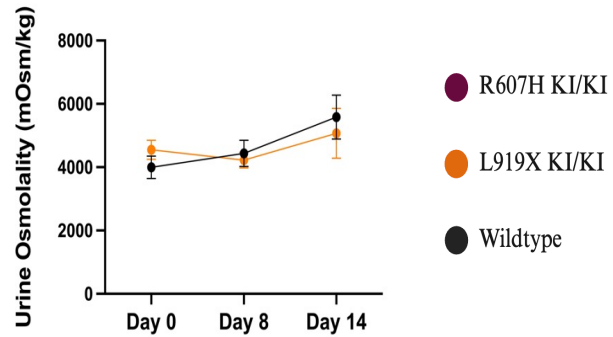


Figure 3.23 There is no significant difference in urine osmolality between the **R607H KI/KI** or **L919X KI/KI** mice and **WT** littermates following the salt-depleted acid load. Urine was frozen and thawed and diluted with water prior to osmolality analysis. **A)** R607H KI/KI and WT counterparts did not differ in urine osmolality (n = 14 WT, n = 18 KI/KI). **B)** L919X KI/KI also did not display different urine osmolality compared to (WT, n = 14 WT, n = 14 KI/KI). All data is presented as mean \pm SEM compared with a 2-way ANOVA, Tukey's multiple comparison test.

dRTA mutant mice display alkaline urine pH and decreased ammonium excretion compared to WT mice.

Consistently with all prior diet challenges, both the L919X KI/KI and R607H KI/KI mice exhibited alkaline urine levels compared with WT counterparts on Day 14 of the salt-depleted acid load (**Figure 3.24 A, C**). Additionally, R607H KI/KI mice excreted less urinary ammonium compared to WT, with a slight trend for less in L919X KI/KI mice (**Figure 3.24 E, F**). While the mutant's urine was still alkaline compared to WT, they do exhibit a decrease in urine pH from Day 0 to Day 14, suggesting the presence of a mechanism for urinary acidification in these mice despite the decreased abundance of A-ICs (**Figure B, D**).

On the salt- depleted acid load, R607H KI/KI and L919X KI/KI mice have a salt wasting nephropathy.

To unveil a potential sodium-wasting phenotype in dRTA mutant mice, we examined their urinary composition after this challenge. On Day 14, a pronounced urinary sodium-loss in both R607H KI/KI and L919X KI/KI dRTA mutant mice was revealed (**Figure 3.25 A, Figure 3.26 A**), in agreement with observations from dRTA patients in similar physiological conditions¹⁰⁰. Interestingly, distinct phenotypes were observed in these dRTA KI/KI mouse models concerning urinary potassium and chloride excretion (**Figure 3.25, Figure 3.26**). R607H KI/KI mice displayed a notably lower urinary excretion of potassium and chloride (**Figure 3.25 B, C**). In contrast, the L919X KI/KI mice displayed a urinary chloride loss (**Figure 3.26 B**), but did not exhibit differences in urinary potassium excretion compared to their WT counterparts (**Figure 3.26 C**). These experiments demonstrate that in mice, the Ae1 L919X KI/KI and R607H KI/KI mutations lead to two major features observed in patients suffering with type 1 dRTA^{73,100,122} such as a urinary sodium losing phenotype and inability to maximally acidify their urine.

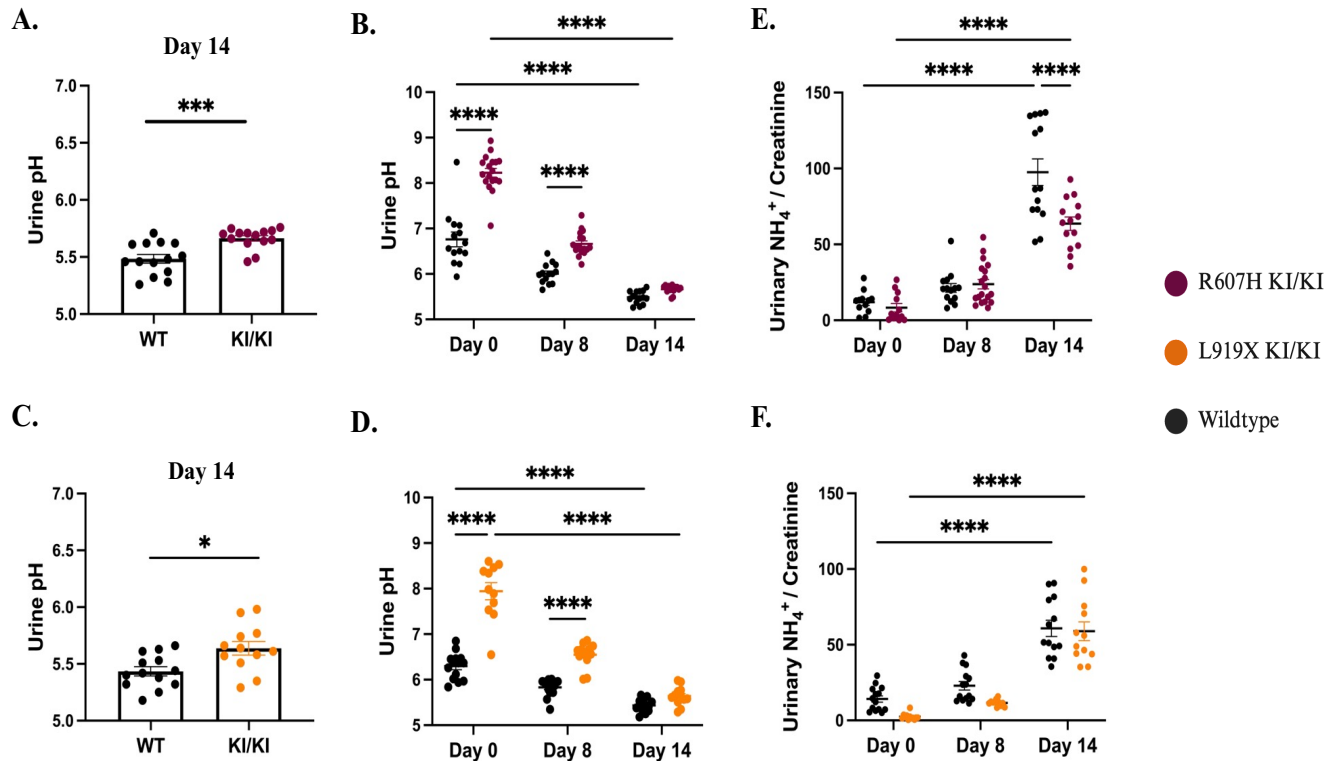


Figure 3.24 The dRTA mutant mice have an alkaline urine and R607H KI/KI mice secrete less urinary ammonium than WT littermates at Day 14 of the salt-depleted acid challenge.

A) R607H KI/KI mice showed alkaline urine following the diet (n = 14 WT, n = 18 KI/KI), with **B)** both genotypes decreasing urine pH. **C)** L919X KI/KI mice also voided alkaline urine on Day 14 of the challenge (n = 14 WT, n = 14 KI/KI, but show **D)** a trend of decreased urine pH throughout the experimental period. **E)** R607H KI/KI mice have decreased urinary ammonium excretion while **F)** L919X KI/KI mice show no difference at Day 14. All data is presented as mean \pm SEM, **P < 0.01, ***P < 0.001, ****P < 0.0001 using an unpaired Student's t-test or Mann-Whitney test. or 2-way ANOVA, Tukey's multiple comparison test.

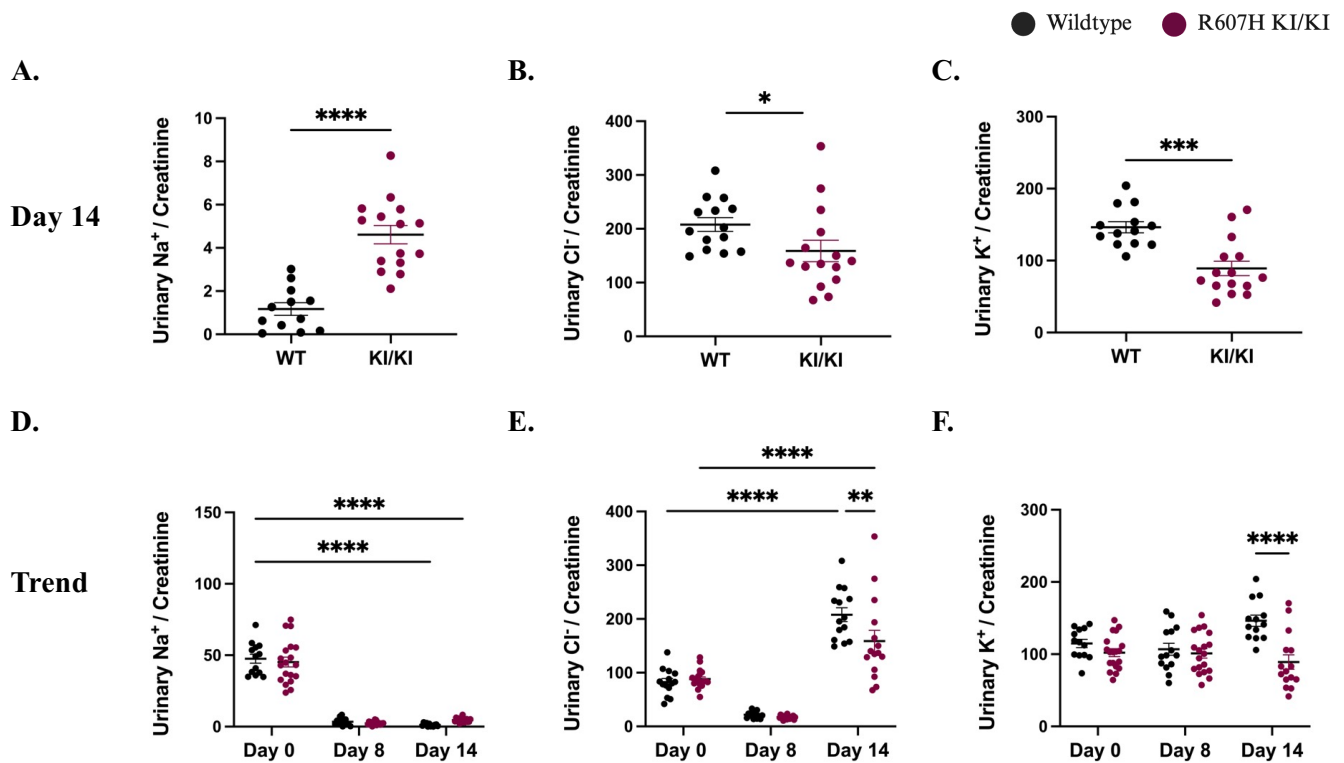


Figure 3.25 R607H KI/KI mice excrete more urinary sodium but less urinary potassium and chloride than WT mice on Day 14 of a salt-restricted acid load. **A)** R607H KI/KI mice exhibit increased urinary sodium but decreased **B)** chloride and **C)** potassium compared to baseline ($n = 14$ WT, $n = 18$ KI/KI). **D - E)** The trend analysis reveals expected responses from WT mice for sodium and chloride (overall decreased), and with **F)** potassium excretion notably increasing under salt-restriction. Data presented as mean \pm SEM; $**P < 0.01$, $***P < 0.001$, $****P < 0.0001$ using with unpaired Student's t-test, Mann-Whitney test, or 2-way ANOVA with Tukey's multiple comparison test. *Only significant comparisons between pre- and post-diet and between genotypes at each time point are shown for clarity.*

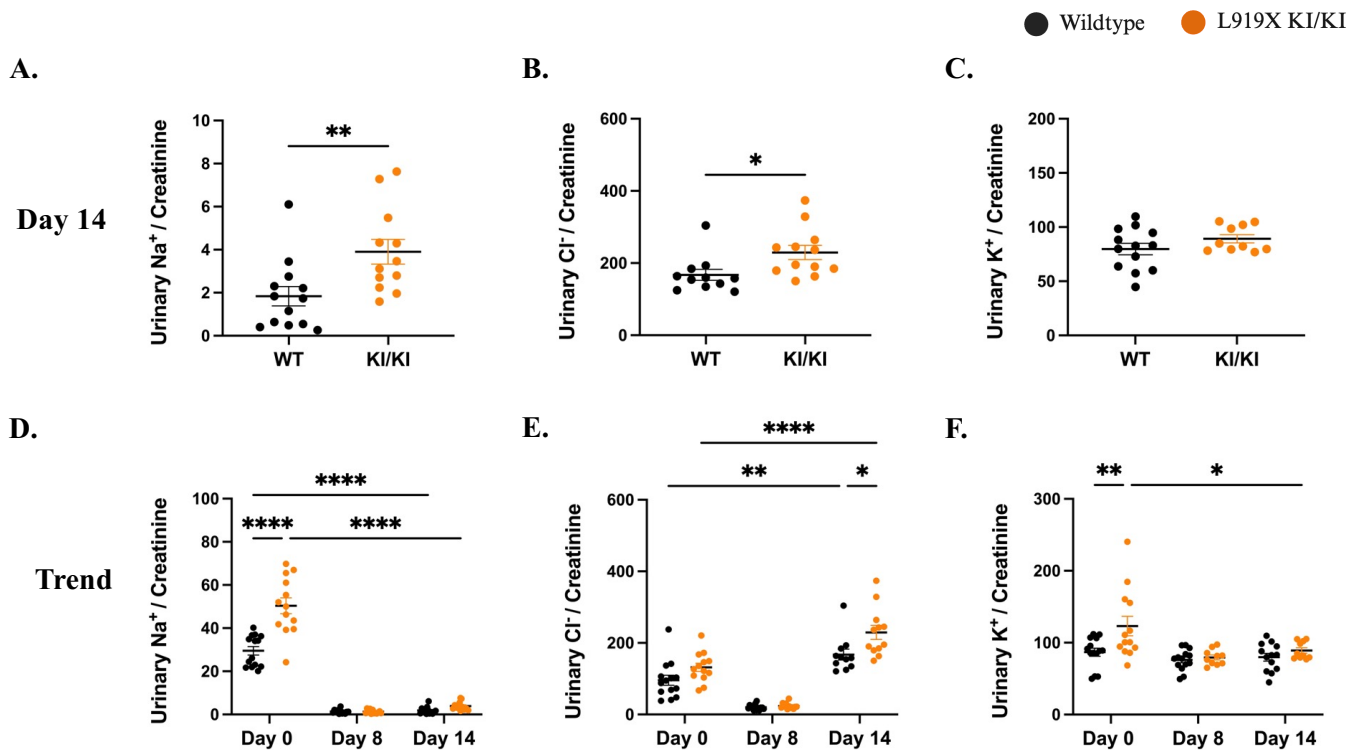


Figure 3.26 L919X KI/KI mice excrete more urinary sodium and chloride than WT mice on Day 14 of a salt-restricted acid load. A) L919X KI/KI mice show increased urinary sodium and B) chloride loss compared to WT, while C) urinary potassium levels were comparable to WT (n = 14 WT, n = 14 KI/KI). Trend analysis (D - F) illustrates changes after salt-restriction alone and following the addition of the acid challenge on Day 8. Data presented as mean \pm SEM, *P < 0.05, **P < 0.01, ****P < 0.0001 using with unpaired Student's t-test, Mann-Whitney test, or 2-way ANOVA with Tukey's multiple comparison test. *Only significant comparisons between pre- and post-diet and between genotypes at each time point are shown for clarity.*

Salt-restricted acid load results in downregulation gene expression of A-IC and B-IC markers, but upregulation of PC makers in R607H KI/KI mice.

Given the alkaline urine and urinary sodium loss observed in R607H KI/KI and L919X KI/KI mice following the salt-restricted acid load, we aimed next to understand the molecular mechanisms involved in contributing to this phenotype. We compared mRNA and protein levels of specific markers in the CD, TAL, and distal convoluted tubule in KI/KI mice and WT littermates (**Figure 3.27, Figure 3.28**). In agreement with the previously reported decreased IC number in R607H KI/KI mouse kidneys⁷³, kAe1 and B1-H⁺-ATPase mRNA abundances were reduced in both KI/KI mice (**Figure 3.27 A, B, Figure 3.28 A, B**). Consistently, B1-H⁺-ATPase protein abundance was also significantly reduced in both KI/KI mouse lines (**Figure 3.27 K, Figure 3.28 K**). Messengers for B-IC markers pendrin and Ae4 were significantly reduced in R607H KI/KI mice (**Figure 3.27 C, E**), with a similar trend in L919X KI/KI mice (**Figure 3.28 C, E**), although an increase in NDCBE mRNA abundance was observed in R607H KI/KI mice with a similar trend in L919X KI/KI mice (**Figure 3.27 D, Figure 3.28 D**). Together, these results highlight an overall decreased in IC markers in the dRTA mutant animals compared to WT, more significantly in the R607H KI/KI mutant mice.

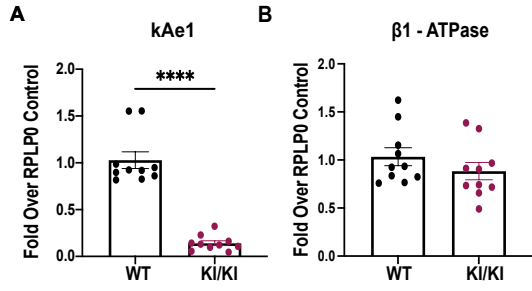
PC marker γ -ENaC mRNA and protein abundance showed a significant increase in R607H KI/KI mice (**Figure 3.27 G, L**) but did not differ in L919X KI/KI mice (**Figure 3.28 G, L**). The messenger and protein abundance of the distal convoluted tubule NCC was significantly lower in L919X KI/KI mice with a similar result in R607H KI mice (**Figure 3.27 J, M, Figure 3.28 J, M**). These results suggest an overall loss of distal nephron makers in the KI/KI mice but a potential upregulation of PC makers in R607H KI/KI mice.

TAL markers, NHE3 and NKCC2 are significantly decreased in R607H KI/KI mice with no changes in L919X KI/KI mice.

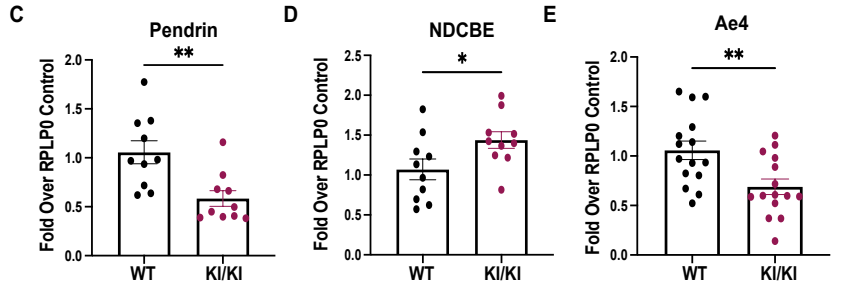
As completed in the acid challenge alone, we investigated markers of the TAL. This was also important given that at steady state, there were no differences in urinary ion excretion between genotypes of either strain. qRT-PCR was performed to assess mRNA abundance of NKCC2 and NHE3 in whole kidneys, with the caveat that NHE3 is also abundantly expressed in the proximal tubule. These levels did not differ between L919X KI/KI and WT counterparts (**Figure 3.28 H, I**) but were significantly decreased in R607H KI/KI mice compared to WT littermates (**Figure 3.27 H, I**). Originally, we hypothesized an increased in TAL markers in the KI/KI mutant strains, due to their dysfunctional CDs, therefore these results were unexpected and suggest other compensatory mechanisms. Overall, however, these results support changes to the Henle's loop during a challenge to acid-base and sodium reabsorption in the dRTA mutant mice.

● Wildtype ● R607H KI/KI

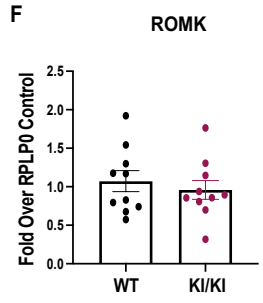
Alpha - Intercalated Cell Markers



Beta - Intercalated Cell Markers



Principal Cell Markers



Prior Nephron Segments

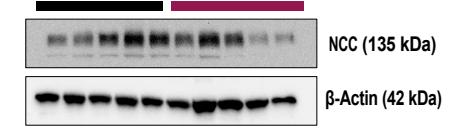
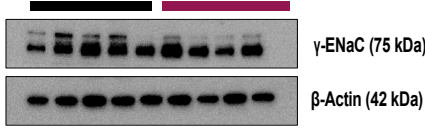
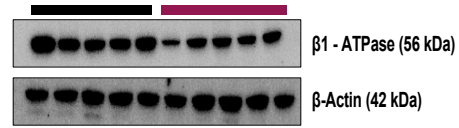
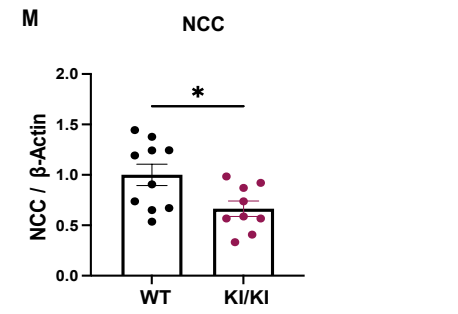
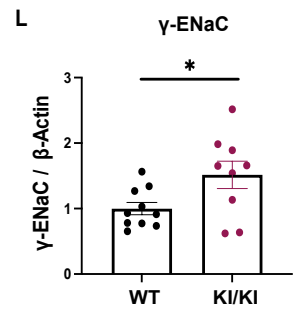
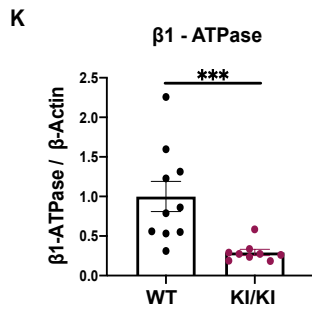
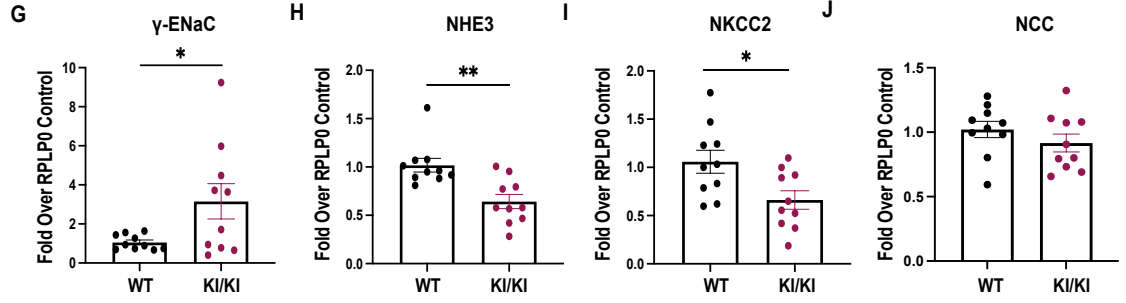
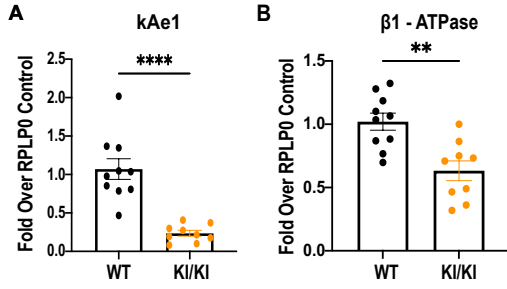


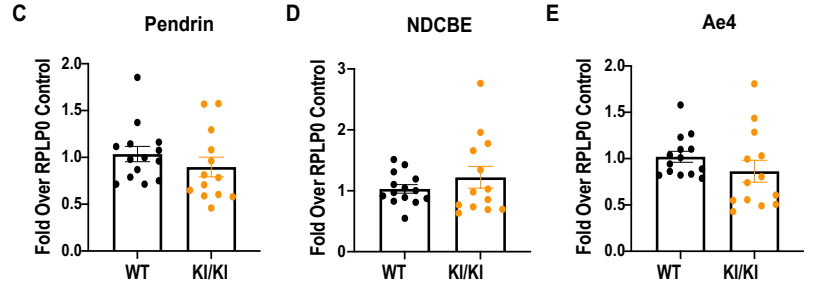
Figure 3.27 Gene expression and protein abundance of markers of the IC, TAL, and distal convoluted tubule are decreased, while ENaC (PC marker) is significantly increased in R607H KI/KI mice versus WT littermates. A) kAe1 B) and B1-ATPase, along with protein expression of K) B1-ATPase was decreased in the KI/KI mice. B-IC markers C) pendrin was significantly decreased, D) NDCBE was significantly increased, and E) Ae4 was significantly decreased in the KI/KI mice. PC marker F) ROMK showed no differences between genotypes but G, L) gamma-ENaC was significantly increased in the KI/KI mice. Gene and protein expression of DCT marker J, M) NCC was reduced in KI/KI mice, while H) NHE3 and I) NKCC2 were significantly lower compared to WT mice. Data presented as mean \pm SEM, **P < 0.01, *P < 0.001, ****P < 0.0001 using with unpaired Student's t-test, Mann-Whitney test.**

● Wildtype ● L919X KI/KI

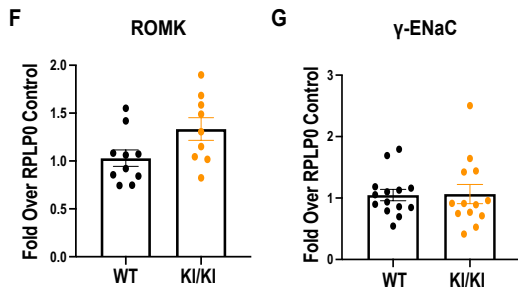
Alpha - Intercalated Cell Markers



Beta - Intercalated Cell Markers



Principal Cell Markers



Prior Nephron Segments

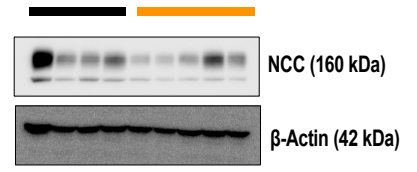
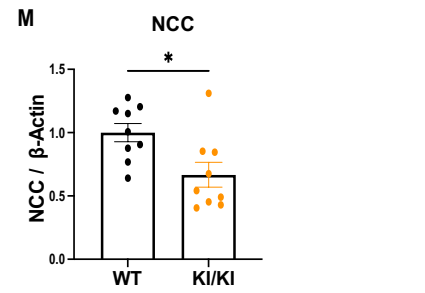
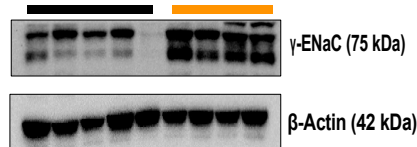
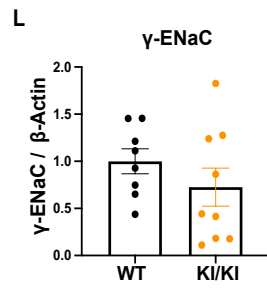
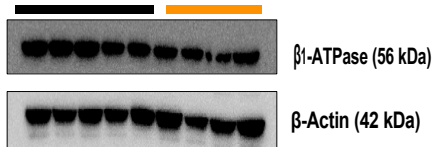
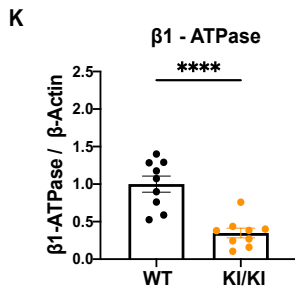
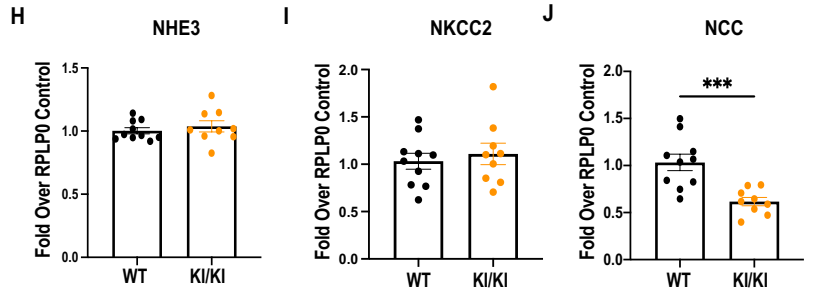


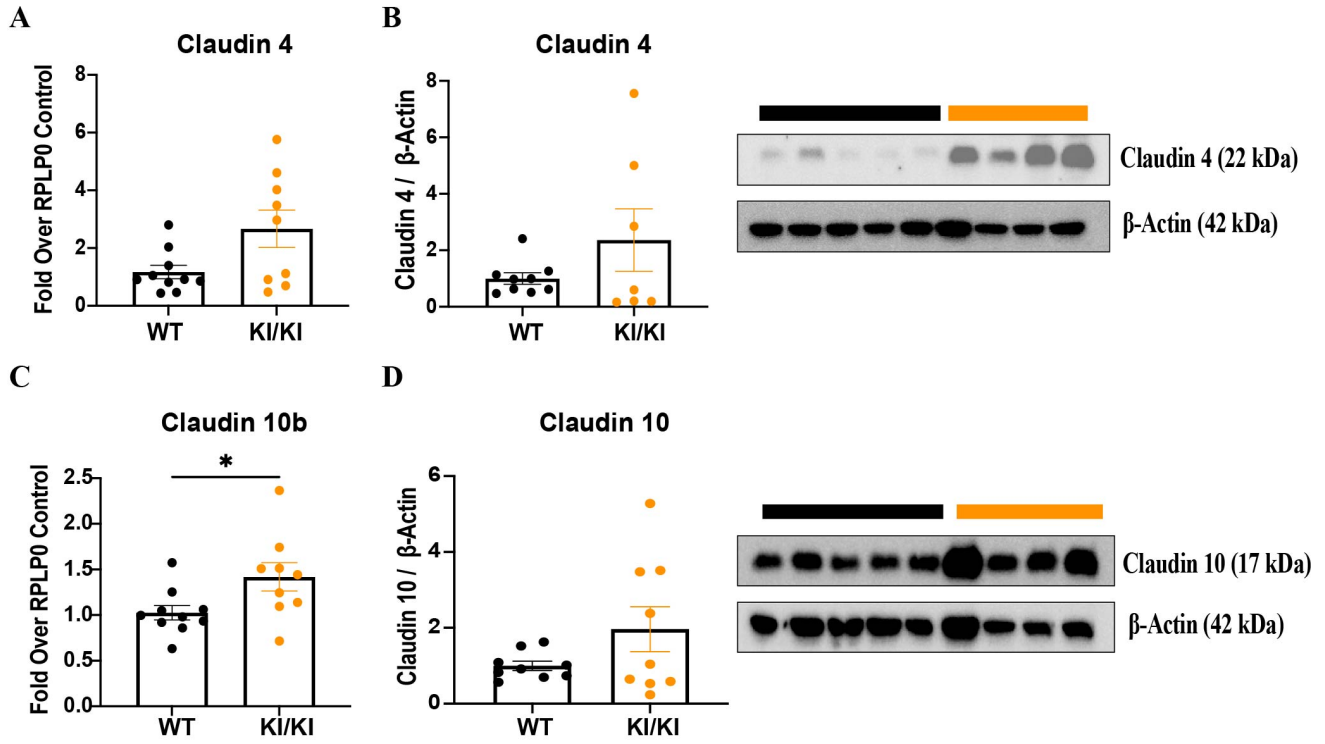
Figure 3.28 Although gene expression and protein abundance of markers of the IC are decreased, PC and TAL markers do not vary significantly in L919X KI/KI mice versus WT littermates. **A)** kAe1 **B)** and B1-ATPase, along with protein expression of **K)** B1-ATPase was decreased in the KI/KI mice. B-IC markers **C)** pendrin, **D)** NDCBE, and **E)** Ae4 have and PC markers **F)** ROMK and **G, L)** gamma-ENaC show no significant difference between genotypes. Gene and protein expression of DCT marker **J M)** NCC was significant reduced in KI/KI mice, while **K)** NHE3 and **L)** NKCC2 showed no difference between genotypes. Data presented as mean \pm SEM, **P < 0.01, ***P < 0.001, ****P < 0.0001 using with unpaired Student's t-test, Mann-Whitney test.

Paracellular markers claudin-10b and claudin-4 are upregulated in dRTA mutant mice compared to WT mice.

Given the decreased abundance of IC markers as well as decreased (or no change to) TAL markers, investigation of other transport mechanisms was needed. Paracellular transport is important in salt homeostasis, which promoted us to look at claudin-4 and claudin-10b as major paracellular salt pores. While claudin-4 acts as a sodium-blocking chloride pore in the thin ascending limb of Henle's loop and the CD, claudin-10b functions as a sodium pore in the TAL^{48,49,89}. Interestingly, in both L919X KI/KI and R607H KI/KI mice, an increase in claudin-4 and claudin-10b mRNA was observed (**Figure 3.29 A, C, E, G**). Consistent trends were observed in these proteins' abundance as well (**Figure 3.29 B, D, F, H**). These findings suggest a common compensatory mechanism via the paracellular pathway in the loop of Henle of both KI/KI mice.

We hypothesized that perhaps the paracellular transport pathway was compensating where disruptions in the transcellular transport existed in the dRTA mice. To complete our analysis, qRT-PCR analysis was done on other claudin proteins present in the CD, claudin-3 (also present in TAL), claudin-8, and claudin-7. Claudin-3 is pivotal in maintaining the integrity of the paracellular barrier, thus regulating urinary pH and the concentration of electrolytes in urine and plasma^{48,64}. Claudin-7 functions as a non-selective chloride and sodium pore¹¹³. Claudin-8, through its interactions with Claudin-4, is an anion channel that modulates permeability to acidic and basic ions and is required for recruiting claudin-4 to the tight junction^{5,49,62}. While the R607H KI/KI did not reveal any changes in these paracellular markers compared to WT littermates (**Figure 3.30 A - C**), L919X KI/KI mice showed increased claudin-3 and claudin-7 (preliminary result) (**Figure 3.30 E, F**). Brought together, these results highlight paracellular adaptations in the KI/KI mutant strains, potentially as an attempt to maintain salt homeostasis.

● Wildtype ● L919X KI/KI



● Wildtype ● R607H KI/KI

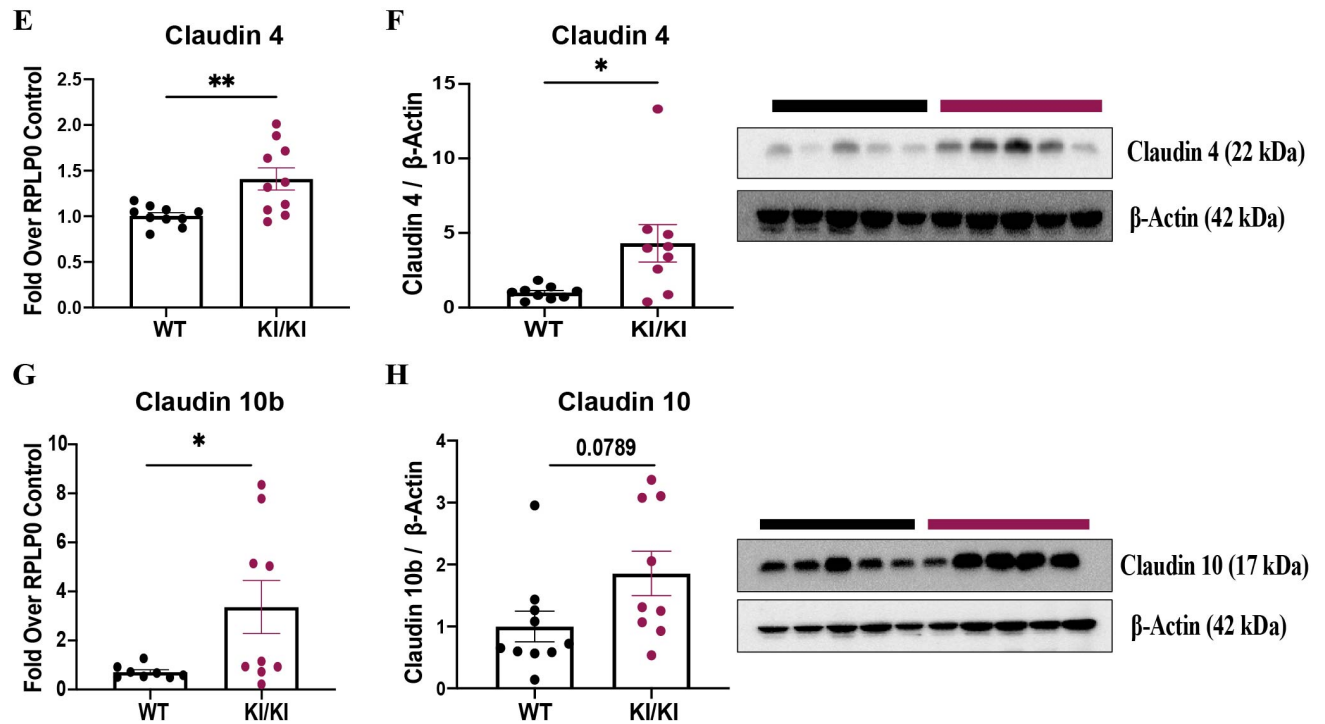


Figure 3.29 Claudin-4 and claudin-10b are upregulated in both L919X and R607H KI/KI mice after a salt-depleted acid diet. A) Claudin-4 gene expression and B) protein abundance was increased in the L919X KI/KI (trends only), compared to WT mice. C) Claudin-10b gene expression and D) claudin-10 protein abundance was also significantly increased in L919X KI/KI mice compared to WT. E - G) These same results were seen in the R607H KI/KI model, with significance. These same results were seen in the R607H KI/KI model, with significance. Data presented as mean \pm SEM, *P < 0.05, **P < 0.01, with unpaired Student's t-test, Mann-Whitney test.

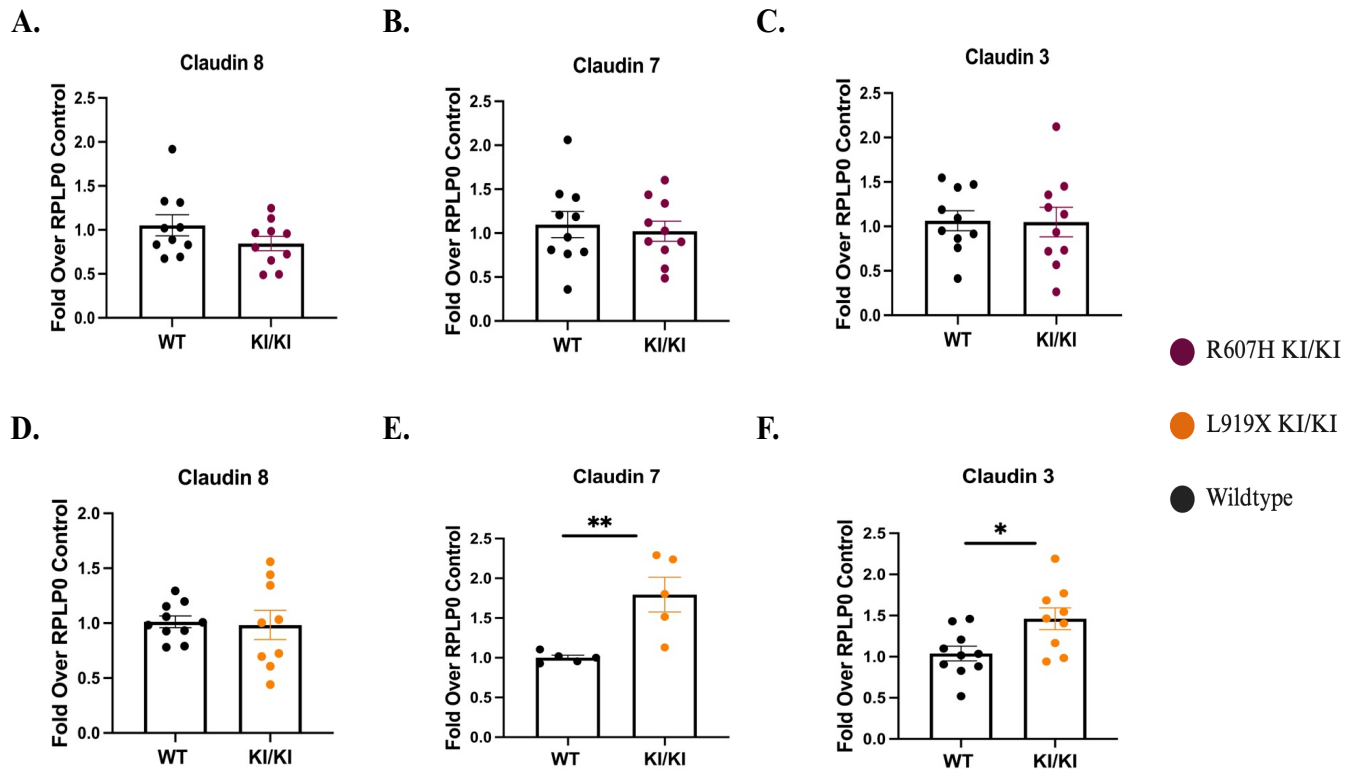


Figure 3.30 Paracellular markers claudin-3 and -7 expressed in the distal nephron are up-regulated in L919X KI/KI mice but not in R607H KI/KI after a salt-depleted acid diet. A - C) Claudin-8, Claudin-7, and Claudin-3 gene expressed showed no significance difference between R607H KI/KI mice compared with WT. In contrast, D) Claudin-8 gene expression showed no difference between genotypes. While F) Claudin-7 gene expression was elevated in the L919X KI/KI mice compared to WT (incomplete analysis). F) Claudin-3 showed significant increase in the L919X KI/KI mice compared to WT. Data presented as mean \pm SEM, *P < 0.05 with unpaired Student's t-test, Mann-Whitney test.

Markers showing significant changes in abundance following the salt-depleted acid challenge were not significantly different at baseline for dRTA mutant mice.

At baseline, our urine analysis had revealed no significant differences in ion excretion between the mutant mice and WT counterparts (**Figure 3.3**). This is in stark contrast to the salt-depleted acid challenge (**Figure 3.25, Figure 3.26**), revealing a urinary sodium loss. As well, after the double salt and acid challenge, we observed differences in mRNA abundance of certain CD and TAL markers in both KI/KI mice. This prompted investigation into the same markers at baseline to determine if prior nephron segments were compensating in the dRTA mutant mice in the absence of a challenge. As expected, both mutant mice exhibited a significant decrease in mRNA abundance of kAe1 compared to WT (**Figure 3.31 A, Figure 3.32 A**), while levels of NDCBE, Ae4, γ -ENaC, remained comparable between WT and both KI/KI mice at steady state (**Figure 3.31 B-D, Figure 3.32 B-D**). mRNA abundance of NHE3 and NKCC2 also showed no significant differences between WT and both KI/KI mice at steady state (**Figure 3.31 E, F, Figure 3.32 E, F**). mRNA abundance of the claudin-4 was similar between WT and R607H KI/KI mice but significantly elevated in L919X KI/KI mice at steady state (**Figure 3.31 G, Figure 3.32 G**). Conversely, mRNA abundance of claudin-10b exhibited no significant differences between WT and both KI/KI mice at steady state (**Figure 3.31 H, Figure 3.32 H**).

In conclusion, our findings highlight little differences in mRNA expression of key markers in dRTA KI/KI mice under baseline conditions, warranting further investigation into compensatory mechanisms in these mutants.

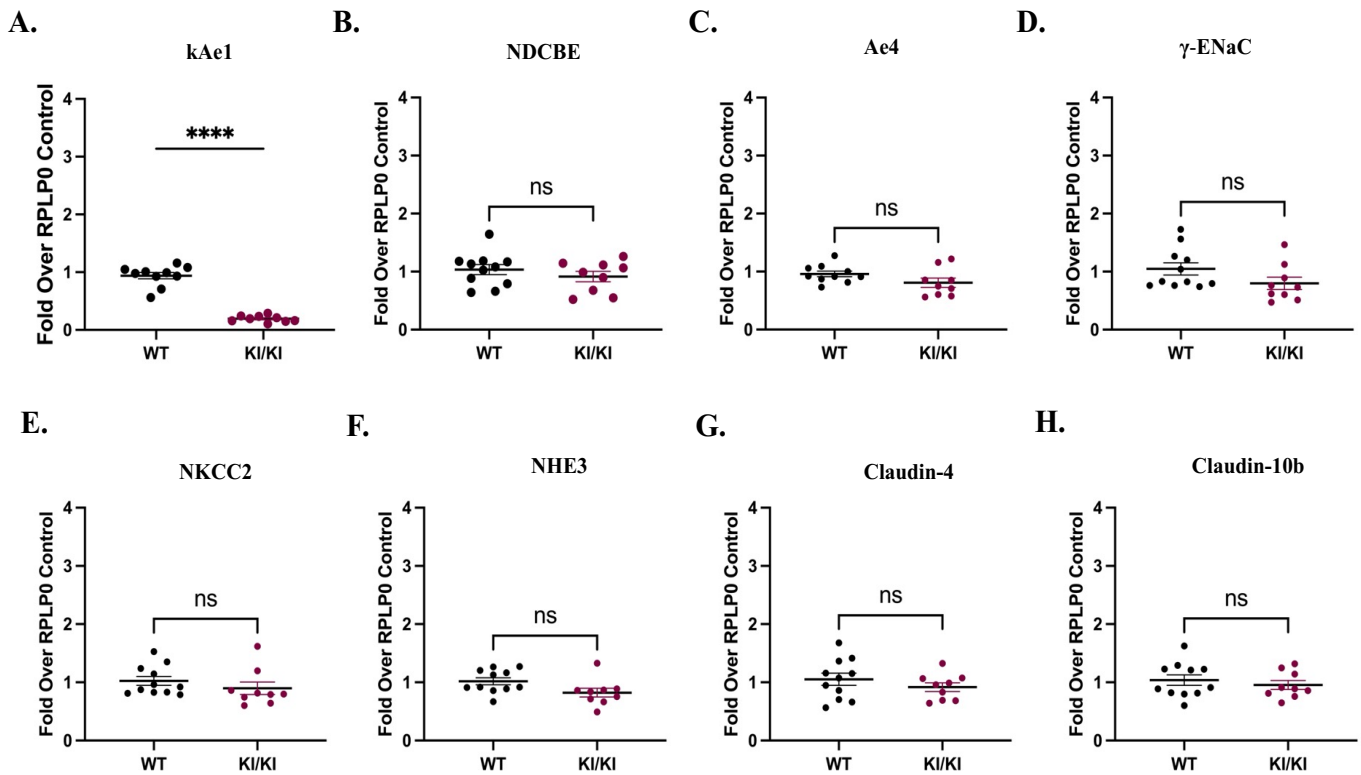


Figure 3.31 kAe1 gene expression of IC and is down regulated in R607H KI/KI mice compared to WT mice at baseline. **A)** As expected, R607H KI/KI mice had significantly decreased kAe1 compared to WT counterparts. There were no significant differences in **B)** NDCBE, **C)** Ae4, **D)** ENaC, **E)** NKCC2, **F)** NHE3, **G)** Claudin-4 or **H)** Claudin-10 between the genotypes at steady state (n = 11 WT, n = 9 KI/KI). Results are normalized to RPLP0 mRNA abundance. Data are presented as mean \pm SEM, ns, not significant, ****P < 0.0001, using unpaired Student's t-test or Mann-Whitney test. The black dots represent WT mice while the magenta dots represent R607H KI/KI mice. *These graphs were created by Saron Gebremariam and arranged here by Priyanka Mungara.*

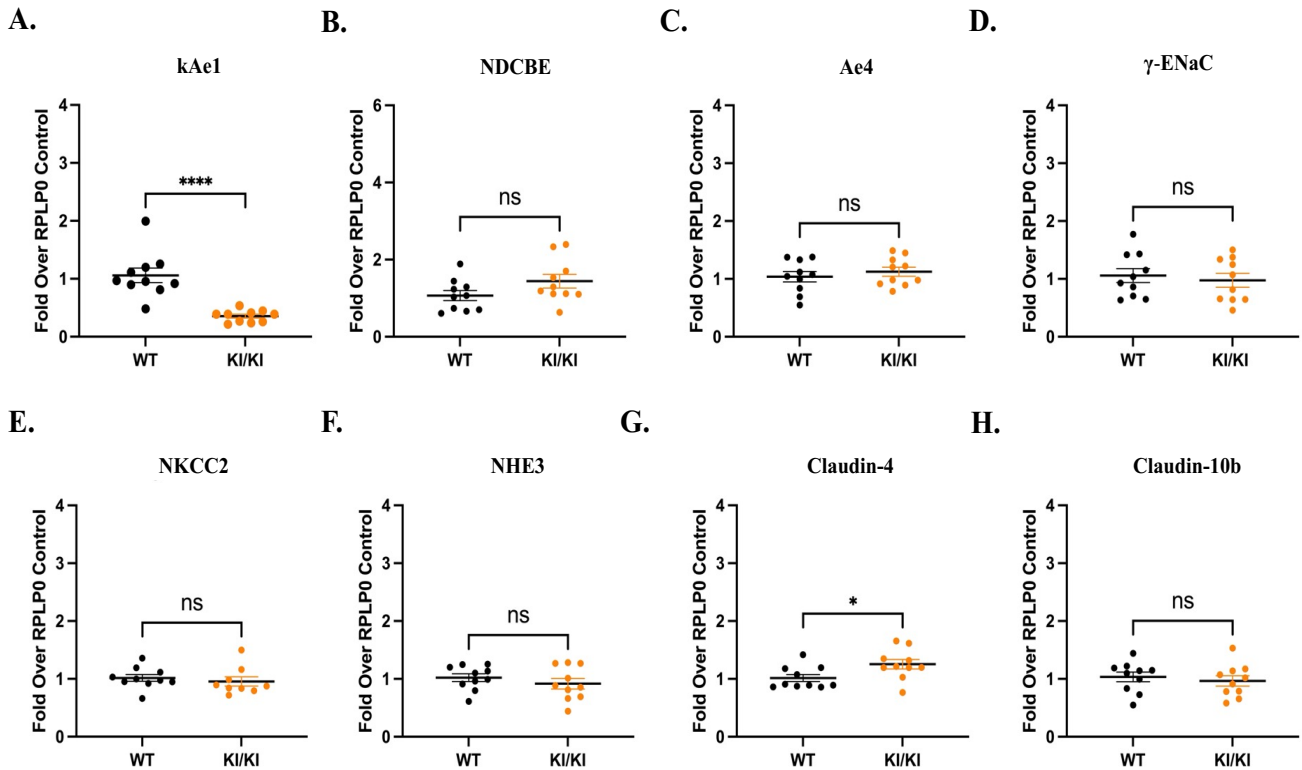


Figure 3.32 kAe1 gene expression is downregulated and claudin 4 is up-regulated in L919X KI/KI mice compared to WT mice at baseline. A) As expected, L919X KI/KI mice had significantly decreased kAe1 compared to WT counterparts. There were no significant differences in B) NDCBE, C) Ae4, D) ENaC, E) NKCC2, F) NHE3 between the genotypes at steady state (n = 10 WT, n = 10 KI/KI). G) Claudin-4 was significantly increased in the KI/KI mice at steady state, but H) Claudin-10 was no different to WT mice. Results are normalized to RPLP0 mRNA abundance. Data are presented as mean \pm SEM, ns, not significant, *P < 0.05, ****P < 0.0001, using unpaired Student's t-test or Mann-Whitney test. The black dots represent WT mice while the orange dots represent L919X KI/KI mice. *These graphs were created by Saron Gebremariam and arranged here by Priyanka Mungara.*

dRTA mutant mice display evidence of potential glomerular disturbance through increased urinary albumin.

Evidence of glomerular dysfunction has been noted in human dRTA patients ¹¹. Notably, kAE1 is present in the glomerulus ⁴⁶ where it interacts with nephrin, a crucial component of the slit diaphragm protein complex ¹²⁶. *Ae1*^{-/-} mice exhibit significantly enlarged glomeruli, albuminuria, and a more diffuse nephrin expression pattern compared with WT mice ¹²⁶. Since alterations in the slit diaphragm can lead to defective filtration and proteinuria, we investigated if this phenotype was present in our dRTA mutant mice. After subjecting the mice to a salt-depleted acid load, we measured urinary albumin levels on Day 14 urine. A marked increase in urinary albumin levels compared to baseline measurements was observed (**Figure 3.33**). To further confirm changes to the filtration barrier, creatinine excretion at steady state compared to Day 14 was quantified in the mice (**Appendix A Figure 3.36**). At steady state, R607H KI/KI mice had less urinary creatinine excretion compared to WT mice but increased it by Day 14, while L919X KI/KI mice showed no difference at steady state or Day 14 compared to WT (**Figure 3.36**).

This preliminary result suggests that altered renal glomerular function or increased glomerular permeability may be a contributor to the renal pathology and sodium wasting phenotype present in the dRTA mutant mice.

Overall, the results from the salt-depleted acid diet reveal a phenotype that aligns with the hypothesis.

The salt-depleted acid diet revealed a sodium wasting phenotype and disrupted collecting duct function in both the R607H KI/KI and L919X KI/KI mice. A summary of the major results provided in this thesis, from steady state to the salt-depleted acid challenge, are summarized in **Table 3.8**.

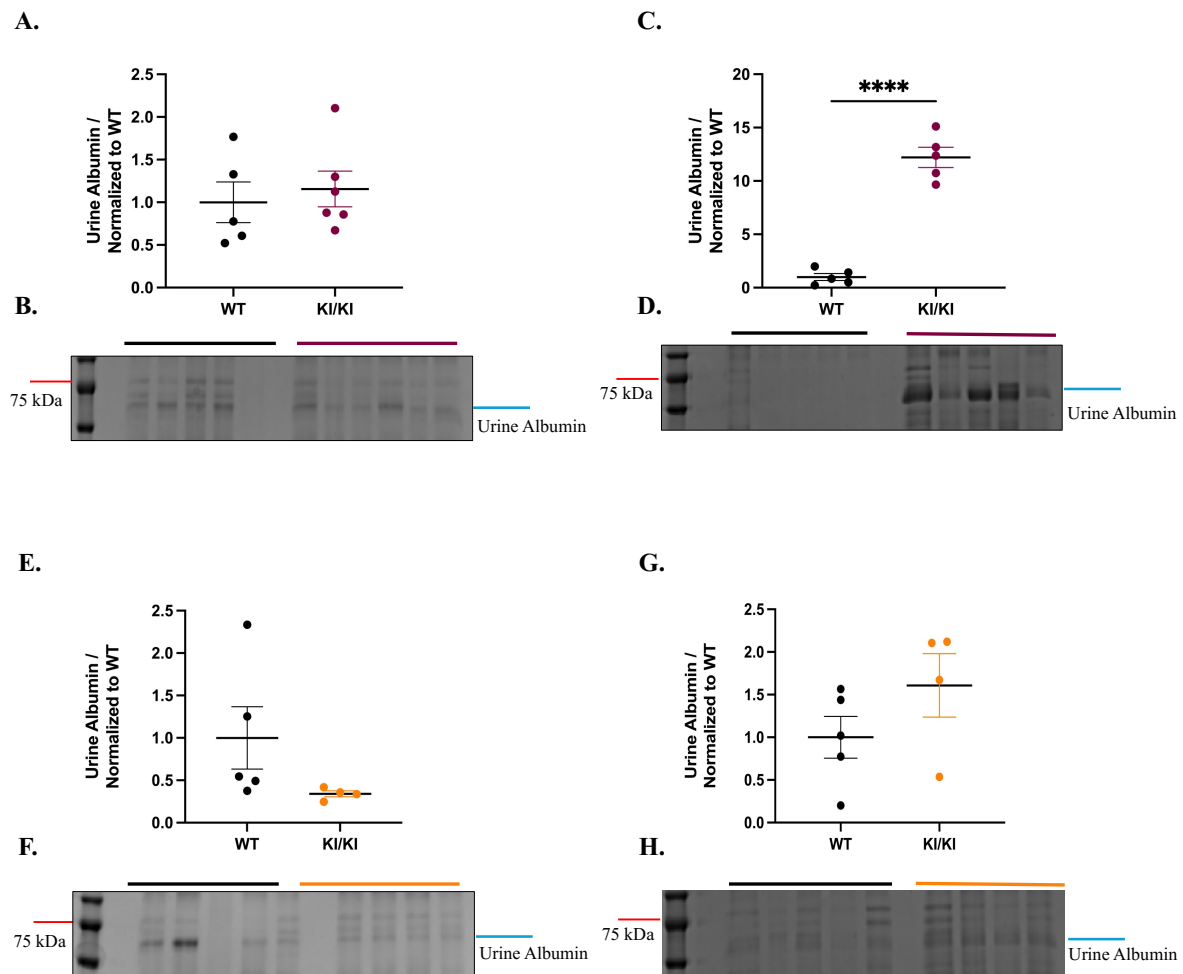


Figure 3.33. Urine albumin abundance is higher in the R607H and L919X KI/KI mice after the salt-depleted acid challenge compared to WT littermates. (A - B) At baseline, no differences in urinary albumin levels in the R607H KI/KI compared to WT. (C - D) After the salt-depleted acid challenge, R607H KI/KI mice have elevated urinary albumin. (E - F) At baseline, no differences in urinary albumin levels in the L919X KI/KI compared to WT. (G - H) After the salt-depleted acid challenge, L919X KI/KI mice have trend for higher urinary albumin after the dietary challenge. All data is presented as mean \pm SEM, **P < 0.0001 using an unpaired Student's t-test or Mann-Whitney test.**

Table 3.8. Summary of the Major Findings Presented in this Thesis

Steady state	<ul style="list-style-type: none"> • Reduced kAe1 gene expression in both mutant mice. • Both mutants excrete alkaline urine (high pH and low ammonium). • Similar Na⁺, Cl⁻, K⁺ excretion between both mutants and WT mice. • Trend for increased NBCn1 protein abundance in both mutant mice.
Salt-Depleted Diet	<ul style="list-style-type: none"> • Both mutants excrete alkaline urine, with evidence of urine acidification. • Both mutant mice excrete Na⁺ and Cl⁻ similarly to WT, but less K⁺ (trend for less in R607H KI/KI mice).
Acid Challenge	<ul style="list-style-type: none"> • Both mutants excrete alkaline urine, with evidence of urine acidification. • Both mutants have high plasma Na⁺, Cl⁻ compared to WT. • Both mutants excrete Cl⁻, K⁺ similarly to WT, but L919X KI/KI mice have increased urinary Na⁺ loss. • L919X KI/KI mice show decreased kAe1 but increased claudin-10b mRNA abundance.
Salt-Depleted Acid Load	<ul style="list-style-type: none"> • Both mutants excrete alkaline urine, with evidence of urine acidification. • Both mutants have high plasma Na⁺, Cl⁻ compared to WT. • Both mutants display a sodium wasting phenotype. • R607H KI/KI mice excrete decreased K⁺ and Cl⁻ compared to WT mice. • L919X KI/KI mice loose Cl⁻, but excrete K⁺ similarly to WT mice. • Both mutants have decreased kAe1 but increased claudin-4 and claudin-10b mRNA (and protein) abundance. • KI/KI mice have increased urinary albumin.

Chapter 4: Discussion

SUMMARY OF FINDINGS

This thesis research project aimed to characterize the novel and unpublished Ae1 L919X KI mouse model and to investigate whether the sodium-wasting phenotype exhibited by human dRTA patients was also present in two dRTA mutant mouse models, the Ae1 R607H KI, and Ae1 L919X KI. The L919X KI mice have been generated in the laboratory of Dr. Christian Hubner but not published (**Appendix A**). We therefore showed that these mice display a similar phenotype as the R607H KI mice, who exhibit a decreased abundance of A-ICs, characterized by a decreased Ae1 mRNA and protein abundance, a decreased percentage of A-ICs compared to B-ICs, and an accumulation of p-62 and autophagic structures in the remaining A-ICs⁷³. Importantly, fewer ICs have been reported in human dRTA patients^{22,121}.

We hypothesized that the two dRTA mutant mice manifest a renal sodium wasting due to their reduced number of ICs. To test this hypothesis, dRTA animals and WT counterparts were fed one of three diets: a salt-depletion, an acid challenge, or a salt-depleted acid challenge. Through the salt-depleted acid challenge, we unveiled a urinary sodium loss in both KI/KI mice, with varied renal handling of urinary potassium and chloride, and elevated plasma sodium and chloride. In the R607H KI/KI mice, there was a general downregulation of transcellular IC and TAL markers, with an upregulation of paracellular markers, claudin-4 and claudin-10b specifically. These results were seen predominantly as trends in the L919X KI/KI mice, although the increase in claudin-4 and claudin-10 was also observed. Interestingly, baseline gene expression levels of these markers was generally not significantly different between WT and both KI/KI mice. The results obtained from this thesis project overall align with the hypothesis and reveal a potential reliance on paracellular transport when transcellular transport is dysfunctional.

THE TWO MOUSE MODELS HAVE INCOMPLETE dRTA

In our experiments, we consistently observed a significantly decreased mRNA abundance of kAe1 (pre- and post-diet conditions) and decreased B1-H⁺-ATPase. Urine pH of both dRTA mutant mice also remained consistently alkaline through all dietary challenges. This data validates our mouse models as it aligns with previous findings⁷³ and because the inability to acidify urine is a fundamental characteristic of dRTA^{1,36,117,123}. Furthermore, while R607H KI/KI mice showed significant changes to ion balance and gene expression of nephron markers, only trends were present in L919X KI/KI mice, suggesting a milder phenotype in the latter model. A report exploring mutations in the AE1 gene in human patients found phenotypic similarities between the R598H and R901X mutations, but patients carrying the R901X dominant mutation developed the disease at an older age, had a ~ 60 % reduction in AE1 abundance, and higher plasma bicarbonate and potassium than patients carrying the R589H mutation^{2,52}, suggesting a milder phenotype in R901X patients. This is in alignment with the results from the L919X KI mouse model.

THE NEPHRON'S RESPONSE TO THE DIETARY CHALLENGES

Urinary Ion Imbalances

Impairments in renal sodium excretion were originally thought to be a reversible consequence of improper renal acidification given the proton/sodium exchange in the distal nephron^{21,100,129}. But direct evidence of a tubular abnormality was revealed when acidotic patients on a sodium-restricted diet, excreted 5 - 27 mEq higher sodium than that of dietary intake¹⁰⁰. Previously, a group using a B1-H⁺-ATPase knockout mouse model fed a salt-restricted diet, revealed that impaired sodium reabsorption via pendrin/NDCBE on B-ICs was responsible for a salt losing phenotype⁴². B-IC dysfunction caused increased urinary ATP and prostaglandin E2 release, which in turn decreased ENaC expression on PCs, further elevating sodium waste^{42,94}.

The results from this mouse model differ from our *Ae1* mutant models, although measuring prostaglandin and ATP levels in the urine may provide insights into the mechanisms at play in our mice. In our experiments, R607H KI/KI mice showed increased γ -ENaC with no change in ROMK gene expression coupled with increased NDCBE gene expression. There was also a trend for decreased NCC gene expression. In L919X KI/KI mice, there was a trend for increased NDCBE, but significantly decreased NCC gene expression.

In a healthy CD during salt-depletion, increased sodium reabsorption via ENaC would facilitate potassium secretion via ROMK^{1,36,65,94}. In WT counterparts of both strains, we observed an expected sharp increase in potassium excretion in response to a salt-depletion, while the opposite trend was observed in mutant animals⁶⁵ highlighting an abnormal CD response in mutant animals. In NCC knockout mice, electroneutral transport becomes the predominant mechanism for salt reabsorption, minimizing potassium loss^{32,128}. Also, upregulation of ENaC and NDCBE/pendrin pathway compensates for the loss of NCC¹⁰³. Therefore, these distal nephrons salt transporters display a functional interplay. Consequently, in our mutant animals exhibiting less NCC gene expression compared to WT, perhaps upregulated NDCBE is the preferred mechanism to reabsorb salt, but at the cost of potassium excretion. As NDCBE reabsorbs bicarbonate, this route of transport may serve as an auxiliary mechanism to acidify urine pH. *In vivo* studies suggest that ENaC is held in intracellular pools under salt-replete conditions, but dietary changes or external cues may facilitate its apical targeting¹⁰. When luminal chloride levels drop, such as during salt-depletion, a decrease in pendrin-mediated bicarbonate secretion is observed¹¹⁹. This results in acidification of the lumen, which in turn diminishes ENaC-mediated sodium reabsorption¹¹⁹. In our dRTA mutant mice, where tubular fluid remains alkaline and with the elevated tubular chloride (from NH₄Cl load), there is a potential for sustained elevated ENaC necessity, as

evidenced by increased gene expression. In addition, specifically in the R607H KI/KI mice, there was significantly decreased gene expression NHE3 and NKCC2. Hence, major salt transporters upstream of the CD fail to properly reabsorb sodium potentially causing a compensatory increase in the CD to initiate maximum salt reabsorption, but with the altered composition of the CD in mutant mice, it may not be as efficient, contributing to the urinary salt loss.

Our study is unique as it highlights potential TAL disturbances in dRTA-related pathogenesis. Salt-depleted conditions typically increase overall NKCC2 mRNA abundance to increase chloride reabsorption⁹⁸. While possible in WT mice, this process appears disrupted in R607H KI/KI animals. Importantly, our findings are limited to gene expression analysis. As mentioned previously, there is a regulatory network that controls NKCC2 protein expression and activity, involving vasopressin^{37,72}, with no lysine kinase proteins⁸⁵, local paracrine and autocrine factors^{58,72,76} as well as post-translational modifications like phosphorylation^{7,12}. NHE3 also exhibits complex protein regulation via phosphorylation, protein partners, and angiotensin II that impact its activity and membrane density^{24,57,38,125}. Therefore, NKCC2 and NHE3's actions in urine concentration are complex and may not be reflected at the gene level only. As well, close to 80 % of NHE3 protein is expressed in the proximal tubule^{66,129}. Because our analysis of NHE3 was done on whole kidney tissues, our results are therefore not specific to the TAL. Interestingly, while proximal sodium reabsorption decreases in NHE3 knockout mice, a tubulo-glomerular feedback mechanism is activated which decreases GFR^{25,57}. Decreased GFR ensures stable level of sodium delivery to the distal tubule, preventing excessive sodium loss^{25,57}. This may have implications in our mouse models, as kAE1 is expressed in the glomerulus and participates in stabilizing the filtration barrier¹²⁶. Our KI/KI mice present preliminary evidence of possible glomerular dysfunction through increased urinary albumin and changes to urinary creatinine excretion

following the salt-depleted acid diet. In fact, previously studied $Ae1^{-/-}$ mice showed increased albuminuria, whereas this was absent in $Ae1^{+/+}$ mice ¹²⁶. Hence, if the filtration barrier is disrupted, GFR might be increased in the KI/KI mice, which may also explain their excessive sodium loss.

Urine Acidification

Following the salt-depleted acid challenge, the decrease in pendrin and $Ae4$ gene expression observed in dRTA mutant mice (significantly in R607H KI/KI) was an initially puzzling finding. We expected a relative increase in B-ICs (reflected in their markers) in the KI mice as previously shown ^{35,73}. However, $Ae4$ and pendrin have recently been identified as an acid-base sensing pair ¹²². It was proposed that metabolic acidosis causes $Ae4$ -mediated decrease in bicarbonate transport by B-ICs, decreasing pendrin abundance and bicarbonate secretion into the urine ¹²². In kidney cortex, $Ae4$ mRNA was decreased by $\sim 60\%$ during acidosis, recovering quickly to normal after bicarbonate loading ⁸⁶. This aligns with our results. It is possible that while dRTA mutant mice have fewer A-ICs to excrete excess acids, their B-IC usage is decreased to indirectly accomplish a similar goal ³⁵. In this way, $Ae4$ and pendrin mRNA would be reduced, more so compared to the WT mice, to maximally decrease bicarbonate secretion into urine.

As previously reported and consistent with our findings, R607H KI/KI mice are unable to decrease urine pH or to increase urinary excretion of ammonium in response to acid load compared to WT mice ⁷³. L919X KI/KI mice also consistently exhibited alkaline urine in all experimental conditions. Despite this, the mutant mice do acidify their urine significantly from steady state. This is noteworthy given the intricate coupling of proton-salt transport in the nephron ^{25,129}, especially in the TAL through NHE3 and NBCn1 activities ^{59,79}. The secretion of protons induced by NKCC1/2 blockade by furosemide results from a decrease in intracellular sodium concentration, amplifying the driving force for NHE3 sodium-proton exchange. TAL-specific NHE3 KO mice

lack furosemide-induced sustained urinary acidification ¹²⁹. Notably, NBCn1, located on the basolateral TAL membrane also facilitates urine acidification during metabolic acidosis ⁷⁹. This protein was upregulated in the R607H KI/KI at baseline ⁷³ and under our experiments reveal a similar preliminary trend. A recent report proposed that NBCn1 enhances sodium/bicarbonate co-transport, which together allows for ammonium reabsorption across the renal tubules, which rapidly restores arterial blood pH and promotes ammonium secretion in the CD ⁷⁹. This evidence may support why significant acidosis is not apparent in the plasma pH of our mutant mice, despite the noticeable increase in urine acidification. Moreover, NBCn1 might play a role in decreasing intracellular sodium levels in the TAL, aiding the actions of NHE3, further promoting urinary acidification.

Paracellular Ion Transport

Our acid challenge and salt-depleted acid diet reflected an increase in paracellular transport reliance in both KI/KI mice compared to WT. Both dRTA mutant mice exhibited elevated claudin-4 and claudin-10b mRNA and protein levels, significantly in the R607H KI model. L919X KI/KI mice also showed upregulation of claudin-7 (preliminary data) and claudin-3 compared to WT counterparts. Previous studies in mouse inner medullary CD 3 cells showed that WT kAe1 expression reduces transepithelial electrical resistance and increases sodium and chloride permeability, an effect mediated by its interactions with claudin-4 ⁶². Therefore, in dRTA where kAe1 expression is abnormal, there may be a tighter CD, preventing sodium and chloride reabsorption, and the increased claudin-4 mRNA abundance may be compensatory to revert this effect. In addition, given the salt-depleted conditions, increased claudin-4 gene may serve as another mechanism for chloride reabsorption in the CD, required for the exchange activity of kAe1 and the buffering of plasma pH during acidosis. Only the isoform b of claudin-10 is localized to

the tight junctions or colocalized with sodium potassium ATPase and chloride channels in the basolateral infoldings of the TAL ⁸⁹. There it serves as a water-impermeable cation-selective channel ⁸⁹. The TAL segments of claudin-10b knockout mice have significantly decreased sodium permeability, replaced by pathological magnesium and calcium imbalance ^{9,89}. The observed upregulation of claudin-10b in our dRTA mutant mice may be an adaptive response to mitigate urinary ion loss and maximize sodium reabsorption where transcellular salt pathways of NKCC2, NHE3, and NCC are failing. Additionally, NKCC2 and ROMK in the TAL cause a net chloride reabsorption creating a lumen-positive transepithelial potential driving paracellular sodium reabsorption through claudin-10b ^{80,89}. Therefore, increased claudin-10b may result in sodium hyperabsorption, creating a net negative lumen that could facilitate proton or ammonium secretion, acidifying the urine. This would also provide explanation for the high plasma sodium seen in both KI/KI mice. Alternatively, the reliance on paracellular transport maybe more energy efficient for the mutant animals, given the double dietary challenge ^{84,130,131}.

Hormonal/Systemic Influence

A critical physiological response to a salt-depletion challenge is RAAS activation ²⁹. After the salt-depleted acid load, both KI/KI mutant strains had high plasma sodium and chloride, and higher renal renin mRNA abundance compared to WT mice. High plasma sodium and chloride was also observed in the acid challenge alone. The RAAS is activated during metabolic acidosis ^{94,97,101,123}. ICs contain a mineralocorticoid receptor which typically remains phosphorylated and inactive. During volume depletion, aldosterone binds to the MR, through dephosphorylating it. This activation causes increased pendrin and apical V-ATPase expression, and ENaC activity in PCs ^{94,101,127}. Considering the decreased abundance of ICs and altered composition of CDs in our mutant animals, it is plausible that the responses and regulation of the RAAS are disrupted.

Hypernatremia typically occurs either due to inadequate water intake or free water loss¹⁰⁵, but both genotypes of either strain significantly reduced water consumption to the same extent, and both mutant strains reduced urine volume/day compared to WT mice, hence there is a dysregulation in ion/water homeostasis. ADH/vasopressin secretion should occur in response to high plasma osmolality or volume depletion to reabsorb water and restore appropriate plasma sodium and chloride concentrations¹⁹. Again, the abnormal CD composition in the KI/KI mice might lead to an abnormal response, leading to the observed phenotype. As discussed in Chapter 1, the hormones within the RAAS cascade can modulate the transporters studied in this thesis. Therefore, analysis of plasma renin and plasma and urine aldosterone, angiotensin II, and ADH, or quantifying mRNA and protein abundance of AQP channels, would clarify the response patterns in the mutant mice to the RAAS cascade and the alterations to water and salt reabsorption.

STUDY LIMITATIONS AND FUTURE DIRECTIONS

In Chapter 4, various limitations and potential future directions were already acknowledged. This section aims to emphasize a few key points.

One current limitation to our experiments is that our only confirmation of a reduced number of A-ICs is the decreased kAe1 gene expression identified by qRT-PCR. Detecting protein abundance in our mouse samples posed a challenge due to the lack of a kAe1-specific antibody (instead of total Ae1). It is possible that despite perfusion, some red blood cells remain within the kidney, skewing the results. Therefore, a kAe1-specific antibody would need to be generated. Immunofluorescence images showing decreased Ae1 staining intensity in the L919X KI/KI mice compared to WT (provided by Dr. Dominique Eladari, **Appendix A**), serve as further support, so this type of analysis can be completed in our mice at baseline as well. In addition, to gain deeper insights into the composition of the CDs in our mutant mice models, single-cell RNA sequencing

could be performed. Single-cell RNA sequencing allows for transcript analysis in individual cells, which would allow us to distinguish between the populations of the cells and their transcriptional similarities or differences within mutant CDs and compared to WT ⁴⁴. Understanding the specific composition of the CD in the mutant mice would potentially better explain or highlight the phenotypes seen here, given the unique and interrelated functions of each CD cell type.

Our experimental results so far are limited by analysis using primarily qRT-PCR and immunoblots. To enhance our analysis, we require information on the phosphorylation state of proteins or their interactions, which as previously discussed, are crucial for understanding the regulation of certain transporters studied in this thesis. Performing immunoblots with antibodies specific to phosphorylated transporters could be one approach. For example, NKCC2 has a cluster of N-terminal threonine's, that when phosphorylated, activate the protein. Therefore, we would use an anti-pNKCC2 specific to these amino acids and then compared to total NKCC2 abundance, providing insight into the protein's activation ⁷². Alternatively, identifying the abundance of prominent kinases (ex: with-no-lysine kinases) responsible for transporters' phosphorylation could be an indirect measure of phosphorylation. As well, our current methods do not distinguish localization. This is notable because claudins, including claudin-4 and claudin-10b, may also be present at the basolateral membrane, likely impacting their role. Immunofluorescence on kidney sections of mice fed the sodium-depleted acid challenge will provide insight into how localization contributes to the phenotype seen here. TAL claudins have a mosaic expression pattern of either claudin-10b or claudin-3/claudin-19/claudin-16 in a complex ^{9,69}. In WT mice claudin-3, claudin-19, and claudin-16 are present in a certain fraction of tight junctions, but in a claudin-10 knockout model, there is a broad expansion of the claudins the TAL ^{9,69,89}. Therefore, changes to the claudin mosaic may also contribute to ion imbalances, and we could detect this via immunofluorescence.

Since we are utilizing an *in vivo* model in these studies, investigating the humoral response to the dietary challenge presented is crucial. While we show preliminary evidence via our quantification of renal renin mRNA abundance, but employing ELISA assays to assess urine or plasma levels of aldosterone, angiotensin II or vasopressin, or urinary levels of prostaglandin E2, ATP, or other local factors that influence salt homeostasis, would offer a more comprehensive characterization of the mice. Lastly, considering the pivotal role of tubular voltage in ion transport within the nephron, isolating the CD or the TAL from the mice post-dietary challenge and assessing the conductance and permeability of each ion would offer valuable insights into the defects present in the mutant mice.

While this thesis project highlighted a potential involvement of the TAL in the pathophysiology of the dRTA mutant mice, it is still unclear. Our laboratory is currently completing an acute furosemide experiment on mice fed the salt-depleted acid diet. Furosemide is an NKCC2 inhibitor and furosemide application is a clinical test for dRTA in human patients^{1,36,123}. When furosemide is applied, it increases salt exposure to the distal nephron, due to NKCC2 blockade, which upregulates ENaC-mediated salt reabsorption and H⁺-ATPase-mediated proton secretion from A-ICs²¹. Therefore, these experiments would likely cause an altered response in the dRTA mutant mice due to their abnormal CDs. Hence, it would allow us to assess the role of the TAL in acid-base and electrolyte homeostasis in our dRTA mutant mice more clearly.

Our mice model can also be used to study glomerular dysfunction. Evidence of glomerular dysfunction has been observed in human dRTA patients, although it is assumed to be caused by long-term nephrocalcinosis and kidney stones¹¹. Our study reported elevated urine albumin following the 14-day sodium-depleted acid load, suggesting a potential disruption to glomerular filtration in dRTA. *Ae1*^{-/-} mice exhibit significantly enlarged glomeruli, albuminuria, and a more

diffuse nephrin expression pattern compared with WT mice ¹²⁶. Since alterations in the slit diaphragm can lead to defective filtration and proteinuria, these results may underscore the importance of kAe1 in maintaining glomerular structural integrity and function through its interactions ¹²⁶. Further investigations into glomerular filtration rate, changes in kAe1 expression in the glomeruli, and glomerular structure in the WT versus mutant animals, would provide valuable insights into glomerular function and structure in our mice.

Although our experimental setup revealed results that align with our hypothesis, there are some limitations to the design that we used. While using an *in vivo* model like mice is more physiologically accurate compared to *in vitro* models, these models may not fully reflect human pathophysiology. Evidence of this species-to-species difference is present in the R607H KI/KI mice ⁷³. Human dRTA patients' typically present with hypercalciuria while our dRTA mutant mice have decreased urinary calcium excretion ⁷³. At baseline, our R607H KI/KI mice had high plasma potassium, but dRTA patients typically present with hypokalemic metabolic acidosis ^{1,123}. Lastly, the sodium wasting phenotype typically affects people with complete dRTA, whereas our mouse models have incomplete dRTA. Therefore, these species-to-species differences in ion handling are important to consider before data translation to humans. Notably, human disease is based on many factors including genetics, environment, and lifestyle which our models may not accurately reflect. There is also a limitation to the dietary challenges used in this study as well. The diets were provided *ad libitum*, and therefore we had little control over the amount of acid consumed by each mouse. This likely increases variability in the results per mouse. We could consider a different method of acid delivery, through a gavage for example, to reduce this variability. Nevertheless, the current mouse models available are still viable options to study dRTA pathogenesis.

Kidney disease affects 1 in 10 individuals in Canada and is the 10th leading cause of death in the country. This project contributes to the growing body of knowledge on the nephron and the transporters that regulate homeostasis in our body. While we are studying electrolyte balance and acid-base homeostasis in the context of dRTA, our findings can be expanded to treat major diseases like chronic kidney disease, hypertension, and kidney stone formation, which all occur due to alterations in ion homeostasis. This thesis research is shedding new light on the renal handling of salt and the crosstalk between nephron segments to maintain ion balance. The hope is that this research eventually opens the path for potential alternative treatments for dRTA patients and patients facing cardiovascular or kidney-related diseases.

BIBLIOGRAPHY

1. Alexander, R. T. & Bitzan, M. Renal Tubular Acidosis. *Pediatric Clinics of North America* **66**, 135–157 (2019).
2. Almomani, E., Lashhab, R., Alexander, R. T. & Cordat, E. The carboxyl-terminally truncated kidney anion exchanger 1 R901X dRTA mutant is unstable at the plasma membrane. *American Journal of Physiology-Cell Physiology* **310**, C764–C772 (2016).
3. Alper, S. L. Familial renal tubular acidosis. *Journal of nephrology* **23 Suppl 16**, S57-76 (2010).
4. Amasheh, S. *et al.* Claudin-2 expression induces cation-selective channels in tight junctions of epithelial cells. *Journal of Cell Science* **115**, 4969–4976 (2002).
5. Angelow, S., Kim, K. & Yu, A. S. L. Claudin-8 modulates paracellular permeability to acidic and basic ions in MDCK II cells. *The Journal of Physiology* **571**, 15–26 (2006).
6. Arakawa, T. *et al.* Crystal structure of the anion exchanger domain of human erythrocyte band 3. *Science* **350**, 680–684 (2015).
7. Ares, G. R., Caceres, P. S. & Ortiz, P. A. Molecular regulation of NKCC2 in the thick ascending limb. *American Journal of Physiology-Renal Physiology* **301**, F1143–F1159 (2011).
8. Assmus, A. *et al.* Loss of Adam10 Disrupts Ion Transport in Immortalized Kidney Collecting Duct Cells. *Function (Oxford, England)* **2**, zqab024 (2021).
9. Breiderhoff, T. *et al.* Deletion of claudin-10 (Cldn10) in the thick ascending limb impairs paracellular sodium permeability and leads to hypermagnesemia and nephrocalcinosis. *Proceedings of the National Academy of Sciences* **109**, 14241–14246 (2012).
10. Butterworth, M. B. Regulation of the epithelial sodium channel (ENaC) by membrane trafficking. *Biochimica et Biophysica Acta (BBA) - Molecular Basis of Disease* **1802**, 1166–1177 (2010).
11. CARUANA, R. J. & BUCKALEW, V. M. The Syndrome of Distal (Type 1) Renal Tubular Acidosis. *Medicine* **67**, 84–99 (1988).
12. Castrop, H. & Schießl, I. M. Physiology and pathophysiology of the renal Na-K-2Cl cotransporter (NKCC2). *American Journal of Physiology-Renal Physiology* **307**, F991–F1002 (2014).

13. Chelangarimiyandoab, F., Mungara, P., Batta, M. & Cordat, E. Urinary Tract Infections: Renal Intercalated Cells Protect against Pathogens. *Journal of the American Society of Nephrology* **34**, 1605–1614 (2023).
14. Chen, L., Higgins, P. J. & Zhang, W. Development and Diseases of the Collecting Duct System. in 165–203 (2017). doi:10.1007/978-3-319-51436-9_7.
15. Cordat, E. & Reithmeier, R. A. F. Structure, function, and trafficking of SLC4 and SLC26 anion transporters. in *Current Topics in Membranes* vol. 73 1–67 (Academic Press Inc., 2014).
16. Cordat, E. *et al.* Dominant and Recessive Distal Renal Tubular Acidosis Mutations of Kidney Anion Exchanger 1 Induce Distinct Trafficking Defects in MDCK Cells. *Traffic* **7**, 117–128 (2006).
17. Cordat, E., Li, J. & Reithmeier, R. A. F. Carboxyl-Terminal Truncations of Human Anion Exchanger Impair its Trafficking to the Plasma Membrane. *Traffic* **4**, 642–651 (2003).
18. Curthoys, N. P. & Moe, O. W. Proximal Tubule Function and Response to Acidosis. *Clinical Journal of the American Society of Nephrology* **9**, 1627–1638 (2014).
19. Cuzzo, B., Padala, S. A. & Lappin, S. L. *Physiology, Vasopressin*. (2024).
20. David Weiner, I. & Verlander, J. W. Role of NHE3 and NHE4 transporters in renal acid-base transport. *Am J Physiol Renal Physiol* **300**, 11–23 (2011).
21. de Bruijn, P. I. A. *et al.* Furosemide-induced urinary acidification is caused by pronounced H⁺ secretion in the thick ascending limb. *American Journal of Physiology-Renal Physiology* **309**, F146–F153 (2015).
22. DeFranco, P. E., Haragsim, L., Schmitz, P. G. & Bastani, B. Absence of vacuolar H(+)-ATPase pump in the collecting duct of a patient with hypokalemic distal renal tubular acidosis and Sjögren's syndrome. *Journal of the American Society of Nephrology* **6**, 295–301 (1995).
23. Dominguez Rieg, J. A. & Rieg, T. New functions and roles of the Na⁺-H⁺-exchanger NHE3. *Pflügers Archiv - European Journal of Physiology* **476**, 505–516 (2024).
24. du Cheyron, D. *et al.* Angiotensin II stimulates NHE3 activity by exocytic insertion of the transporter: Role of PI 3-kinase. *Kidney International* **64**, 939–949 (2003).
25. Eaton, D. C., Pooler, J. & Vander, A. J. *Vander's Renal Physiology*. (McGraw-Hill Medical, 2009).

26. Eladari, D. & Hübner, C. A. Novel mechanisms for NaCl reabsorption in the collecting duct. *Current Opinion in Nephrology & Hypertension* **20**, 506–511 (2011).
27. Ellison, D. H., Velázquez, H. & Wright, F. S. Adaptation of the distal convoluted tubule of the rat. Structural and functional effects of dietary salt intake and chronic diuretic infusion. *Journal of Clinical Investigation* **83**, 113–126 (1989).
28. Fisher, A. B. Peroxiredoxin 6: A Bifunctional Enzyme with Glutathione Peroxidase and Phospholipase A₂ Activities. *Antioxidants & Redox Signaling* **15**, 831–844 (2011).
29. Fountain, J. H., Kaur, J. & Lappin, S. L. *Physiology, Renin Angiotensin System*. (2024).
30. Frömter, E., Rumrich, G. & Ullrich, K. J. Phenomenologic description of Na⁺, Cl⁻ and HCO₃⁻ absorption from proximal tubules of rat kidney. *Pflügers Archiv European Journal of Physiology* **343**, 189–220 (1973).
31. Fuster, D. G. & Moe, O. W. Incomplete Distal Renal Tubular Acidosis and Kidney Stones. *Advances in Chronic Kidney Disease* **25**, 366–374 (2018).
32. Gallafassi, E. A., Bezerra, M. B. & Rebouças, N. A. Control of sodium and potassium homeostasis by renal distal convoluted tubules. *Brazilian Journal of Medical and Biological Research* **56**, (2023).
33. Gamba, G. & Friedman, P. A. Thick ascending limb: the Na⁺:K⁺:2Cl⁻ co-transporter, NKCC2, and the calcium-sensing receptor, CaSR. *Pflügers Archiv - European Journal of Physiology* **458**, 61–76 (2009).
34. Gao, C. *et al.* Generation of Distal Renal Segments Involves a Unique Population of Aqp2⁺ Progenitor Cells. *Journal of the American Society of Nephrology* **32**, 3035–3049 (2021).
35. Genini, A., Mohebbi, N., Daryadel, A., Bettoni, C. & Wagner, C. A. Adaptive response of the murine collecting duct to alkali loading. *Pflügers Archiv - European Journal of Physiology* **472**, 1079–1092 (2020).
36. Giglio, S., Montini, G., Trepiccione, F., Gambaro, G. & Emma, F. Distal renal tubular acidosis: a systematic approach from diagnosis to treatment. *Journal of Nephrology* **34**, 2073–2083 (2021).
37. Giménez, I. & Forbush, B. Short-term Stimulation of the Renal Na-K-Cl Cotransporter (NKCC2) by Vasopressin Involves Phosphorylation and Membrane Translocation of the Protein. *Journal of Biological Chemistry* **278**, 26946–26951 (2003).

38. Girardi, A. C. C. & di Sole, F. Deciphering the mechanisms of the Na⁺/H⁺ exchanger-3 regulation in organ dysfunction. *American Journal of Physiology-Cell Physiology* **302**, C1569–C1587 (2012).
39. Gong, Y. *et al.* The Cap1–claudin-4 regulatory pathway is important for renal chloride reabsorption and blood pressure regulation. *Proceedings of the National Academy of Sciences* **111**, (2014).
40. Gonzalez-Vicente, A., Saez, F., Monzon, C. M., Asirwatham, J. & Garvin, J. L. Thick Ascending Limb Sodium Transport in the Pathogenesis of Hypertension. *Physiological Reviews* **99**, 235–309 (2019).
41. Grinstein, M., Dingwall, H. L., Shah, R. R., Capellini, T. D. & Galloway, J. L. A robust method for RNA extraction and purification from a single adult mouse tendon. *PeerJ* **6**, e4664 (2018).
42. Gueutin, V. *et al.* Renal β -intercalated cells maintain body fluid and electrolyte balance. *Journal of Clinical Investigation* **123**, 4219–4231 (2013).
43. Hamm, L. L., Nakhoul, N. & Hering-Smith, K. S. Acid-Base Homeostasis. *Clinical Journal of the American Society of Nephrology* **10**, 2232–2242 (2015).
44. Haque, A., Engel, J., Teichmann, S. A. & Lönnberg, T. A practical guide to single-cell RNA-sequencing for biomedical research and clinical applications. *Genome Medicine* **9**, 75 (2017).
45. Harrison, M. L., Isaacson, C. C., Burg, D. L., Geahlen, R. L. & Low, P. S. Phosphorylation of human erythrocyte band 3 by endogenous p72syk. *The Journal of biological chemistry* **269**, 955–9 (1994).
46. Hazen-Martin, D. J., Pasternack, G., Hennigar, R. A., Spicer, S. S. & Sens, D. A. Immunocytochemistry of Band 3 Protein in Kidney and Other Tissues of Control and Cystic Fibrosis Patients. *Pediatric Research* **21**, 235–237 (1987).
47. Hebert, S. C. & Andreoli, T. E. Control of NaCl transport in the thick ascending limb. *American Journal of Physiology-Renal Physiology* **246**, F745–F756 (1984).
48. Hou, J., Rajagopal, M. & Yu, A. S. L. Claudins and the Kidney. *Annual Review of Physiology* **75**, 479–501 (2013).

49. Hou, J., Renigunta, A., Yang, J. & Waldegger, S. Claudin-4 forms paracellular chloride channel in the kidney and requires claudin-8 for tight junction localization. *Proceedings of the National Academy of Sciences* **107**, 18010–18015 (2010).
50. Huang, D. Y., Osswald, H. & Vallon, V. Sodium reabsorption in thick ascending limb of Henle's loop: effect of potassium channel blockade *in vivo*. *British Journal of Pharmacology* **130**, 1255–1262 (2000).
51. Jarolim, P. *et al.* Autosomal Dominant Distal Renal Tubular Acidosis Is Associated in Three Families with Heterozygosity for the R589H Mutation in the AE1 (Band 3) Cl⁻/HCO₃⁻-Exchanger. *Journal of Biological Chemistry* **273**, 6380–6388 (1998).
52. Karet, F. E. *et al.* Mutations in the chloride-bicarbonate exchanger gene *AE1* cause autosomal dominant but not autosomal recessive distal renal tubular acidosis. *Proceedings of the National Academy of Sciences* **95**, 6337–6342 (1998).
53. Keskanokwong, T. *et al.* Interaction of Integrin-linked Kinase with the Kidney Chloride/Bicarbonate Exchanger, kAE1. *Journal of Biological Chemistry* **282**, 23205–23218 (2007).
54. Khayyat, N. H., Zaika, O., Tomilin, V. N., Pyshev, K. & Pochynyuk, O. Angiotensin II increases activity of the ClC-K2 Cl⁻ channel in collecting duct intercalated cells by stimulating production of reactive oxygen species. *Journal of Biological Chemistry* **296**, 100347 (2021).
55. Kim, E. Y. *et al.* Altered Regulation of Renal Acid Base Transporters in Response to Ammonium Chloride Loading in Rats. *The Korean Journal of Physiology & Pharmacology* **16**, 91 (2012).
56. Kittanakom, S., Cordat, E. & Reithmeier, R. A. F. Dominant-negative effect of Southeast Asian ovalocytosis anion exchanger 1 in compound heterozygous distal renal tubular acidosis. *Biochemical Journal* **410**, 271–281 (2008).
57. Knepper, M. A. & Brooks, H. L. Regulation of the sodium transporters NHE3, NKCC2 and NCC in the kidney. *Current Opinion in Nephrology and Hypertension* **10**, 655–659 (2001).
58. KNEPPER, M. A., KIM, G.-H., FERNÁNDEZ-LLAMA, P. & ECELBARGER, C. A. Regulation of Thick Ascending Limb Transport by Vasopressin. *Journal of the American Society of Nephrology* **10**, 628–634 (1999).

59. Kwon, T.-H. *et al.* Chronic metabolic acidosis upregulates rat kidney Na-HCO₃ – cotransporters NBCn1 and NBC3 but not NBC1. *American Journal of Physiology-Renal Physiology* **282**, F341–F351 (2002).
60. Laghmani, K., Richer, C., Borensztein, P., Paillard, M. & Froissart, M. Expression of rat thick limb Na/H exchangers in potassium depletion and chronic metabolic acidosis. *Kidney International* **60**, 1386–1396 (2001).
61. Lapointe, J.-Y., Laamarti, A. & Bell, P. D. Ionic transport in macula densa cells. *Kidney International* **54**, S58–S64 (1998).
62. Lashhab, R. *et al.* The kidney anion exchanger 1 affects tight junction properties via claudin-4. *Scientific Reports* **9**, 3099 (2019).
63. Lashhab, R., Ullah, A. K. M. S. & Cordat, E. Renal collecting duct physiology and pathophysiology. *Biochemistry and Cell Biology* vol. 97 234–242 at <https://doi.org/10.1139/bcb-2018-0192> (2019).
64. Leiz, J. & Schmidt-Ott, K. M. Claudins in the Renal Collecting Duct. *International Journal of Molecular Sciences* **21**, 221 (2019).
65. Leviel, F. *et al.* The Na⁺-dependent chloride-bicarbonate exchanger SLC4A8 mediates an electroneutral Na⁺ reabsorption process in the renal cortical collecting ducts of mice. *Journal of Clinical Investigation* **120**, 1627–1635 (2010).
66. Li, X. C. *et al.* Proximal Tubule-Specific Deletion of the NHE3 (Na⁺/H⁺ Exchanger 3) Promotes the Pressure-Natriuresis Response and Lowers Blood Pressure in Mice. *Hypertension* **72**, 1328–1336 (2018).
67. Livak, K. J. & Schmittgen, T. D. Analysis of Relative Gene Expression Data Using Real-Time Quantitative PCR and the 2– $\Delta\Delta$ CT Method. *Methods* **25**, 402–408 (2001).
68. Loffing, J. *et al.* Differential subcellular localization of ENaC subunits in mouse kidney in response to high- and low-Na diets. *American Journal of Physiology-Renal Physiology* **279**, F252–F258 (2000).
69. Milatz, S. *et al.* Mosaic expression of claudins in thick ascending limbs of Henle results in spatial separation of paracellular Na⁺ and Mg²⁺ transport. *Proceedings of the National Academy of Sciences* **114**, (2017).
70. MINETTI, G. *et al.* Characterization of the hypertonically induced tyrosine phosphorylation of erythrocyte band 3. *Biochemical Journal* **335**, 305–311 (1998).

71. MINETTI, G., PICCININI, G., BALDUINI, C., SEPPI, C. & BROVELLI, A. Tyrosine phosphorylation of band 3 protein in Ca²⁺/A23187-treated human erythrocytes. *Biochemical Journal* **320**, 445–450 (1996).
72. Mount, D. B. Thick ascending limb of the loop of henle. *Clinical Journal of the American Society of Nephrology* **9**, 1974–1986 (2014).
73. Mumtaz, R. *et al.* Intercalated Cell Depletion and Vacuolar H⁺-ATPase Mistargeting in an Ae1 R607H Knockin Model. *Journal of the American Society of Nephrology* **28**, 1507–1520 (2017).
74. Mungara, P., Waiss, M., Hartwig, S., Burger, D. & Cordat, E. Unraveling the Molecular Landscape of kAE1: A Narrative Review. *Canadian Journal of Physiology and Pharmacology* (2024) doi:10.1139/cjpp-2023-0482.
75. Mustaqeem, R. & Arif, A. *Renal Tubular Acidosis*. (2024).
76. Mutig, K. *et al.* Activation of the Bumetanide-sensitive Na⁺,K⁺,2Cl⁻ Cotransporter (NKCC2) Is Facilitated by Tamm-Horsfall Protein in a Chloride-sensitive Manner. *Journal of Biological Chemistry* **286**, 30200–30210 (2011).
77. Nuiplot, N. *et al.* Transmembrane protein 139 (TMEM139) interacts with human kidney isoform of anion exchanger 1 (kAE1). *Biochemical and Biophysical Research Communications* **463**, 706–711 (2015).
78. Olinger, E., Houillier, P. & Devuyst, O. Claudins: a tale of interactions in the thick ascending limb. *Kidney International* **93**, 535–537 (2018).
79. Olsen, J. S. M. *et al.* NBCn1 Increases NH₄⁺ Reabsorption Across Thick Ascending Limbs, the Capacity for Urinary NH₄⁺ Excretion, and Early Recovery from Metabolic Acidosis. *Journal of the American Society of Nephrology* **32**, 852–865 (2021).
80. Palmer, L. G. & Schnermann, J. Integrated Control of Na Transport along the Nephron. *Clinical Journal of the American Society of Nephrology* **10**, 676–687 (2015).
81. Pang, A. J., Bustos, S. P. & Reithmeier, R. A. F. Structural Characterization of the Cytosolic Domain of Kidney Chloride/Bicarbonate Anion Exchanger 1 (kAE1). *Biochemistry* **47**, 4510–4517 (2008).
82. Patterson, S. T. & Reithmeier, R. A. F. Cell Surface Rescue of Kidney Anion Exchanger 1 Mutants by Disruption of Chaperone Interactions. *Journal of Biological Chemistry* **285**, 33423–33434 (2010).

83. Pearce, D. *et al.* Collecting Duct Principal Cell Transport Processes and Their Regulation. *Clinical Journal of the American Society of Nephrology* **10**, 135–146 (2015).
84. Pei, L. *et al.* Paracellular epithelial sodium transport maximizes energy efficiency in the kidney. *Journal of Clinical Investigation* **126**, 2509–2518 (2016).
85. Ponce-Coria, J. *et al.* Regulation of NKCC2 by a chloride-sensing mechanism involving the WNK3 and SPAK kinases. *Proceedings of the National Academy of Sciences* **105**, 8458–8463 (2008).
86. Purkerson, J. M., Heintz, E. v., Nakamori, A. & Schwartz, G. J. Insights into acidosis-induced regulation of SLC26A4 (pendrin) and SLC4A9 (AE4) transporters using three-dimensional morphometric analysis of β -intercalated cells. *American Journal of Physiology-Renal Physiology* **307**, F601–F611 (2014).
87. QUILTY, J. A., CORDAT, E. & REITHMEIER, R. A. F. Impaired trafficking of human kidney anion exchanger (kAE1) caused by hetero-oligomer formation with a truncated mutant associated with distal renal tubular acidosis. *Biochemical Journal* **368**, 895–903 (2002).
88. Quilty, J. A., Li, J. & Reithmeier, R. A. Impaired trafficking of distal renal tubular acidosis mutants of the human kidney anion exchanger kAE1. *American Journal of Physiology-Renal Physiology* **282**, F810–F820 (2002).
89. Quintanova, C. *et al.* Unrecognized role of claudin-10b in basolateral membrane infoldings of the thick ascending limb. *Annals of the New York Academy of Sciences* **1517**, 266–278 (2022).
90. Reeves, W. B., Winters, C. J. & Andreoli, T. E. Chloride Channels in the Loop of Henle. *Annual Review of Physiology* **63**, 631–645 (2001).
91. Reithmeier, R. A. F. *et al.* Band 3, the human red cell chloride/bicarbonate anion exchanger (AE1, SLC4A1), in a structural context. *Biochimica et Biophysica Acta (BBA) - Biomembranes* **1858**, 1507–1532 (2016).
92. Rodríguez Soriano, J. Renal Tubular Acidosis. *Journal of the American Society of Nephrology* **13**, 2160–2170 (2002).
93. Rossi, G. M., Regolisti, G., Peyronel, F. & Fiaccadori, E. Recent insights into sodium and potassium handling by the aldosterone-sensitive distal nephron: a review of the relevant physiology. *Journal of Nephrology* **33**, 431–445 (2020).

94. Roy, A., Al-Bataineh, M. M. & Pastor-Soler, N. M. Collecting duct intercalated cell function and regulation. *Clinical Journal of the American Society of Nephrology* **10**, 305–324 (2015).
95. Sassi, A. *et al.* Expression of claudin-8 is induced by aldosterone in renal collecting duct principal cells. *American Journal of Physiology-Renal Physiology* **321**, F645–F655 (2021).
96. Saxena, V. *et al.* Kidney intercalated cells are phagocytic and acidify internalized uropathogenic Escherichia coli. *Nature Communications* **12**, 2405 (2021).
97. Schambelan, M., Sebastian, A., Katuna, B. A. & Arteaga, E. Adrenocortical hormone secretory response to chronic NH₄Cl-induced metabolic acidosis. *American Journal of Physiology-Endocrinology and Metabolism* **252**, E454–E460 (1987).
98. Schieβl, I. M. *et al.* Dietary salt intake modulates differential splicing of the Na-K-2Cl cotransporter NKCC2. *American Journal of Physiology-Renal Physiology* **305**, F1139–F1148 (2013).
99. Schwaderer, A. L., Rajadhyaksha, E., Canas, J., Saxena, V. & Hains, D. S. Intercalated cell function, kidney innate immunity, and urinary tract infections. *Pflügers Archiv - European Journal of Physiology* **476**, 565–578 (2024).
100. Sebastian, A., McSherry, E. & Morris, R. C. Impaired renal conservation of sodium and chloride during sustained correction of systemic acidosis in patients with type 1, classic renal tubular acidosis. *Journal of Clinical Investigation* **58**, 454–469 (1976).
101. Sebastian, A., Sutton, J. M., Hulter, H. N., Schambelan, M. & Poler, S. M. Effect of mineralocorticoid replacement therapy on renal acid-base homeostasis in adrenalectomized patients. *Kidney International* **18**, 762–773 (1980).
102. Sherwood, L. W. C. I. S. *Human Physiology: From Cells to Systems*. (2019).
103. Sinning, A. *et al.* Double Knockout of the Na⁺-Driven Cl⁻/HCO₃⁻ Exchanger and Na⁺/Cl⁻ Cotransporter Induces Hypokalemia and Volume Depletion. *Journal of the American Society of Nephrology* **28**, 130–139 (2017).
104. Soi, V. & Yee, J. Sodium Homeostasis in Chronic Kidney Disease. *Advances in Chronic Kidney Disease* **24**, 325–331 (2017).
105. Sonani, B., Naganathan, S. & Al-Dhahir, M. A. *Hypernatremia*. (2024).

106. Stehberger, P. A. *et al.* Distal Renal Tubular Acidosis in Mice Lacking the AE1 (Band3) Cl⁻/HCO₃⁻ Exchanger (slc4a1). *Journal of the American Society of Nephrology* **18**, 1408–1418 (2007).
107. Sterling, D., Reithmeier, R. A. F. & Casey, J. R. A Transport Metabolon. *Journal of Biological Chemistry* **276**, 47886–47894 (2001).
108. Stockand, J. D. Vasopressin regulation of renal sodium excretion. *Kidney International* **78**, 849–856 (2010).
109. Su, Y. *et al.* Glyceraldehyde 3-phosphate dehydrogenase is required for band 3 (anion exchanger 1) membrane residency in the mammalian kidney. *American Journal of Physiology-Renal Physiology* **300**, F157–F166 (2011).
110. Su, Y. *et al.* PDLIM5 links kidney anion exchanger 1 (kAE1) to ILK and is required for membrane targeting of kAE1. *Scientific Reports* **7**, 39701 (2017).
111. Su, Y. *et al.* Physical and Functional Links between Anion Exchanger-1 and Sodium Pump. *Journal of the American Society of Nephrology* **26**, 400–409 (2015).
112. Subramanya, A. R. & Ellison, D. H. Distal Convolute Tubule. *Clinical Journal of the American Society of Nephrology* **9**, 2147–2163 (2014).
113. Tatum, R. *et al.* Renal salt wasting and chronic dehydration in claudin-7-deficient mice. *American Journal of Physiology-Renal Physiology* **298**, F24–F34 (2010).
114. Toka, H. R. *et al.* Deficiency of the Calcium-Sensing Receptor in the Kidney Causes Parathyroid Hormone-Independent Hypocalciuria. *Journal of the American Society of Nephrology* **23**, 1879–1890 (2012).
115. Toye, A. M., Banting, G. & Tanner, M. J. A. Regions of human kidney anion exchanger 1 (kAE1) required for basolateral targeting of kAE1 in polarised kidney cells: mis-targeting explains dominant renal tubular acidosis (dRTA). *Journal of Cell Science* **117**, 1399–1410 (2004).
116. Toye, A. M., Bruce, L. J., Unwin, R. J., Wrong, O. & Tanner, M. J. A. Band 3 Walton, a C-terminal deletion associated with distal renal tubular acidosis, is expressed in the red cell membrane but retained internally in kidney cells. *Blood* **99**, 342–347 (2002).
117. Trepiccione, F. *et al.* New Findings on the Pathogenesis of Distal Renal Tubular Acidosis. *Kidney Diseases* **3**, 98–105 (2017).

118. Tsukita, S., Tanaka, H. & Tamura, A. The Claudins: From Tight Junctions to Biological Systems. *Trends in Biochemical Sciences* **44**, 141–152 (2019).
119. V. Pech, *et al.* Pendrin Modulates ENaC Function by Changing Luminal HCO₃⁻. *Journal of the American Society of Nephrology* **21**, 1928–1941 (2010).
120. van Beusecum, J. P. *et al.* Novel Concepts in Nephron Sodium Transport: A Physiological and Clinical Perspective. *Advances in Kidney Disease and Health* **30**, 124–136 (2023).
121. Vichot, A. A. *et al.* Loss of kAE1 expression in collecting ducts of end-stage kidneys from a family with SLC4A1 G609R-associated distal renal tubular acidosis. *Clinical Kidney Journal* sfw074 (2016) doi:10.1093/ckj/sfw074.
122. Vitzthum, H. *et al.* The AE4 transporter mediates kidney acid-base sensing. *Nature Communications* **14**, (2023).
123. Wagner, C. A. *et al.* The pathophysiology of distal renal tubular acidosis. *Nature Reviews Nephrology* **19**, 384–400 (2023).
124. Wagner, C. A., Devuyst, O., Bourgeois, S. & Mohebbi, N. Regulated acid–base transport in the collecting duct. *Pflügers Archiv - European Journal of Physiology* **458**, 137–156 (2009).
125. Watts, B. A., George, T. & Good, D. W. Aldosterone inhibits apical NHE3 and HCO₃⁻ absorption via a nongenomic ERK-dependent pathway in medullary thick ascending limb. *American Journal of Physiology-Renal Physiology* **291**, F1005–F1013 (2006).
126. Wu, F. *et al.* Anion Exchanger 1 Interacts with Nephrin in Podocytes. *Journal of the American Society of Nephrology* **21**, 1456–1467 (2010).
127. Wu, P. *et al.* Effect of Angiotensin II on ENaC in the Distal Convoluted Tubule and in the Cortical Collecting Duct of Mineralocorticoid Receptor Deficient Mice. *Journal of the American Heart Association* **9**, (2020).
128. Xu, J., Barone, S., Brooks, M.-B. & Soleimani, M. Double Knockout of Carbonic Anhydrase II (CAII) and Na⁺-Cl⁻ Cotransporter (NCC) Causes Salt Wasting and Volume Depletion. *Cellular Physiology and Biochemistry* **32**, 173–183 (2013).

129. Xue, J., Thomas, L., Dominguez Rieg, J. A., Fenton, R. A. & Rieg, T. NHE3 in the thick ascending limb is required for sustained but not acute furosemide-induced urinary acidification. *American Journal of Physiology-Renal Physiology* **323**, F141–F155 (2022).
130. Yu, A. S. L. Paracellular transport and energy utilization in the renal tubule. *Current Opinion in Nephrology and Hypertension* **26**, 398–404 (2017).
131. Yu, A. S. L. Paracellular transport as a strategy for energy conservation by multicellular organisms? *Tissue Barriers* **5**, e1301852 (2017).
132. Zacchia, M., Capolongo, G., Rinaldi, L. & Capasso, G. The importance of the thick ascending limb of Henle's loop in renal physiology and pathophysiology. *International Journal of Nephrology and Renovascular Disease* **Volume 11**, 81–92 (2018).
133. Zhekova, H. R. *et al.* CryoEM structures of anion exchanger 1 capture multiple states of inward- and outward-facing conformations. *Communications Biology* **5**, 1372 (2022).

APPENDIX A

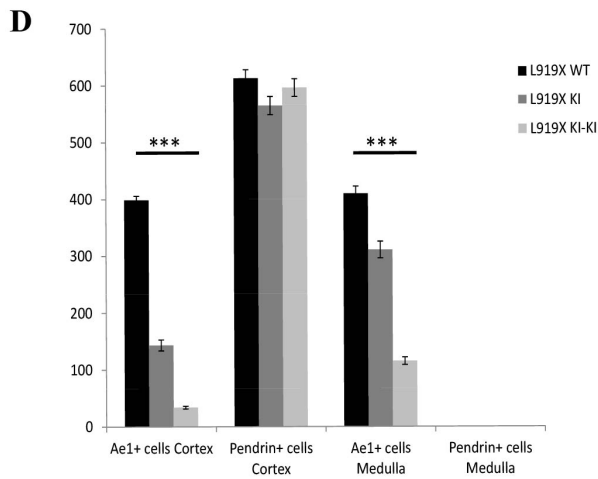
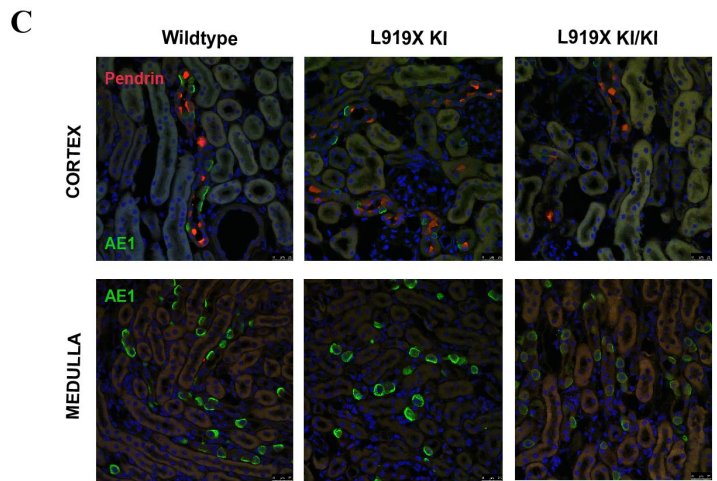
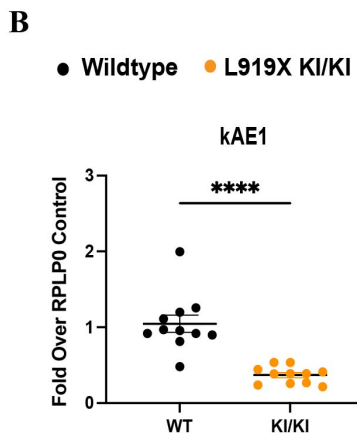
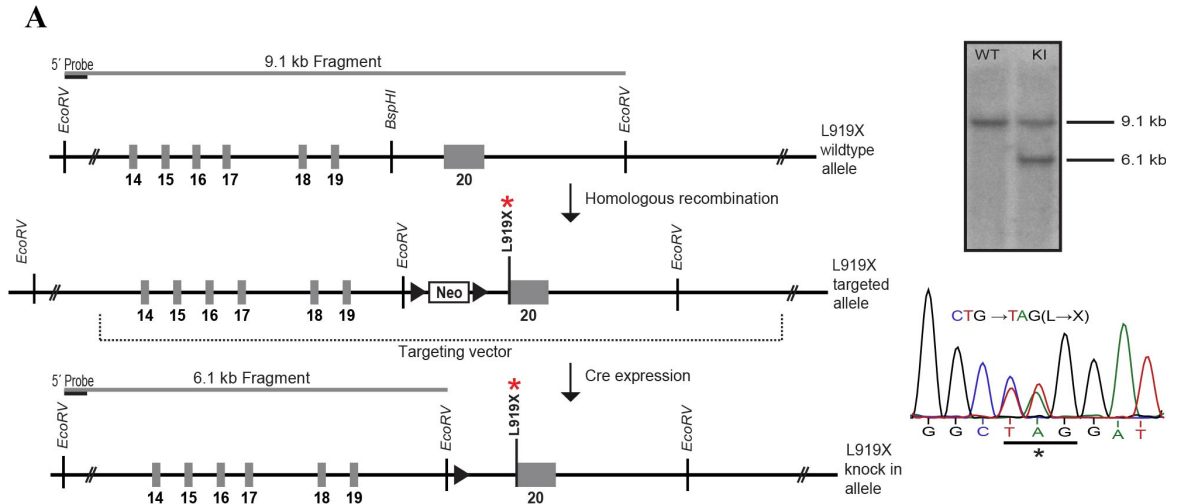


Figure 3.34 The generation and preliminary characterization of the L919X KI mice. **A)** A strategy for targeting and screening using the murine *Ae1* locus (top) and the targeted locus (middle), followed by the locus post selection cassette removal through Cre recombination. Additionally, validation of the introduced mutation with Southern blotting and sequencing. **B)** Gene expression of *kAe1* in perfused whole kidney from WT or L919X KI/KI mice. **C)** Immunofluorescence images from confocal microscopy of WT, heterozygous or homozygous L919X KI/KI mice medullary or cortical kidney sections stained for pendrin (red) or *Ae1* (green). **D)** Quantification of **(C)** showing A-IC and B-IC in the cortex and medulla of WT, heterozygous or homozygous *Ae1* L919X KI mice. Error bars correspond to means \pm SEM (n = 4-6 kidney sections). ***P < 0.001 using Two-way ANOVA. *Each image in this figure, except for panel B, was provided by Dr. Dominique Eladari.*

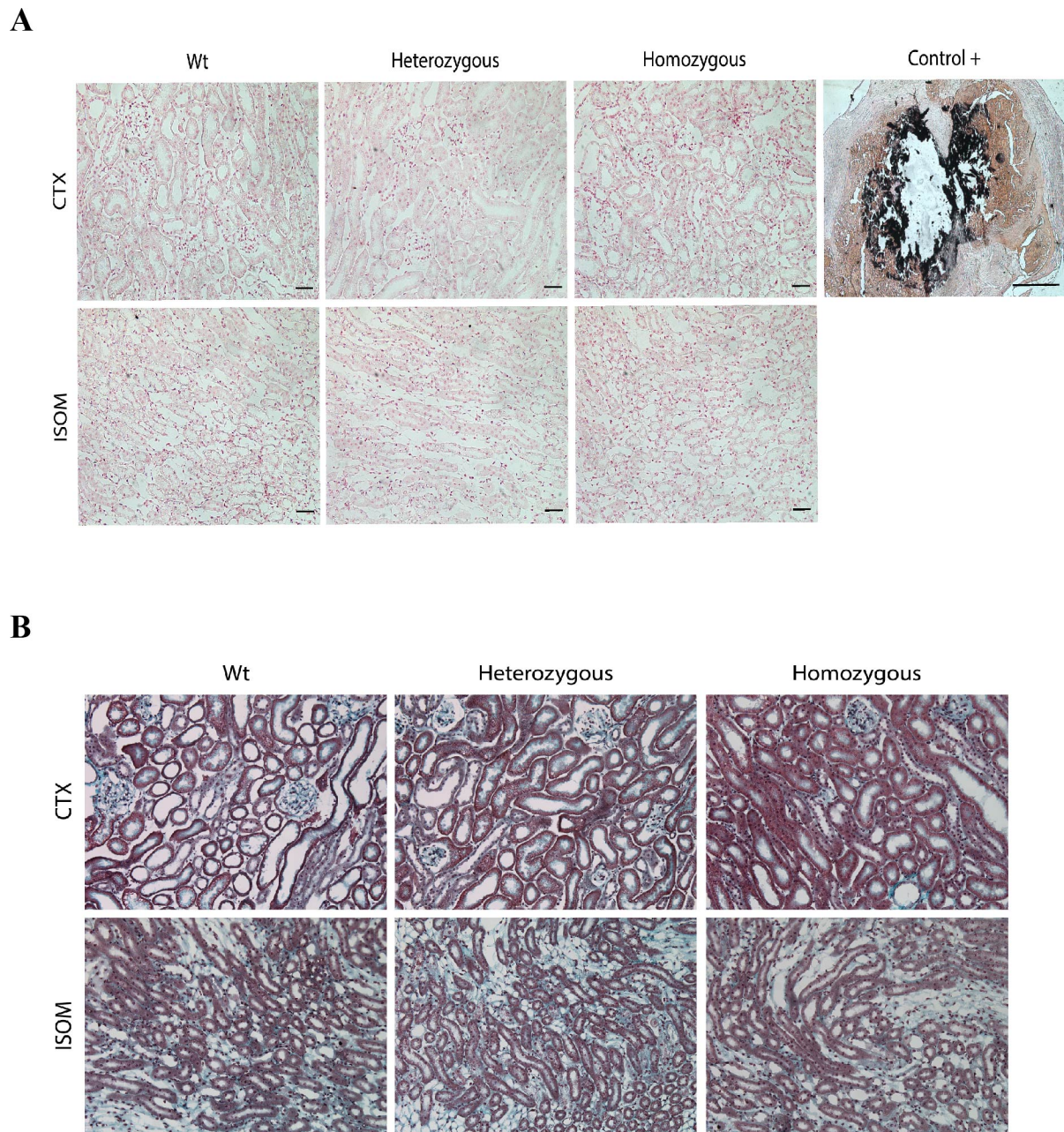


Figure 3.35 Further preliminary characterization of the L919X KI mice via Von Kossa and Masson Trichome Staining. **A)** Van Kossa staining to determine calcification within the kidney tissues revealed no significant difference between the wildtype, or the L919X KI heterozygous or homozygous in either the cortex or medulla. **B)** Masson Trichome staining to assess fibrosis in the kidney also revealed no significant differences between wildtype or L919X KI heterozygous or

homozygous mice. Together this suggests no gross abnormalities in these Ae1 mutant mice. *The images shown in this figure were provided by Dr. Dominique Eladari.*

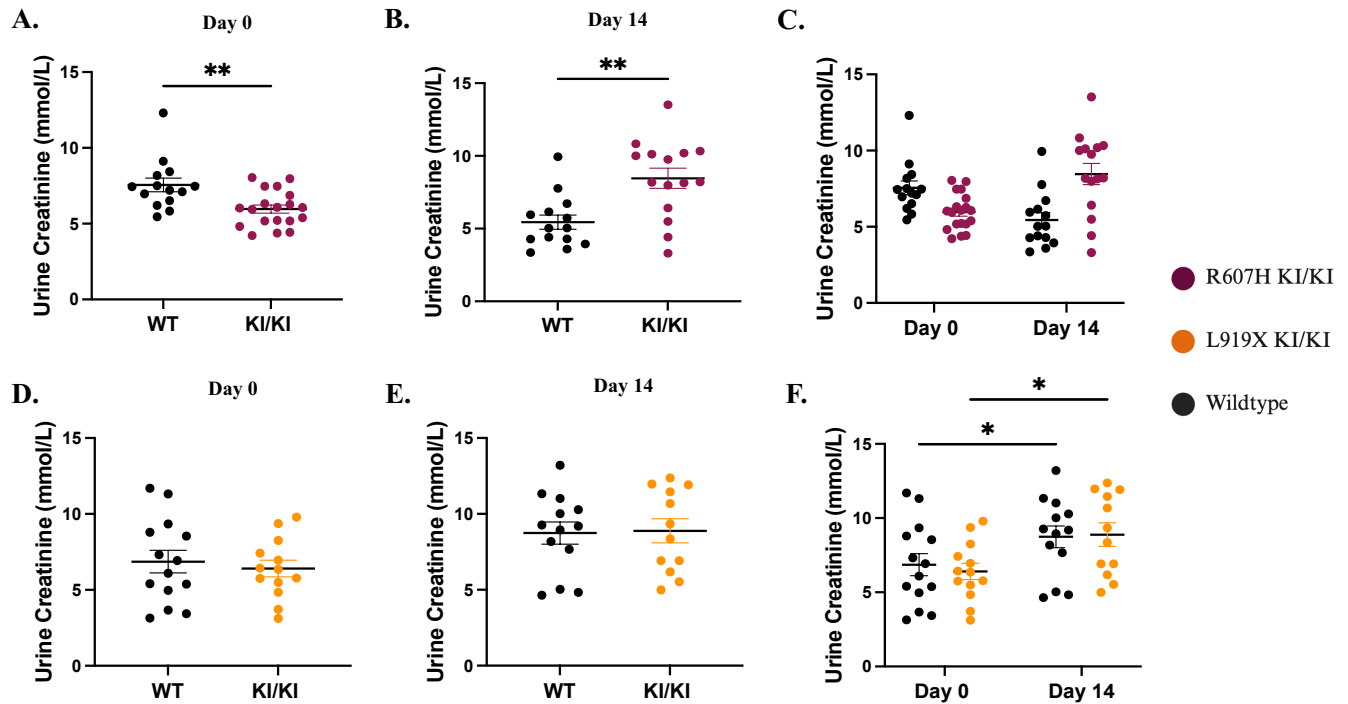


Figure 3.36 R607H KI/KI and L919X KI/KI mice following the salt-depleted acid load show changes in urinary creatinine excretion. **A)** At steady state, R607H KI/KI mice had less urinary creatinine excretion compared to WT mice, but by **B)** Day 14, the KI/KI mice increased urinary creatinine compared to WT counterparts. **C)** The trend of urine creatinine excretion over the 14-day experimental period for R607H KI/KI mice and WT counterparts. **D)** At steady state and **E)** at Day 14, L919X KI/KI mice had no difference to urinary creatinine excretion compared to WT **F)** The trend of urine creatinine excretion over the 14-day experimental period for L919X KI/KI mice and WT counterparts reveal both significantly increased creatinine excretion from baseline. Data presented as mean \pm SEM, * $P < 0.05$, ** $P < 0.01$, with unpaired Student's t-test, Mann-Whitney test, and 2-way ANOVA with Tukey's multiple comparison test.